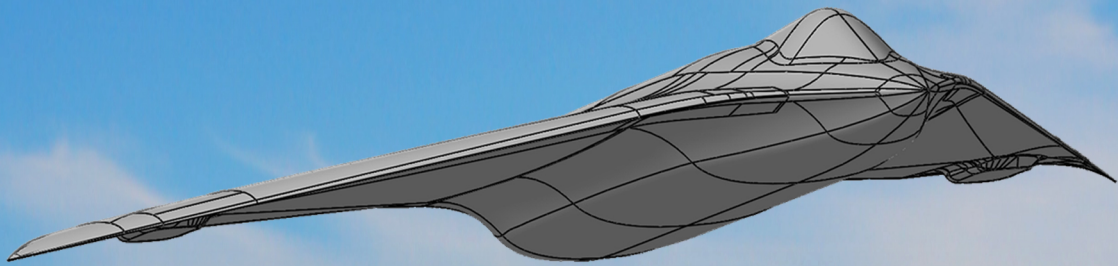


Upset Recovery Controller Based on Maximum Control Effectiveness for a High-Performance Over-Actuated Aircraft

Master of Science Thesis
D.J. van Oorspronk



Upset Recovery Controller Based on Maximum Control Effectiveness for a High-Performance Over-Actuated Aircraft

Master of Science Thesis

by

D.J. van Oorspronk

to obtain the degree of Master of Science
at the Delft University of Technology,
to be defended publicly on Friday May 25, 2018 at 14:00.

Student number: 4220838
Project duration: June 6, 2017 – May 25, 2018
Thesis committee: Dr. ir. Q.P. Chu, TU Delft, chair of assessment committee and supervisor
Dr. ir. C.C. de Visser, TU Delft, supervisor
Dr. ir. E. van Kampen, TU Delft
Dr. ir. E. Mooij, TU Delft

Image of ICE aircraft on cover is property of Lockheed Martin Aeronautics.

Summary

High-performance aircraft require an upset recovery controller which is capable of recovering the aircraft from any upset condition back to the safe flight envelope. In aircraft upset conditions, aircraft encounter nonlinear effects and reduced control authority over the control effectors. Currently, no adequate method in the field of upset recovery in aviation is available to properly handle this issue. Existing upset recovery methods are focused on recovery by neglecting current flight conditions and nonlinear effects.

This thesis implements a novel method for aircraft upset recovery that combines maximum control effectiveness of each control effector with a sophisticated upset recovery strategy to control key aircraft states to an acceptable level by means of incremental nonlinear dynamic inversion during off-nominal flight conditions that are specified as loss of control.

A recovery control strategy based on reducing angular body rates and aerodynamic angles generates inner and outer loop commands. Pseudo control inputs defined as required moment increments are derived using a nonlinear Jacobian model of the control effectors. This pseudo control input and Jacobian determine the direction of control effector effectiveness gradient optimization. The upset recovery system is implemented on the Innovative Control Effectors (ICE) aircraft, a high performance over-actuated aircraft with 13 highly nonlinear, interacting and coupled control effectors. Real-time simulation results show that the upset recovery system is fault tolerant, considerably faster, and more reliable compared to nominal flight control systems in terms of recovering angular body rates and aerodynamic angles, and is applicable in every aircraft upset condition.

Acknowledgements

I would like to express my deep gratitude to Dr. Q.P. Chu, for his patient guidance, enthusiastic attitude, long conversations, and insights into control methodologies of aerospace vehicles. These insights have led to the completion of my thesis with an innovative result. I would also like to thank Dr. C.C. de Visser, for his advice and assistance in taking the academic contribution to the next level. His involvement and eagerness to understand the concept from start to end has brought new interesting ideas.

Furthermore I want to thank my friends for the fun and great time we had in Delft that I leave behind now. Moreover, thank you to Lisanne for all her love and support. Last but not least I want to express my deepest gratitude to my parents and family for the support over the years, without their support it would have been impossible to obtain my MSc degree in Aerospace Engineering in Delft.

Dennis van Oorspronk
Delft, The Netherlands
May 25, 2018

Contents

Summary	iii
Acknowledgements	v
Nomenclature	ix
List of Figures	xi
List of Tables	xiii
1 Introduction	1
2 Aircraft Upset Conditions	3
2.1 Aircraft Upset Definition	3
2.2 Causes of Aircraft Upsets	3
2.2.1 Environmental Causes	4
2.2.2 Aircraft Failure Causes	4
2.2.3 Pilot Induced Causes.	4
2.2.4 Mission Dependent Causes	5
2.3 Aircraft Critical Motions.	5
2.4 Aircraft Upset Recovery Strategies.	5
2.4.1 Nose-High Recovery Strategy	6
2.4.2 Nose-Low Recovery Strategy	6
2.5 All-Encompassing Upset Recovery Strategies	6
3 Incremental Nonlinear Dynamics	11
3.1 Nonlinear Dynamic System	11
3.2 Incremental Effector Constraints	13
3.3 Control Effector Dynamics Compensation	13
3.4 Control Effectiveness	14
3.4.1 Control Effectiveness Optimization	14
3.4.2 Gradient Information Algorithm	16
3.4.3 Stochastic Search Algorithms	16
4 Innovative Control Effectors Aircraft	17
4.1 Innovative Control Effectors	18
4.2 Aerodynamic Model of Innovative Control Effector Aircraft	19
4.3 Upset Recovery for Innovative Control Effector Aircraft	21
5 Project Definition	23
5.1 Research Objective and Questions	23
5.2 Upset Recovery Using Maximum Control Effectiveness and Incremental Control Design	24
5.3 Experimental Setup and Analysis of Results.	25
5.4 Proof of Concept	25
5.4.1 Proof of Concept Design	25
5.4.2 Spin Recovery Demonstration	26
6 Upset Recovery Controller Design	29
6.1 Upset Recovery Strategy Planner	29
6.1.1 Angular Rate Control Loop.	29
6.1.2 Aerodynamic Angle Control Loop	30
6.2 Multivariate Simplex B-Splines Jacobian	32
6.2.1 Aerodynamic Multivariate Simplex B-Splines Jacobian.	32
6.2.2 Multi-Axis Thrust Vectoring Jacobian	32

6.3	Control Effector Selection	33
6.4	Control Effectiveness Optimization	33
6.5	Actuator Dynamics Compensation	34
6.6	Fault Tolerant Control Capabilities	35
6.7	Control Effector Saturation	35
6.8	Low Altitude Control	36
6.9	Upset Recovery Controller Design Overview	36
7	Simulation and Results	39
7.1	Simulation Equipment	39
7.2	Critical Upset Motions	40
7.2.1	Deep Stall	40
7.2.2	Spin	42
7.3	External Caused Aircraft Upsets	46
7.3.1	Environmental Caused Upset	46
7.3.2	Mission Dependent Caused Upset	46
7.4	Fault Tolerant Control Capabilities	48
7.5	Low Altitude Control	49
7.6	Actuator Dynamics Compensation	52
8	Conclusions and Recommendations	53
	Bibliography	57
A	Conference Paper	61
B	Additional Results	91

Nomenclature

Latin Symbols

\mathbb{A}	Feasible set	[-]
A_x	Body frame acceleration in X	[ft/s ²]
A_y	Body frame acceleration in Y	[ft/s ²]
A_z	Body frame acceleration in Z	[ft/s ²]
C_L	Dimensionless rolling moment coefficient	[-]
C_M	Dimensionless pitching moment coefficient	[-]
C_N	Dimensionless yawing moment coefficient	[-]
C_X	Dimensionless axial force coefficient	[-]
C_Y	Dimensionless lateral force coefficient	[-]
C_Z	Dimensionless vertical force coefficient	[-]
d	Distance	[ft]
g	Gravitational acceleration	[ft/s ²]
h	Altitude	[ft]
I	Inertia matrix	[-]
M	Mach number	[-]
p	Angular roll rate	[deg/s]
q	Angular pitch rate	[deg/s]
r	Angular yaw rate	[deg/s]
\mathbb{R}	Set of real numbers	[-]
t	Time	[s]
V	Airspeed	[ft/s]
x	State vector	[-]
y	Output vector	[-]

Greek Symbols

α	Angle of attack	[deg]
β	Angle of sideslip	[deg]
Δ	Increment	[-]
δ	Control effector deflection angle	[deg]
ε	Equality constraint index	[-]
γ	Flight path angle	[deg]
θ	Pitch angle	[deg]
ϑ	Inequality constraint index	[-]
ν	Virtual control	[-]
τ	Aerodynamic input vector	[-]
Φ	Nonlinear aerodynamic control input	[-]
ϕ	Roll angle	[deg]
ω	Angular body rates	[deg/s]
Ω	Available feasible space	[-]

Sub- and superscripts

0	Current
.	Time derivative
a	Airframe
b	Body frame
c	Command
c.g.	Center of gravity
k	Step direction
l	Lower
u	Upper
max	Maximum
min	Minimum
step	Step size

Abbreviations

AMT	All moving wing tips
CAT	Clear air turbulence
DLEF	Differential leading edge flap
DRUD	Deployable rudder
IATA	International Air Transport Association
ICAO	International Civil Aviation Organization
ICE	Innovative Control Effectors
INCA	Incremental nonlinear control allocation
INDI	Incremental nonlinear dynamic inversion
LAMT	Left all moving wing tip
LED	Leading edge down
LEL	Left elevon
LIBLEF	Left inboard leading edge flap
LOBLEF	Left outboard leading edge flap
LOC	Loss of control
LSP	Lower surface spoiler
LSSD	Left spoiler slot deflector
MTV	Multi-axis thrust vectoring
PF	Pitch flap
RAMT	Right all moving wing tip
RCS	Radar cross section
REL	Right elevon
RIBLEF	Right inboard leading edge flap
ROBLEF	Right outboard leading edge flap
RSSD	Right spoiler slot deflector
SSD	Spoiler slot deflector
TED	Trailing edge down
TEU	Trailing edge up
TVP	Pitch thrust vectoring
TVY	Yaw thrust vectoring

List of Figures

2.1	Upset recovery strategy	9
4.1	Land based baseline configuration [12]	17
4.2	Carrier based baseline configuration [12]	17
4.3	Innovative control effectors [28]	18
5.1	Control flow diagram for the upset recovery controller	25
5.2	Control flow diagram for the proof of concept upset recovery controller	26
5.3	Body angular rates q and r during yaw spin demonstration	27
5.4	Aerodynamic angles during yaw spin demonstration	27
5.5	Airspeed and Mach number during yaw spin demonstration	28
6.1	Actuator dynamics compensation scheme	35
6.2	Actuator dynamics compensation high-bandwidth transfer function	35
6.3	Upset recovery controller design overview	37
7.1	Body angular rates in a deep stall upset at low airspeed	41
7.2	Aerodynamic angles and airspeed in a deep stall upset at low airspeed	41
7.3	Body angular rates in a deep stall upset at zero airspeed	42
7.4	Aerodynamic angles and airspeed in a deep stall upset at zero airspeed	43
7.5	Body angular rates in a yaw spin upset	44
7.6	Aerodynamic angles and airspeed in a yaw spin upset	44
7.7	Body angular rates in a pitch spin upset	45
7.8	Aerodynamic angles and airspeed in a pitch spin upset	45
7.9	Body angular rates while encountering a 1,000 ft/s wind gust	47
7.10	Aerodynamic angles and airspeed while encountering a 1,000 ft/s wind gust	47
7.11	Body angular rates while being hit by missile	48
7.12	Aerodynamic angles and airspeed while being hit by missile	49
7.13	Body angular rates while being hit by missile, left wing control effector failure for "Recovery FT"	50
7.14	Aerodynamic angles and airspeed while being hit by missile, left wing control effector failure for "Recovery FT"	50
7.15	Pitch angle, angle of attack, and flightpath angle in stall condition near ground	51
7.16	Altitude and airspeed in stall condition near ground	51
7.17	Performance comparison between having/not having actuator dynamics compensation and INCA	52
B.1	Control effector inputs during low speed deep stall recovery	91
B.2	Control effector inputs during zero speed deep stall recovery	92
B.3	Control effector inputs during yaw spin recovery	93
B.4	Control effector inputs during pitch spin recovery	94
B.5	Control effector inputs while encountering a 1,000 ft/s wind gust	95
B.6	Control effector inputs while being hit by missile	96
B.7	Control effector inputs while being hit by missile, no failure in left wing control effectors	97
B.8	Control effector inputs while being hit by missile, failure in left wing control effectors	98
B.9	Control effector inputs with low altitude control system during low altitude stall	99

List of Tables

2.1	Nose-high recovery strategy [4].	6
2.2	Nose-low recovery strategy [4].	7
4.1	Control effectors overview of the ICE aircraft, sign convention, position and rate limits, abbreviations, and effector dynamics [12, 29].	19
4.2	Sub coefficients of the ICE aircraft and corresponding parameters, data range, and number of datapoints	22
5.1	Flight conditions during yaw spin demonstration	27
6.1	Envelope limits of inner and outer control loop parameters	30
7.1	Gains used during simulation of upset recovery controller	40
7.2	Close explosion moment properties of missile impact	48
7.3	Fault tolerant close explosion moment properties of missile impact	48

Introduction

Recent statistics show that loss of control (LOC) is the largest contributor of fatal accidents in aviation for commercial and military aircraft [1, 2, 16, 33, 45]. In order to increase safety and reduce the number of fatal accidents in aviation, LOC requires more in-depth research. In general LOC is associated with flying outside the save flight envelope, where pilots encounter nonlinear influences such as kinematic coupling, oscillatory or divergent aircraft responses and experience reduced capabilities to control the aircraft [8, 24, 45]. Also high angular rates and displacements together with the lack to maintain aircraft attitude can be expected [45]. Despite the improvements made to reduce aircraft accidents, some factors are still not fully described and well understood [8].

Although modern commercial and military aircraft are equipped with autonomous envelope protection in order to keep the aircraft in the safe envelope, aircraft still end-up in critical regions (upset) due to pilot inputs, aircraft failures, or environmental causes. For these occurrences of flying outside the save envelope where aircraft are not capable of responding to pilot inputs as in nominal flight conditions, upset recovery is essential for preventing a fatal incident. In this context recovery is defined as the capability to control key aircraft states to an acceptable level during off-nominal flight conditions that are specified as LOC [8].

Traditionally, flight control systems have been developed for nominal flight conditions in which the pilot has full control authority. Since aircraft upsets occur outside the safe nominal flight envelope, development of effective algorithms for off-nominal flight conditions is crucial. Guidance laws that recover the aircraft are investigated, by using a pilot-activated recovery system based on genetic search [42], linear quadratic regulator state feedback controller [5], sliding mode controller [34, 36, 47], high order sliding mode controller [9–11, 46], and nonlinear dynamic inversion [22, 32]. Other systems are limited to incomplete pilot recovery guidelines by using reinforcement learning systems [13, 20] or online model predictive control [37]. In order reduce the number of LOC accidents, it is vital to enhance current flight control systems with algorithms that cope with off-nominal conditions where nonlinear dynamics and uncertainties are present [6].

Flight control systems require a more advanced upset recovery methodology which is able to recover from extreme angles of attack far away from the safe flight envelope. Current methods are more focused on how to recover as fast as possible taking only into account the current states of the aircraft while neglecting nonlinear aircraft dynamics, and control effector nonlinearities and interactions. However, in off-nominal conditions together with maximum control effector deflections, usage of linear models is of limited value [7, 30]. A method implementing maximum aircraft control effectiveness is focusing instead of only aircraft states also on the maximum control authority of an aircraft in critical/upset flight conditions while taking into account nonlinearities.

This thesis describes a methodology for designing an aircraft upset recovery system which is able to recover from any type of aircraft upset condition for a high performance over-actuated aircraft. Currently no adequate method in the field of upset recovery is available. Based on maximum control effectiveness of control effectors given the flight condition, key aircraft states are controlled to an acceptable condition within the safe flight envelope. By means of a reformulation of nonlinear dynamics in incremental form, known as

incremental nonlinear dynamic inversion (INDI), a pseudo control input defined as the required moment increment generated by control effectors is derived using a nonlinear Jacobian model of the control effectors. This pseudo control input is fundamental in determining the heading of optimization of future control effector deflections for highest aircraft control effectiveness. Inner and outer control loops for determining a pseudo control input are derived from an all-encompassing upset recovery strategy sequence necessary for quick recovery.

The research objective of this thesis is to contribute to the development of an upset recovery controller for a highly maneuverable over-actuated fighter aircraft which is capable of recovering from any loss of control situation, by designing an advanced recovery flight control system which uses maximum control effectiveness for recovering the Innovative Control Effectors (ICE) aircraft.

In order to meet this research objective, the following research questions are defined:

1. How to design an upset recovery method based on maximum control effectiveness for a high-performance over-actuated aircraft which is capable of recovering from any loss of control situation?
 - (a) Can the method be constructed for any aircraft upset condition?
 - (b) Which aircraft states and inputs determine the performance of upset recovery?
 - (c) Which upset recovery strategy is applicable in every upset condition?
2. How to determine the maximum control effectiveness of an aircraft?
 - (a) Which aircraft states and inputs have influence on the control effectiveness?
 - (b) Which multidimensional optimization method is able obtain optimal control authority?

This thesis report contains the findings of an extensive literature study, combined with a novel method for upset recovery, and a demonstration to show the working principle and the feasibility of the method. The remainder of the report is structured as follows. In chapter 2 definitions, causes, and strategies are provided for upset recovery. Chapter 3 presents the general equations of motion of a nonlinear system and how to derive the control effectiveness. Chapter 4 elaborates on the ICE aircraft simulation model and the corresponding available aerodynamic database. In chapter 5 the full project definition is presented together with a detailed explanation of the research objective and research questions, the chosen method, and a demonstration of a proof of concept. Followed by describing the implemented maximum control effectiveness concept for upset recovery in chapter 6 in which the new flight control systems is designed. Simulations and results are described in chapter 7 where different upset scenarios are simulated. This report is concluded in chapter 8 together with recommendations for future work.

2

Aircraft Upset Conditions

In this chapter an introduction is given into aircraft upset conditions in a LOC situation. Recent statistics show that LOC is the largest contributor of fatal accidents in aviation for commercial and military aircraft [1, 2, 16, 33, 45]. In order to increase safety and reduce the number of fatal accidents in aviation, LOC requires more in-depth research. In general LOC is associated with flying outside the save flight envelope into upset conditions, where pilots encounter nonlinear influences such as kinematic coupling, oscillatory or divergent aircraft responses and experience reduced capabilities to control the aircraft [8, 24, 45]. Also high angular rates and displacements together with the lack to maintain aircraft attitude can be expected [45]. Despite the improvements made to reduce aircraft accidents, some factors are still not fully described and well understood [8]. This chapter contains an elaboration on the correct definition of aircraft upset presented in section 2.1. Followed by section 2.2 that explains the causes how to depart from the safe flight envelope. Section 2.3 explains the possible critical motions followed from the upset causes. Finally section 2.4 explains on available upset recovery guidelines and an all-encompassing upset recovery strategy is presented in section 2.5.

2.1. Aircraft Upset Definition

Within the commercial aviation industry different terms and definitions are used to describe aircraft upset. Therefore, from this point on aircraft upset will be used for the rest of the report. Aircraft upset can be defined as an undesired aircraft state which is characterized by unintentional exceeding parameters usually experienced during normal operations [4, 18, 19]. The first aspect of the definition is unintentional. In aircraft upset the aircraft is not doing what it is commanded to do and is close to the boundary of the safe envelope. The second aspect is controllers and pilots should not wait until the aircraft is in upset before corresponding actions are taken to return to the safe envelope. Defining specific values for aircraft approaching upset condition vary among aircraft specification. However, for airplane upset recovery training programs the following values may be used [4].

- Nose up pitch attitude larger than 25 degrees.
- Nose down pitch attitude smaller than 10 degrees.
- Bank angle larger than 45 degrees.
- Within the above mentioned flight conditions, but at a reasonable low airspeed for current flight parameters.

However, these values are specified for civil aviation and therefore can not be applied to aircraft in general.

2.2. Causes of Aircraft Upsets

For commercial aircraft, aircraft upset is not a common occurrence. Today's certification requirements are of such a high level that aircraft have become more reliable. Furthermore pilot training programs have increased the pilot awareness close to aircraft upsets [4]. Despite this fact, incidents of this type still occur. This section describes the four most common aircraft upsets.

2.2.1. Environmental Causes

A significant number of aircraft upsets are caused by environmental factors where aircraft often have no influence on [4].

- **Turbulence** Turbulent air contains large variations in flow velocity over a short distance. The main causes of turbulence are windshear, jet streams, and wind obstructions.
 - **Clear air turbulence (CAT)** can be encountered at any altitude but is known as high-level turbulence (usually above 15,000 ft.). CAT is mainly caused by jet streams.
 - **Mountain Wave** belongs to the category wind obstruction. In case of severe turbulence it may cause large variations in airspeed and the aircraft might be out of control for some time.
 - **Windshear** is defined as wind variations at low altitude which may cause hazards during take-off and approach. These wind variations are caused by local meteorological conditions.
 - **Thunderstorms** produce strong gusts and high precipitation. Due to accelerating airflow within the storm, large changes in windspeed could occur.
 - **Micro-burst** is defined as a concentrated, more powerful downdraft (downward moving column of air). Micro-bursts occur in convective weather conditions. Still micro-burst accidents occur from which cannot be successfully escaped with known techniques.
- **Wake Turbulence** is the dominant cause of aircraft upset by environmental conditions. Due to high pressure air on the lower wing surface and low pressure air on the upper wing surface, air flows from the lower to the upper surface. This phenomenon creates a pair of counter rotating vortices. Those vortices are generally very strong dependent on mainly the weight of the aircraft. Other aircraft flying into the vortices encounter usually induced roll and pitch moments.
- **Aircraft Icing** causes large aerodynamic performance degradation due to disturbed flow around the airfoil. These adverse effects vary with location and reduced aircraft handling.

2.2.2. Aircraft Failure Causes

Over the years, aircraft designs become better and are equipped with more safety systems than before. This is required by the ever-improved certification process of aircraft. Furthermore aircraft manufacturers log aircraft incidents to prevent equipment failure from happening again. Despite the increasing level of control, failure of components can not be completely prevented. Some of these failures can lead to aircraft upset if mitigation or training is not applied. Possible upset causes due to aircraft failures are listed below [4].

- **Flight Instruments** occasionally fail during operation. However the pilot or system needs to be aware of information displayed by the aircraft might be incorrect.
- **Autopilot** systems are integrated systems that keep track of altitude, heading, and airspeed with high accuracy. Pilots tend to have high confidence in the autopilot which makes pilot unconscious in case the system fails.
- **Flight Control** anomalies such as control effectors that stuck at a certain deflection angle reduces aircraft control authority. Engine failure also belongs to this category.

2.2.3. Pilot Induced Causes

The third category is aircraft upset due to pilot control inputs or unawareness. Sensory input can lead to misconception in the case of low visibility or extreme flight conditions. Flight instruments help the pilot to provide additional information. Possible upset causes induced by pilots are listed below [4].

- **Misinterpretation** during the cross-check of instruments can lead to upset due to incorrect applying control inputs.
- **Inattention** or neglecting to monitor current aircraft states can result into small deviations from the planned flight path. Slowly changing aircraft states are more difficult to notice by a pilot.
- **Disorientation** causes a significant proportion of aircraft upset accidents induced by pilots. Pilots are no longer able to align themselves with the Earth's surface.

- **Pilot Flying Skills** are despite the fact that every pilot gets a basic level of training, not the same for every pilot. Aircraft are developed and certified such that it behaves easily and well in the entire envelope. It is assumed that pilots use certain routine techniques. In some circumstances, control inputs can lead to unwanted aircraft motion such as pilot-induced oscillations.

2.2.4. Mission Dependent Causes

There are particular aircraft upset conditions where military aircraft have to deal with more often than commercial aircraft, one of those examples is an in-air missile attack. Missiles that aircraft might encounter come in different types: surface-to-air and air-to-air missiles. An impact from such a missile has dramatic impact on the current flight condition of the aircraft depending on the power of the missile warhead and impact location. High angular rates and control effector failures can be expected.

2.3. Aircraft Critical Motions

Various events can contribute to LOC during the flight mission, these events may depend on the type of mission but may also depend on meteorological, aircraft failure, or pilot induced causes. Section 2.2 gives an introduction to a variety of different events that can lead to aircraft upset. Investigation of aircraft LOC shows that in flight LOC is much more complicated than just the failure of components and other known factors [1]. Analysis shows that there can be concluded that in flight LOC can be the consequence of maneuverability near the boundary of the safe envelope [11]. At those boundaries of the safe envelope the angle of attack α might be so high that the aircraft has no full control authority to return to the safe envelope. Before an upset recovery strategy can be determined, a number of critical motions will first be discussed.

- **Stall:** An aircraft is in stall conditions if the angle of attack α exceeds the stall angle [4, 11]. The stall angle is the maximum angle at which the wings ability to produce lift is equal to the weight and the aircraft is able to maintain steady flight [3, 41]. Wings can stall at any airspeed and any altitude.
- **Departure:** Defined as the post-stall flight condition which accelerates entry into deep stall, spin, or post-stall gyration. Departure is the aircraft motion that indicates the transition from controlled flight into uncontrolled flight conditions. Departure is characterized by sudden uncommanded aircraft motions [43].
- **Deep stall:** In deep stall conditions the aircraft is unable to generate a nose-down moment. In order to prevent the deep stall from getting worse, turning around the velocity vector is advised [11].
- **Wing rock:** An aircraft is in wing rock mode if dominant oscillation in the roll axis are detected [23]. The motion is characterized by instability of the Dutch roll mode [11].
- **Spin:** A high yaw rate r at angles of attack α above stall angle. Additional body rates may cause oscillation in pitch q and roll p . In the severe case of a fully developed spin, the trajectory is approximately vertical and no major changes in the spin are observed [43].
- **Falling leaf:** The interchange of both aerodynamic and kinematic effects which causes a continuous motion about all three moment axes is called the falling leaf mode [17]. In the case of a falling leaf maneuver the aircraft is wings-level stalled and is forced into a spin motion. At the moment the spin develops, the spin is reversed by opposite rudder such that the spin starts developing in opposite direction.

2.4. Aircraft Upset Recovery Strategies

This section describes available recommended aircraft upset recovery strategies/techniques from literature. In October 2008, an airplane upset recovery team with representatives from airplane manufacturers, airlines, pilot associations, and government aviation and regulatory agencies developed a training aid that is not necessarily procedural [4]. Also International Civil Aviation Organization (ICAO) developed a "Manual on Aeroplane Upset Prevention and Recovery Training" [19]. Finally International Air Transport Association (IATA) published in 2015 guidance material and best practices in the scope of upset prevention and recovery training [14].

The training programs just mentioned are constructed for civil aviation, which means that it is application dependent. However the general idea behind the strategies is applicable for aircraft in general.

In the training programs mentioned above a clear difference has been made between two groups of flight controls, primary and secondary flight controls respectively. Primary flight controls such as aileron, elevator, and rudder are recommended to use. Secondary flight controls such as stabilizer trim, thrust, and speedbrakes can serve as an addition to assist primary flight controls. The use of both primary and secondary flight control in the process of recovery from an upset are discussed in section 2.4.1 and 2.4.2, where two different upset recovery strategies are described.

Strategies explained in this section are described in [4, 14, 19]. Note that the given aircraft upset recovery strategies given in this chapter assume the aircraft is not stalled.

2.4.1. Nose-High Recovery Strategy

This nose-high recovery strategy starts with a nose up pitch attitude larger than 25 degrees. The first step is to recognize the upset situation, and disengage the autopilot and autothrottle. Followed by direct nose-down elevator to obtain a nose-down pitch rate, maximum control inputs might be required. If there is still no pitch rate control at this time, there is an alternative technique to be tried. The use of different techniques strongly depends on the flight conditions and aircraft control authority. In the event the recommended procedure does not apply, the following alternatives are available:

- Rolling the aircraft to a bank angle starts a nose-down motion. Nose-down elevator will ensure that the angle of attack α remains as low as possible which makes aileron control effective. This rolling maneuvers ensures that the pitch decreases.
- In the case of underwing-mounted engines, reducing thrust setting will reduce pitch up moment. However this method is only permitted at safe altitude.
- If ailerons and spoilers are stalled, rudder input may solves the recovery by inducing a rolling maneuver. Only a small rudder input is allowed to prevent a spin from developing.

In order to complete the recovery, only gentle inputs are recommended to avoid entering another upset. Roll wings to level flight and check airspeed. The complete recommended procedure is given in Table 2.1.

Table 2.1: Nose-high recovery strategy [4].

Situation	Situation description	Recovery strategy
Nose-high	$\theta > 25 \text{ deg}$ $q > 0 \text{ deg/s}$ $\dot{V} < 0 \text{ m/s}$	Recognize situation Disengage autopilot and autothrottle Full nose-down elevator Roll (if necessary) to obtain $q < 0$ Reduce thrust (in case of underwing-mounted engines) Recover to level flight

2.4.2. Nose-Low Recovery Strategy

This nose-low recovery strategy starts with a nose down pitch attitude smaller than -10 degrees. The first step is to recognize the upset situation, and disengage the autopilot and autothrottle. Since attitude is not directly related to whether the aircraft is stalled or not, the aircraft may be in stalled condition despite the relatively low pitch. If it is necessary, recover from stall first by applying nose down elevator which might be counter intuitive. Apply thrust once the aircraft is recovered from the stall. Return aircraft attitude by applying nose up elevator. In order to complete the recovery, only gentle inputs are recommended to avoid entering another upset or exceeding g-force limitations. If required, reduce thrust or extend speedbrakes as secondary control input. Roll wings to level flight and check airspeed. The complete recommended procedure is given in Table 2.2.

2.5. All-Encompassing Upset Recovery Strategies

To ensure a higher chance of survival for a recovery controller, the controller must have an adequate plan for each flight condition. Setting up a correct strategy plan is therefore essential. In section 2.3, critical motions

Table 2.2: Nose-low recovery strategy [4].

Situation	Situation description	Recovery strategy
Nose-low	$\theta < -10$ deg V is low/high	Recognize situation Disengage autopilot and autothrottle Recover from stall if necessary Roll in the shortest direction to wings level Recover to level flight

are displayed as a start-condition for the recovery controller. After this section available recovery strategies for civil aviation are described in section 2.4.

Section 2.4 is limited to describing two different recommended procedures that assume that the aircraft is not stalled. These procedures cover part of the potentially critical motions. However, these procedures are not applicable to worse upset conditions such as a flat spin or falling leaf. In order to also have an answer to these critical motions, a more complete procedure has to be designed, this procedure is described in this section.

A good working strategy should be designed for every condition, including stall conditions since this is one of the critical motions in which an aircraft is in upset conditions. Critical motions can be divided into two groups where the greatest differences can be found in the movement of the aircraft. The first group has been characterized by large aerodynamic angles without angular rates. This group includes for example the critical motions stall and deep stall. Stall is described as a condition in which the angle of attack α exceeds the stall angle [4, 11], this is true for each critical motion described before. However, only large aerodynamic and attitude angles can be recognized with these types of upsets. The second group is characterized by large aerodynamic angles and angular rates that are higher compared to flying in normal flight conditions. An example of this critical motion is the spin, in which large variations in angle of attack α and beta β can be observed and at the same time large angular rates that characterize the spin. Important to mention is that high angular rates must first be reduced before attempting to restore the aerodynamic envelope. With this information together with the prescribed pilot upset recovery procedures introduced in section 2.4 and multi-mode upset recovery strategy [15] interpreted, the following sequence of actions are defined as aircraft upset recovery strategy.

1. Start upset recovery
2. Reduce angular rates p, q, r
3. Recover aerodynamic angles α, β
4. Recover attitude angles ϕ, γ
5. Recover altitude h and airspeed V
6. Normal flight control

In every given situation when the aircraft is experiencing high angular rates, first the rates must be reduced before attempting to recover aerodynamic angles. These fast rotational dynamics of the aircraft require damping moments. These damping effects can be created by the natural damping of the aircraft, however this is highly dependent on the type of control effectors installed on the aircraft. In advanced upsets, reliance on natural damping will not be sufficient and primary control effectors will have to reduce the measured angular rate. This way of fast-rotational dynamics reduction is difficult due to the aerodynamic uncertainty in the forces and moments produced by the control effectors in these upset conditions.

Next step after reducing high angular rates is to return the aircraft to the normal aerodynamic envelope, i.e. recover angle of attack α , sideslip angle β , and low airspeed. If there is underspeed, a speed increase will also have to be achieved at the same time. Gravity allows the aircraft to recover the airspeed, by trading altitude for airspeed. This airspeed recovery procedure is only valid when there is sufficient altitude to trade for airspeed. For the aerodynamic angles a moment will be created to point the nose of the aircraft directly into the airflow which means that the aerodynamic angles are close to zero. Active control for reducing α and β is required if the natural stability of the aircraft is insufficient.

Assuming that the aerodynamic angles are returned into the aerodynamic envelope, the next phase is to return the aircraft to steady level flight, i.e. bank angle ϕ to wings level and flight path angle γ to level flight. Because the angle of attack, sideslip angle, and airspeed are back in the normal flight envelope, control effectors will produce known aerodynamic forces and moments. Furthermore, the normal flight control will again be available to satisfy the attitude recovery. The advantage of this is that the normal flight control laws are valid that take into account the limitations of the aircraft.

Once the attitude envelope has also been restored, the last part of the upset recovery that remains is the limitation of any over-speed and to regain altitude. Reduced throttle setting and aiming for positive flight path angle to reduce the airspeed is required. Once the airspeed has been reduced, the upset recovery procedure has been completed and normal flight may be continued.

This entire upset recovery strategy is visualized in Fig. 2.1. Rounded square boxes represent the action that is required, those actions are described in this section. Next to that there are two diamonds that contain the question if certain rates and angles are reduced to a certain level such that the upset recovery strategy can be continued. The arrows in the figure indicate the process within the flow diagram and indicate the direction for certain conditions.

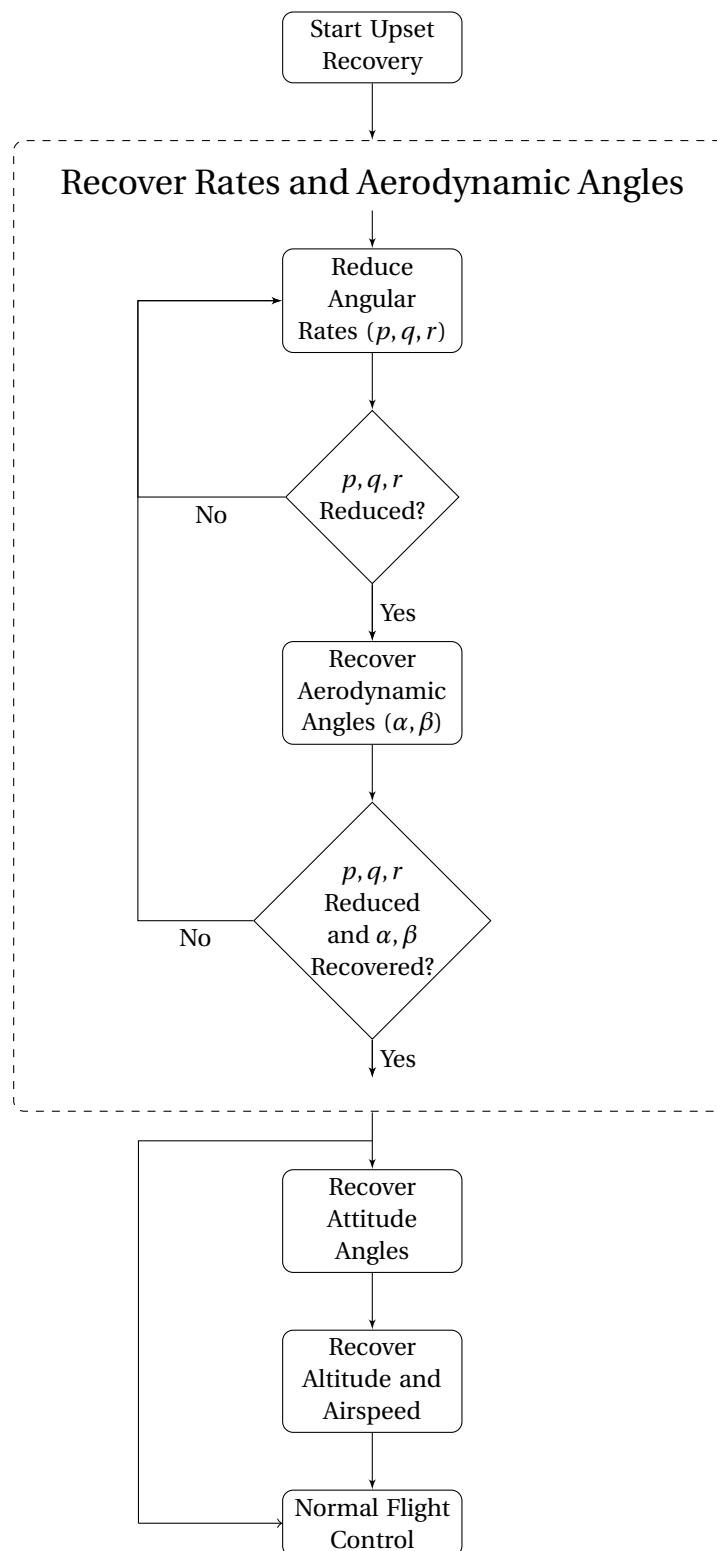


Figure 2.1: Upset recovery strategy

Incremental Nonlinear Dynamics

Selecting the maximum control effectiveness is the process of searching optimal control inputs for available control effectors, this process is strongly application dependent. This chapter describes the general idea of maximum control effectiveness for a given nonlinear system, in this case an aircraft. The combination of control effectiveness together with upset recovery has not been used before. Section 3.1 shows the general nonlinear dynamics of a system. Followed by an incremental formulation of those dynamics in section 3.2. Finally section 3.4 describes how to obtain maximum control effectiveness in any situation.

3.1. Nonlinear Dynamic System

In general, dynamics of an aircraft in upset/critical conditions can be described as Eq. (3.1).

$$\dot{x}(t) = f(x) + g(x)\tau \quad (3.1)$$

where $x \in \mathbb{R}^n$ is the state vector containing n scalars, $g(x)$ is control effectiveness, $\tau \in \mathbb{R}^m$ containing the input vector of size m . In Eq. (3.1) the state equation is only influenced externally by the input vector τ . This τ is often defined as (aerodynamic) moments generated. Equation (3.2) shows the separation of the largest moment contributors.

$$\tau = \tau_a + \tau_\delta \quad (3.2)$$

Where τ_a consist of moments generated only by the airframe, and τ_δ of moments generator by control effectors. Model τ_δ for nonlinear functions can be expressed as $\Phi(x, \delta)$ for nonlinear mapping. Here, $\delta \in \mathbb{R}^c$ describes c control effector deflections/positions. For conventional aircraft configurations where control effectors are far apart from each other, the influence of interactions between control effectors is small and can be assumed as separable. However, if multiple control effectors are installed close together, the influence of the interactions will be larger [31]. Equation (3.2) can be rewritten for a nonlinear mapping of (aerodynamic) moments generated by the control effectors, this rewritten equation is shown in Eq. (3.3).

$$\tau = \tau_a + \Phi(x, \delta) \quad (3.3)$$

By using this aerodynamic control vector formulation the general aircraft dynamics of Eq. (3.1) can be rewritten as

$$\dot{x} = [f(x) + g(x)\tau_a] + g(x)\Phi(x, \delta) = F(x) + g(x)\Phi(x, \delta) \quad (3.4)$$

where $F(x)$ contains all the effects that are not generated by the control effectors.

In the case the system operates in a discrete-time scheme, the dynamic equations as written in general form in Eq. (3.4) can be locally linearized at time steps around current state x_0 and control effector position δ_0 as a first-order Taylor expansion equation:

$$\dot{x} \approx \dot{x}_0 + \frac{\partial}{\partial x} [F(x) + g(x)\Phi(x, \delta)](x - x_0) + \frac{\partial}{\partial \delta} [F(x) + g(x)\Phi(x, \delta)](\delta - \delta_0) \quad (3.5)$$

With regard to the upset recovery problem, the proposed upset recovery method is aiming for maximum control effectiveness for each flight condition. Determining a control effector position δ that produces a given

(i.e. maximum or minimum) force or moment is key for this problem. For over-actuated systems where $c > m$ this upset recovery problem becomes more challenging, since multiple solutions could exist. Control effectiveness Jacobian can be deduced from the locally linearized system at every time step around the current state x_0 and current control effector positions δ_0 as a Taylor expansion (Eq. (3.5)).

The time scale separation principle states that if a moment acts on an aircraft, this mainly causes angular rate changes and attitude angles remain roughly the same for small time steps [25, 35, 38]. For Eq. (3.5) time scale separation may be used since the derivative of the state vector \dot{x} have notably faster dynamics compared to the state itself x . Therefore the second term on the right-hand side of Eq. (3.5) is small enough to be neglected with high sampling rates. The third term containing δ changes significantly faster than x in one time step, therefore the influence of δ is expected to be higher. Applying the time scale separation principle to Eq. (3.5) results into Eq. (3.6).

$$\dot{x} \approx \dot{x}_0 + \frac{\partial}{\partial \delta} [F(x) + g(x)\Phi(x, \delta)](\delta - \delta_0) \approx \dot{x}_0 + g(x_0) \frac{\partial \Phi(x_0, \delta_0)}{\partial \delta} \Delta \delta \quad (3.6)$$

Where $g(x)\partial\Phi(x_0, \delta_0)/\partial\delta$ in Eq. (3.6) represents the control effectiveness Jacobian function that contains (non)linear behavior of control effectors. For this thesis project, the Jacobian control effectiveness matrix is derived from a multivariate simplex spline-based aerodynamic model identified from a high-fidelity aerodynamic database of the Lockheed Martin ICE aircraft [44]. This spline model maintains the aerodynamic structure including nonlinear aerodynamics as stated in Eq. (3.7).

$$C_i = \sum C_{i_c}(\alpha, \beta, M, \delta) \quad (3.7)$$

With $i = \{X, Y, Z, l, m, n\}$ and c the number of aerodynamic coefficients. A 0th-order simplex model is constructed from the original ICE aerodynamic database using linear regression techniques in [44], the total number of spline functions to aerodynamic moment and force coefficients for this model is 108. Using this simplex model the partial derivatives of the aerodynamic force and moment coefficients with respect to δ is calculated, in Eq. (3.8) the control effectiveness Jacobian matrix is defined.

$$\frac{\partial \Phi(x, \delta)}{\partial \delta} = \begin{bmatrix} \frac{\partial C_X(x, \delta)}{\partial \delta_1} & \frac{\partial C_X(x, \delta)}{\partial \delta_2} & \dots & \frac{\partial C_X(x, \delta)}{\partial \delta_n} \\ \frac{\partial C_Y(x, \delta)}{\partial \delta_1} & \frac{\partial C_Y(x, \delta)}{\partial \delta_2} & \dots & \frac{\partial C_Y(x, \delta)}{\partial \delta_n} \\ \vdots & \vdots & \ddots & \vdots \\ \frac{\partial C_n(x, \delta)}{\partial \delta_1} & \frac{\partial C_n(x, \delta)}{\partial \delta_2} & \dots & \frac{\partial C_n(x, \delta)}{\partial \delta_n} \end{bmatrix} \quad (3.8)$$

In the case of an over-actuated aircraft with more control effectors to control compared to the degrees of freedom, this Jacobian becomes a non-square matrix.

Setting the virtual control input $v(x) = \dot{x}$, Eq. (3.6) can be simplified to

$$v(x) = \dot{x} \approx \dot{x}_0 + g(x_0) \frac{\partial \Phi(x_0, \delta_0)}{\partial \delta} \Delta \delta \quad (3.9)$$

For a general problem of this form with three moments to be controlled in the equation, the time derivative of the state vector x_0 contains body angular accelerations. These body angular accelerations are sometimes not immediately measurable therefore state estimation methods can be used to obtain those parameters. The system can be linearized by rewriting Eq. (3.9) into Eq. (3.10).

$$\Delta \delta = \left[\frac{\partial \Phi(x_0, \delta_0)}{\partial \delta} \right]^{-1} g(x_0)^{-1} [v(x) - \dot{x}_0] \quad (3.10)$$

Where $g(x)\partial\Phi(x_0, \delta_0)/\partial\delta$ is the control effectiveness Jacobian and $g(x_0)^{-1}[v(x) - \dot{x}_0]$ the pseudo-control input command. The approach in Eq. (3.10) is also known as INDI which uses the properties of the system together with nonlinear dynamic inversion by using body angular accelerations and has been proven to work in many aerospace applications [38–40]. This body angular acceleration feedback eliminates sensitivity to model mismatch, that certainly occurs close to or in upset conditions. The principle of elimination of model mismatch increases robustness compared with conventional nonlinear dynamic inversion. Furthermore no or little gain scheduling is required in comparison with other nonlinear dynamic inversion methods [38].

When controlling aircraft attitude the acceleration feedback is dependent on the current state x_0 , angular acceleration $\dot{\omega}_0$, the virtual control input v , angular acceleration command $\dot{\omega}_c$, and $g(x)^{-1}$ is dependent on the inertia of the aircraft I . Therefore the pseudo-control input in Eq. (3.10) can be rewritten as

$$\Delta \tau_c = I[\dot{\omega}_c - \dot{\omega}_0] = I\dot{\omega}_c - I\dot{\omega}_0 \quad (3.11)$$

where the commanded angular acceleration $\dot{\omega}_c$ is provided by the control loop v and the current angular acceleration $\dot{\omega}_0$ is provided by feedback control using state estimation or angular acceleration measurement.

The linearized system defined in Eq. (3.10) is controlled by providing the virtual input v from the control loop such that the system output follows the commanded state. This can be achieved by using a state-feedback PID controller that is defined as Eq. (3.12).

$$v = K_P(y_c - y) + K_I \int (y_c - y) dt + K_D \frac{d(y_c - y)}{dt} \quad (3.12)$$

Writing Eq. (3.10) in incremental control form provides an effector position increment with respect to the current effector position such that the new effector position command δ_c becomes:

$$\delta_c = \delta_0 + \Delta \delta \quad (3.13)$$

This equation makes the linearization between the virtual control input $v(x)$ and x complete.

3.2. Incremental Effector Constraints

In section 3.1 the incremental formulation of the aircraft dynamics require also a new formulation for the constraints on the control effectors. Control effectors have constraints on deflection angles and deflection rates which in discrete-time are formulated into local constraints due to the deflection rate limits. Due to these constraints, unlimited position increments can not be achieved. Effector position and rate constraints are formulated in Eq. (3.14) and 3.15) respectively.

$$\delta_{min} \leq \delta \leq \delta_{max} \quad (3.14)$$

$$|\dot{\delta}| \leq \dot{\delta}_{max} \quad (3.15)$$

In discrete-time simulation environments, rate constraints determine the maximum effector position increment for each time step Δt as can be seen in Eq. (3.16) [30].

$$\Delta \delta_{max} = \dot{\delta}_{max} \Delta t \quad (3.16)$$

Using Eq. (3.16), Eq. (3.14) can be rewritten as Eq. (3.17) where incremental position constraints are taken into account in order to define a lower and upper constraint for the current effector position.

$$\delta_l \leq \delta \leq \delta_u \quad (3.17)$$

with [30]

$$\delta_l = \min(\delta_{max}, \delta + \dot{\delta}_{max} \Delta t) \quad (3.18)$$

$$\delta_u = \max(\delta_{min}, \delta - \dot{\delta}_{max} \Delta t) \quad (3.19)$$

where δ_l and δ_u selects the most restrictive constraint.

The relations defined in Eq. (3.18) and Eq. (3.19) defines at the same time the local search space for maximum control effectiveness optimization.

3.3. Control Effector Dynamics Compensation

Investigation into control allocation methods for advanced controllers have received increased attention since those controllers become more complex [26]. These advanced flight controllers are often faced with over-actuated systems with more control effectors than to be controlled variables. Despite the complexity of most advanced flight controllers, most existing control allocation algorithms neglect actuator dynamics [21, 26, 27]. Control allocation algorithms and closed-loop control laws are usually designed separately. The

idea behind this principle dictates the main objective for control allocation to give the appropriate commands to the actuators in order to have the desired system input.

In the case actuator dynamics are neglected, there is a possibility that control allocation algorithm, dynamics of actuators, and aircraft control commands may not match and loses control effectiveness [26, 27]. In the end this may result into losing adequate tracking performance or control stability of the closed loop system. Decreased overall effective bandwidth of the control system and the effect of unmodeled nonlinearities is one reason for this event [26].

In general an actuator dynamics problem can be described as a relation between a commanded control input and a actual control input. Eq. (3.20) shows the problem at hand.

$$\delta_{act} = \delta_c H \quad (3.20)$$

where δ_{act} represents the actual effector deflection to the aircraft, δ_c the commanded effector deflection by the controller, and H the actuator dynamics. The effect of actuator dynamics may be solved with feedback and feedforward control on the actuator input channel. By propagating the error and the current actuator position, actuator dynamics are taken into account.

3.4. Control Effectiveness

Control effectiveness is an important property of the flight characteristics of an aircraft. It more or less determines how the handling qualities of the aircraft are in certain conditions. In upset conditions, the control effectiveness of certain control effectors will change positively or negatively. This section describes what control effectiveness is and how this can be determined based on aerodynamic data from the aircraft.

Control effectiveness can be defined as the contribution of a certain control effector to the parameter coefficient to be controlled. A high contribution to the parameter coefficient means that the control effectiveness of this specific control effector is high. In the general equation for aircraft dynamics there is a control effectiveness matrix in the equation as can be seen in the following equation

$$\dot{x}(t) = f(x) + g(x)\tau \quad (3.21)$$

where $x \in \mathbb{R}^n$ is the state vector containing n vectors, $g(x)$ is control effectiveness, $\tau \in \mathbb{R}^m$ containing the aerodynamic input vector of size m and t is time. Equation (3.21) can be rewritten for a nonlinear mapping of aerodynamic forces and moments generated by the control effectors, this rewritten equation is shown in Eq. (3.22).

$$\tau = \tau_a + \Phi(x, \delta) \quad (3.22)$$

The control effector derivative of the control effectiveness matrix is defined as the following Jacobian.

$$\frac{\partial \Phi(x, \delta)}{\partial \delta} = \begin{bmatrix} \frac{\partial C_X(x, \delta)}{\partial \delta_1} & \frac{\partial C_X(x, \delta)}{\partial \delta_2} & \dots & \frac{\partial C_X(x, \delta)}{\partial \delta_n} \\ \frac{\partial C_Y(x, \delta)}{\partial \delta_1} & \frac{\partial C_Y(x, \delta)}{\partial \delta_2} & \dots & \frac{\partial C_Y(x, \delta)}{\partial \delta_n} \\ \vdots & \vdots & \ddots & \vdots \\ \frac{\partial C_n(x, \delta)}{\partial \delta_1} & \frac{\partial C_n(x, \delta)}{\partial \delta_2} & \dots & \frac{\partial C_n(x, \delta)}{\partial \delta_n} \end{bmatrix} \quad (3.23)$$

In upset conditions nonlinear effects may cause the aircraft to be less effective to control commands. In order to get out of this upset condition as quickly as possible, optimal control theory is recommended. Optimal control theory is finding a control law for a given system and condition such that the commanded control is accomplished. Solving this problem for nonlinear dynamic systems is computationally expensive in real-time and therefore optimal control is beyond possibilities for the upset recovery controller. In order to approach this optimal control theory anyway, there will be aimed for maximum control effectiveness in any given flight condition.

3.4.1. Control Effectiveness Optimization

Aiming for maximum control effectiveness must ensure that commanded states are achieved in the most effective way. In order to obtain this, every control effector must be used as efficient as possible. The optimality

criterion in the case of controlling the angular rates of an aircraft is to achieve the highest possible (maximum) control effectiveness. Achieving maximum control effectiveness to generate a maximum moment is a multi-dimensional optimization problem that can be tackled in different ways. There are two ways of determining maximum control effectiveness.

- Determine the maximum possible moment that could be generated based on current flight conditions and effector deflection settings. This moment does not necessarily have to be the maximum moment that can be generated by the aircraft, but can be seen as a local maximum.
- Determine the maximum moment that could be generated regardless of current flight conditions and effector deflection settings. This is the maximum moment that can be achieved by the aircraft and can therefore be seen as a global maximum.

It can be said that the second way of determining the maximum control effectiveness does not apply in the case of upset conditions. This is in the first place because it may not be the same condition as specified in the upset recovery strategy from section 2.5. The first way is limited to optimizing the maximum control effectiveness in local search space which is defined in 3.2.

Optimization is an important tool for making decisions and analysis of physical systems like aircraft. The objective of this optimization in regarding to aircraft upset recovery will be maximum control effectiveness selection. This objective depends on certain characteristics of the aircraft, called aircraft states and control effector deflections. The goal of this section is to find an appropriate method to find the values of the variables that optimize the before mentioned objective. Often variables are restricted or constrained due to physical limits, these restrictions are described in section 3.2.

Once the optimization problem is formulated, an optimization algorithm should be used to find its solution. Unfortunately there is no universal optimization method that is able to solve each and every problem. There is a collection of optimization methods, each of which is tailored for particular use. The choice in optimization method determined whether or not the solution whether the solution will be found and if it is solved rapidly or slowly. Mathematical expressions known as optimality conditions are recommended for checking if the current set of variables is indeed the solution of the problem. If this optimality condition is not met, a new iteration of the optimization method is required. To improve the optimization, sensitivity analysis could be used that reveals the sensitivity to changes in data.

Optimization algorithms use the iterative process with a first guess of the vector of variables x and start improving these estimates what is called iterating. This process is repeated until the solution criteria are met. Based on information from the current value of the objective function, the predetermined constraints, and possible first and second derivatives a direction is determined for the next iteration. In any case, a good algorithm must meet the following properties:

- **Accuracy:** The algorithm must be able to approach the solution with a certain degree of precision without being sensitive to data fluctuations and errors.
- **Efficiency:** The algorithm must be efficient with the available computational power and storage delivered with the problem. The extent to which the selected number of variables needs the required computational resources must be limited.
- **Robustness:** The algorithm should perform outstanding for a wide variety of reasonable initial points. In the sense that the algorithm shows the same performance each time.

In mathematical terms, optimization is the minimization or the maximization of a function that is subjected to constraints on its variables. In general the following notation in Eq. (3.24) is used to describe an optimization problem.

$$\min_{x \in \mathbb{R}^n} F(x) = [f_1(x), f_2(x), \dots, f_k(x)] \quad \text{subject to} \quad \begin{cases} h_i(x) = 0 & i \in \varepsilon \\ g_j(x) \geq 0 & j \in \vartheta \end{cases} \quad (3.24)$$

Where x is the vector of variables, $F(x)$ is the objective function, and $h_i(x)$ and $g_j(x)$ are the function equality and inequality constraints respectively which are functions of x that define certain equations the vector x

should satisfy. Here ε and ϑ are sets of indices for equality and inequality constraints respectively. The available space of feasible solutions also called the feasible set is a set of all points that satisfy the constraints $h_i(x)$ and $g_j(x)$.

$$\Omega = \{y \in \mathbb{R}^n : h_i(y) = 0, i = 1, \dots, m_{eq} \text{ and } g_j(y) \geq 0, j = 1, \dots, m_{ineq}\} \quad (3.25)$$

Which results into the following equation that shows the range of the feasible set for the objective function $F(x)$.

$$\mathbb{A} = \{F(x) : x \in \Omega\} \quad (3.26)$$

3.4.2. Gradient Information Algorithm

The first algorithms for optimization that will be discussed are the gradient methods. By using the gradient of an objective function, the direction of the function can be determined. On the basis of the direction of the function, a next step can then be taken to where the optimum is expected. In order to find the solution vector x^* , the following general form for obtaining a guaranteed local optimum may be used. Where d_k is

Algorithm 1: General iterative descent algorithm

Data: Objective function $F(x)$, initial point x_0
while $\Delta F(x) \approx 0$ **do**
 Determine a descent direction d_k ;
 Determine a step length d_{step} ;
 Update variables $x_{k+1} = x_k + d_{step} \cdot d_k$;
end
Result: Minimum of objective function $F(x)$

the selected descent direction and d_{step} the step size. This is a mathematical way of optimizing problems. Based on your current solution choose a better candidate solution and repeat until the optimality conditions are satisfied.

3.4.3. Stochastic Search Algorithms

There are ways to do numerical optimization for functions that are not continuous or differentiable, for these methods there are approaches for calculating future iteration points that rely on non-deterministic algorithmic steps. These methods guess what could be the best search direction for the next iteration.

The simplest form of this type of algorithm is the random search method. Random search algorithms compare solutions between iterations, the current iteration is updates if there are better solutions available in neighbor points. Next possible iteration points are determined by two components: the search direction d_k and step size d_{step} .

Algorithm 2: Random search algorithm

Data: Objective function $F(x)$, initial point x_0 , number of iterations i_{max}
while Iterations $\in i_{max}$ **do**
 Select candidate variable x_k ;
 if $F(x_k) < F(x_{optimal})$ **then**
 | $x_{optimal} = x_k$
 end
end
Result: Minimum of objective function $F(x)$

4

Innovative Control Effectors Aircraft

The ICE program was introduced in 1993 in order to investigate innovative methods for aircraft control and stabilization of high performance, low signature fighters. This ICE program was sponsored by both Wright Laboratory and the Naval Air Warfare Center. Low signature technologies have led to limitations in the design of a high performance fighter. These low signature related discussion together with a higher requirement for maneuverability are a guideline for devising new concepts for innovative control for fighter aircraft. To lower the radar cross section (RCS) adjustments in the design in the form of external shaping, removing the vertical control surfaces, and the placement of control surfaces have lead to a reduced detection signature and increased survivability for current fighters. These adjustments forced fighter aircraft in the direction of tailless designs who lack vertical control surfaces, which raises issues for directional stability. This implies that low RCS designs require new innovative control concepts that fulfill the requested maneuverability requirements.

Two different fighter concepts were introduced. The first one is a land based fighter aircraft developed for the US Air Force which is 65 degrees sweep angle delta wing shown in Fig. 4.1. The second fighter was designed as a carrier based fighter aircraft which has a 42 degrees leading edge sweep canard-delta wing shown in Fig. 4.2 especially designed for navy purposes. Both fighter aircraft are equipped with a single engine with internal weapons-carriage measures for reduced RCS.

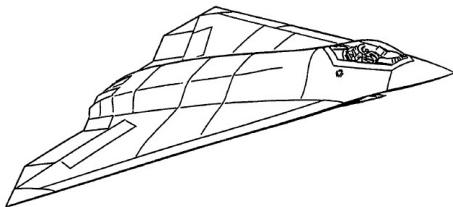


Figure 4.1: Land based baseline configuration [12]

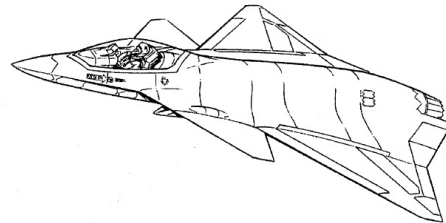


Figure 4.2: Carrier based baseline configuration [12]

The objective of the ICE program was to evaluate the impact of innovative aerodynamic control surfaces on tailless fighters and to quantify the high angle of attack α flying qualities potentials. The ICE program is divided into two phases. Phase one includes the selection of the baseline vehicle and the selection of innovative control concepts, performance investigation of each control effector, and the evaluation of the impact of integrating the control effectors. Furthermore impact of high angle of attack α on control effectors has been studied. In phase two of the program the best combinations of innovative control effectors were tested in more detail.

Five innovative control concepts were investigated for their ability to produce lateral control for a highly maneuverable tailless fighter. Control concepts evaluated were the all moving wing tip (AMT), spoiler slot deflector (SSD), differential leading edge flap (DLEF), deployable rudder (DRUD), and the lower surface spoiler (LSP). Only the first three control concepts have been selected for further research. This research consisted of testing low speed, high speed and high angle of attack α flying qualities performance, signature performance, structural weight impacts, and transonic acceleration impacts. After evaluation the AMT was concluded to

be the best all-round control effector followed by the SSD and DLEF respectively. Performance of RCS has been evaluated using computational analysis tools where different deflection angles were analyzed. For the remainder of this thesis there will be focused on the land based fighter aircraft (Fig. 4.1). Section 4.1 gives an introduction to the innovative control effectors and their use. In section 4.2 the aerodynamic model of the ICE aircraft is presented. Finally section 4.3 explains the shortcomings of the ICE aircraft with respect to upset recovery.

4.1. Innovative Control Effectors

The land based 65 degree sweep flying wing is used as baseline for analysis of the newly introduced innovative control effectors and can be seen in Fig. 4.3. The goals for these innovative control effectors is improved low signature characteristics compared to conventional controls, improved control effectiveness at high angles of attack α , applicable to tailless fighters, weight and drag reduction compared to conventional controls, and reduced hinge moment and reduced sensitivity to aeroelastic effects [12]. Control effectors installed on the ICE aircraft configuration are described below.

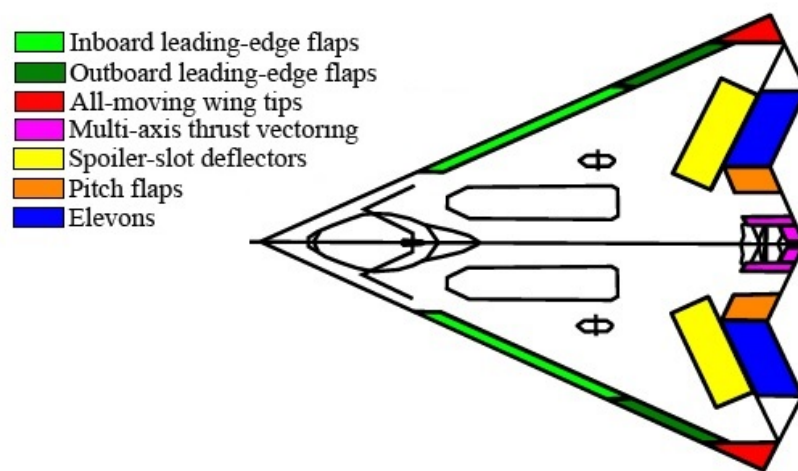


Figure 4.3: Innovative control effectors [28]

- **All Moving Tips (AMT) [12]:** AMT provides yaw control up to very high angles of attack α . Trailing edge down deflections increases profile and induced drag that will create a yaw motion. At large deflections of the AMT yaw control magnitude can be compared to T-tail fighters. Compared to more conventional control concepts, AMT shows less sideslip angle β impact. Besides yaw control, AMT trailing edge up deflections provide good roll effectiveness up to high angles of attack α .
- **Differential Leading Edge Flaps (DLEF) [12]:** DLEF provides lateral control at moderate to high angle of attack α . In regions where conventional yaw control lose effectiveness, DLEF shows tendencies in lateral directional stability. Control effectiveness at high Mach numbers can be maintained, although the effectiveness at high angles of attack α decreases above Mach 0.6. Furthermore the aerodynamic interaction of other DLEF (inboard versus outboard) is significant. DLEF control is most useful for stability augmentation and roll coordination at low speed flight.
- **Elevons: [12]** Elevons are more conventional control effectors that combines the function of both elevator and aileron in one control surface. Usually there is an elevon pair installed that makes symmetrical use result in pitch moments, and asymmetrical use result in roll moments. For ICE aircraft the nose down pitch loses effectiveness at angle of attack α larger than 45 degrees.
- **Multi-axis Thrust Vectoring (MTV) [12]:** The ICE aircraft is equipped with MTV at the center of the trailing edge that provides thrust in both pitch and yaw direction. Yaw thrust vectoring is very powerful at low speeds, however at moderate to high speeds load limitations on the engine and structure

limits its usefulness. The major advantage of using MTV over the conventional rudder is the ability to provide large control moments throughout the entire angle of attack α range whereas the rudder loses effectiveness at high angle of attack α . This is due to the fact that thrust is generally function of Mach, altitude, and power setting.

- **Pitch Flaps (PF):** [12] Pitch flaps provide pitch control throughout the entire range of angle of attack α . Pitch flaps are located inboard of the elevon position. Pitch flaps deflect simultaneously in the same direction such that it only provides pitch control, therefore these pitch flaps can be seen as one control effector. The interaction with the SSD is assumed to be much less severe compared to the elevon.
- **Spoiler Slot Deflectors (SSD)** [12]: SSD provide improved high angle of attack α and transonic flight characteristics for lateral control effectors which can result in lower actuator requirements. A properly designed SSD provides better lateral control effectiveness over a conventional spoiler. Furthermore the SSD is less affected by high speed flexibility effects compared to a conventional aileron. The drawback of SSD is decreased trailing edge control surface effectiveness when SSD is deflected.

In Table 4.1 the different control effectors are listed. The total number of control effectors installed is 13 and therefore the ICE aircraft is highly redundant. The table also provides position and rate limits that apply to the ICE aircraft. Furthermore sign convention is presented for what is considered to be a positive deflection. There are three different conventions: Trailing edge up (TEU), trailing edge down (TED), or leading edge down (LED). When the project was initialized back in the mid 1990s, the main part of the research was focused on the aerodynamics of the various control effectors and therefore no actuator dynamics are taken into account [29]. Dynamics of the control effectors are modeled as second-order transfer functions for low and high-bandwidth in Eq. (4.1) and Eq. (4.2) respectively. The last column in Table 4.1 shows the second order dynamics of each control effector indicated with H_l and H_h .

$$H_l = \frac{1800}{s^2 + 118s + 1800} \quad (4.1)$$

$$H_h = \frac{4000}{s^2 + 140s + 4000} \quad (4.2)$$

Table 4.1: Control effectors overview of the ICE aircraft, sign convention, position and rate limits, abbreviations, and effector dynamics [12, 29].

Control effector	Positive deflection	Position limits [deg]	Rate limits [deg/s]	Abbreviation	Effector dynamics
All moving tips	TED	[0, 60]	150	LAMT, RAMT	H_h
Inboard leading edge flaps	LED	[0, 40]	40	LIBLEF, RIBLEF	H_l
Outboard leading edge flaps	LED	[-40, 40]	40	LOBLEF, ROBLEF	H_l
Elevons	TED	[-30, 30]	150	LEL, REL	H_h
Pitch thrust vectoring	$\dot{q} > 0$	[-15, 15]	150	TVP	H_h
Yaw thrust vectoring	$\dot{p} > 0$	[-15, 15]	150	TVY	H_h
Pitch flaps	TED	[-30, 30]	150	PF	H_h
Spoiler slot deflectors	TEU	[0, 60]	150	LSSD, RSSD	H_h

4.2. Aerodynamic Model of Innovative Control Effector Aircraft

During phase 1 and phase 2 of the ICE program wind tunnel test data that has been generated which is collected in a high-fidelity aerodynamic database. From this aerodynamic database a model is created in Matlab Simulink as a lookup table which has been released by Lockheed Martin for academic purposes presented in [29].

This model contains of six different parts that represent the aerodynamic force and moment coefficients. There are three main force coefficients defined where the axial component is indicated by C_X , the side component by C_Y , and the normal component by C_Z . The same is done for the moment coefficients where the roll component is indicated by C_l , the pitch component by C_m , and finally the yaw component by C_n . These six main aerodynamic coefficients are further subdivided into sixteen to eighteen sub coefficients. All these

aerodynamic sub coefficient represent a state or control effector of the aircraft and are function of aircraft states at the current flight condition. Aerodynamic flexibility factors included in the model will be neglected and are not part of the simulation model. Equation (4.3) to Eq. (4.5) show the formulation of aerodynamic force coefficients.

$$\begin{aligned}
C_X = & C_{X_1}(\alpha, M) + C_{X_2}(\alpha, \beta, M) + C_{X_3}(\alpha, \beta, \delta_{LIBLEF}) + C_{X_4}(\alpha, \beta, \delta_{LIBLEF}, \delta_{OBLEF}, M) \\
& + C_{X_5}(\alpha, \delta_{LSSD}, \delta_{LEL}, M) + C_{X_6}(\alpha, \delta_{LSSD}, \delta_{RSSD}, \delta_{PF}, M) + C_{X_7}(\alpha, \beta, \delta_{LAMT}) \\
& + C_{X_8}(\alpha, \delta_{LEL}, \delta_{LAMT}) + C_{X_9}(\alpha, \delta_{LOBLEF}, \delta_{LAMT}) + C_{X_{10}}(\alpha, \delta_{REL}, \delta_{RAMT}) \\
& + C_{X_{11}}(\alpha, \delta_{ROBLEF}, \delta_{RAMT}) + C_{X_{12}}(\alpha, \beta, \delta_{LSSD}) + C_{X_{13}}(\alpha, \beta, \delta_{RIBLEF}) \\
& + C_{X_{14}}(\alpha, \beta, \delta_{RIBLEF}, \delta_{ROBLEF}, M) + C_{X_{15}}(\alpha, \delta_{RSSD}, \delta_{REL}, M) + C_{X_{16}}(\alpha, \beta, \delta_{RAMT}) \\
& + C_{X_{17}}(\alpha, \beta, \delta_{RSSD})
\end{aligned} \tag{4.3}$$

$$\begin{aligned}
C_Y = & C_{Y_1}(\alpha, M) + C_{Y_2}(\alpha, \beta, M) + C_{Y_3}(\alpha, \beta, \delta_{LIBLEF}) - C_{Y_4}(\alpha, \beta, \delta_{LIBLEF}, \delta_{OBLEF}, M) \\
& + C_{Y_5}(\alpha, \delta_{LSSD}, \delta_{LEL}, M) + C_{Y_6}(\alpha, \delta_{LSSD}, \delta_{RSSD}, \delta_{PF}, M) + C_{Y_7}(\alpha, \beta, \delta_{LAMT}) \\
& + C_{Y_8}(\alpha, \delta_{LEL}, \delta_{LAMT}) + C_{Y_9}(\alpha, \delta_{LOBLEF}, \delta_{LAMT}) - C_{Y_{10}}(\alpha, \delta_{REL}, \delta_{RAMT}) \\
& - C_{Y_{11}}(\alpha, \delta_{ROBLEF}, \delta_{RAMT}) + C_{Y_{12}}(\alpha, \beta, \delta_{LSSD}) + C_{Y_{13}}(\alpha, \beta, \delta_{RIBLEF}) \\
& + C_{Y_{14}}(\alpha, \beta, \delta_{RIBLEF}, \delta_{ROBLEF}, M) - C_{Y_{15}}(\alpha, \delta_{RSSD}, \delta_{REL}, M) + C_{Y_{16}}(\alpha, \beta, \delta_{RAMT}) \\
& - C_{Y_{17}}(\alpha, \beta, \delta_{RSSD})
\end{aligned} \tag{4.4}$$

$$\begin{aligned}
C_Z = & C_{Z_1}(\alpha, M) + C_{Z_2}(\alpha, \beta, M) + C_{Z_3}(\alpha, \beta, \delta_{LIBLEF}) + C_{Z_4}(\alpha, \beta, \delta_{LIBLEF}, \delta_{OBLEF}, M) \\
& + C_{Z_5}(\alpha, \delta_{LSSD}, \delta_{LEL}, M) + C_{Z_6}(\alpha, \delta_{LSSD}, \delta_{RSSD}, \delta_{PF}, M) + C_{Z_7}(\alpha, \beta, \delta_{LAMT}) \\
& + C_{Z_8}(\alpha, \delta_{LEL}, \delta_{LAMT}) + C_{Z_9}(\alpha, \delta_{LOBLEF}, \delta_{LAMT}) + C_{Z_{10}}(\alpha, \delta_{REL}, \delta_{RAMT}) \\
& + C_{Z_{11}}(\alpha, \delta_{ROBLEF}, \delta_{RAMT}) + C_{Z_{12}}(\alpha, \beta, \delta_{LSSD}) + C_{Z_{13}}(\alpha, \beta, \delta_{RIBLEF}) \\
& + C_{Z_{14}}(\alpha, \beta, \delta_{RIBLEF}, \delta_{ROBLEF}, M) + C_{Z_{15}}(\alpha, \delta_{RSSD}, \delta_{REL}, M) + C_{Z_{16}}(\alpha, \beta, \delta_{RAMT}) \\
& + C_{Z_{17}}(\alpha, \beta, \delta_{RSSD}) + \frac{cq}{2V} C_{Z_{18}}(\alpha, M)
\end{aligned} \tag{4.5}$$

From Eq. (4.3) to Eq. (4.5) it can be seen where aerodynamic sub coefficients depend on. All coefficients are significantly dependent on angle of attack α , followed by a variation of control surfaces and other airflow characteristics. In the normal force coefficient, there is an extra term in the formulation. This term comes from a component of pitch rate q , this aerodynamic sub coefficient is therefore multiplied by the normalized factor by $\frac{cq}{2V}$.

Next the moment coefficients are approximated by the following formulation as can be seen in Eq. (4.6) to Eq. (4.8). These aerodynamic coefficients show an equal formulation as the force coefficients.

$$\begin{aligned}
C_L = & C_{L_1}(\alpha, M) + C_{L_2}(\alpha, \beta, M) - C_{L_3}(\alpha, \beta, \delta_{LIBLEF}) - C_{L_4}(\alpha, \beta, \delta_{LIBLEF}, \delta_{OBLEF}, M) \\
& + C_{L_5}(\alpha, \delta_{LSSD}, \delta_{LEL}, M) + C_{L_7}(\alpha, \beta, \delta_{LAMT}) + C_{L_8}(\alpha, \delta_{LEL}, \delta_{LAMT}) \\
& + C_{L_9}(\alpha, \delta_{LOBLEF}, \delta_{LAMT}) - C_{L_{10}}(\alpha, \delta_{REL}, \delta_{RAMT}) - C_{L_{11}}(\alpha, \delta_{ROBLEF}, \delta_{RAMT}) \\
& + C_{L_{12}}(\alpha, \beta, \delta_{LSSD}) + C_{L_{13}}(\alpha, \beta, \delta_{RIBLEF}) + C_{L_{14}}(\alpha, \beta, \delta_{RIBLEF}, \delta_{ROBLEF}, M) \\
& - C_{L_{15}}(\alpha, \delta_{RSSD}, \delta_{REL}, M) - C_{L_{16}}(\alpha, \beta, \delta_{RAMT}) - C_{L_{17}}(\alpha, \beta, \delta_{RSSD}) \\
& + \frac{bp}{2V} C_{L_{18}}(\alpha, M) + \frac{br}{2V} C_{L_{19}}(\alpha, M)
\end{aligned} \tag{4.6}$$

$$\begin{aligned}
C_M = & C_{M_1}(\alpha, M) + C_{M_2}(\alpha, \beta, M) + C_{M_3}(\alpha, \beta, \delta_{LIBLEF}) + C_{M_4}(\alpha, \beta, \delta_{LIBLEF}, \delta_{OBLEF}, M) \\
& + C_{M_5}(\alpha, \delta_{LSSD}, \delta_{LEL}, M) + C_{M_6}(\alpha, \delta_{LSSD}, \delta_{RSSD}, \delta_{PF}, M) + C_{M_7}(\alpha, \beta, \delta_{LAMT}) \\
& + C_{M_8}(\alpha, \delta_{LEL}, \delta_{LAMT}) + C_{M_9}(\alpha, \delta_{LOBLEF}, \delta_{LAMT}) + C_{M_{10}}(\alpha, \delta_{REL}, \delta_{RAMT}) \\
& + C_{M_{11}}(\alpha, \delta_{ROBLEF}, \delta_{RAMT}) + C_{M_{12}}(\alpha, \beta, \delta_{LSSD}) + C_{M_{13}}(\alpha, \beta, \delta_{RIBLEF}) \\
& + C_{M_{14}}(\alpha, \beta, \delta_{RIBLEF}, \delta_{ROBLEF}, M) + C_{M_{15}}(\alpha, \delta_{RSSD}, \delta_{REL}, M) + C_{M_{16}}(\alpha, \beta, \delta_{RAMT}) \\
& + C_{M_{17}}(\alpha, \beta, \delta_{RSSD}) + \frac{cq}{2V} C_{M_{18}}(\alpha, M)
\end{aligned} \tag{4.7}$$

$$\begin{aligned}
C_N = & C_{N_1}(\alpha, M) + C_{N_2}(\alpha, \beta, M) - C_{N_3}(\alpha, \beta, \delta_{LIBLEF}) - C_{N_4}(\alpha, \beta, \delta_{LIBLEF}, \delta_{OBLEF}, M) \\
& + C_{N_5}(\alpha, \delta_{LSSD}, \delta_{LEL}, M) + C_{N_7}(\alpha, \beta, \delta_{LAMT}) + C_{N_8}(\alpha, \delta_{LEL}, \delta_{LAMT}) \\
& + C_{N_9}(\alpha, \delta_{LOBLEF}, \delta_{LAMT}) - C_{N_{10}}(\alpha, \delta_{REL}, \delta_{RAMT}) - C_{N_{11}}(\alpha, \delta_{ROBLEF}, \delta_{RAMT}) \\
& + C_{N_{12}}(\alpha, \beta, \delta_{LSSD}) + C_{N_{13}}(\alpha, \beta, \delta_{RIBLEF}) + C_{N_{14}}(\alpha, \beta, \delta_{RIBLEF}, \delta_{ROBLEF}, M) \\
& - C_{N_{15}}(\alpha, \delta_{RSSD}, \delta_{REL}, M) - C_{N_{16}}(\alpha, \beta, \delta_{RAMT}) - C_{N_{17}}(\alpha, \beta, \delta_{RSSD}) \\
& + \frac{bp}{2V} C_{N_{18}}(\alpha, M) + \frac{br}{2V} C_{N_{19}}(\alpha, M)
\end{aligned} \tag{4.8}$$

As can be seen for the aerodynamic moment coefficients (Eq. (4.6) to Eq. (4.8)), it shows a similar structure as the aerodynamic force coefficients with the only difference that non-symmetric moment coefficients C_l and n have an additional term for roll and yaw rate while symmetric moment coefficient C_m has a pitch rate term included.

4.3. Upset Recovery for Innovative Control Effector Aircraft

As just discussed in section 4.2, the aerodynamic model depends on many dimensions. The wind tunnel data of which the model is generated is determined on a predefined grid. Furthermore, the grid size that depends on the measuring frequency and is limited to certain maximum values. Table 4.2 shows for each sub coefficients of the ICE aircraft their corresponding parameters, data range, and number of datapoints.

What can be seen from Table 4.2 is that the number of datapoints is limited. Between wind tunnel datapoints no value has been determined for the coefficients. Because some coefficients are highly nonlinear, local variations in value can not be observed. For now the unknown data between datapoints has been approached by interpolation. In the constructed Matlab Simulink model of the ICE aircraft, these sub coefficients are estimated by linear interpolation or cubic spline [29]. What is more striking is the fact that for the airflow characteristics the data range is limited to a certain value. For angle of attack α , sideslip angle β , and Mach M the limits are [-5, 90], [-30, 30], and [0.3, 2.16] respectively. For certain upset conditions these values can be exceeded. In the event that the datapoints are exceeded, while flying outside the data tables, datapoints are extrapolated or clipped at the border value of the model. The danger of using this data is that nonlinear behavior of the aircraft may not be observed.

Table 4.2: Sub coefficients of the ICE aircraft and corresponding parameters, data range, and number of datapoints

Coefficient	Parameter	Data range	Datapoints
C_1	α	[-5, 90]	48
	M	[0.3, 2.16]	10
C_2	α	[-5, 90]	30
	β	[-30, 30]	15
	M	[0.3, 2.16]	8
C_3	α	[-2.5, 45]	20
	β	[-10, 10]	3
	δ_{LIBLEF}	[0, 40]	2
C_4	α	[-2.5, 45]	20
	β	[-10, 10]	3
	δ_{LIBLEF}	[0, 40]	2
	δ_{LOBLEF}	[-40, 40]	5
	M	[0.3, 1.2]	4
C_5	α	[-2.5, 90]	28
	δ_{LSSD}	[0, 60]	4
	δ_{LEL}	[-30, 30]	5
	M	[0.3, 2.16]	7
C_6	α	[-2.5, 90]	29
	δ_{LSSD}	[0, 60]	2
	δ_{RSSD}	[0, 60]	2
	δ_{PF}	[-30, 30]	5
	M	[0.3, 2.16]	7
C_7	α	[-2.5, 90]	29
	β	[-30, 30]	7
	δ_{LAMT}	[0, 60]	5
C_8	α	[-2.5, 42.5]	19
	δ_{LEL}	[-30, 30]	3
	δ_{LAMT}	[0, 60]	3
C_9	α	[-2.5, 42.5]	19
	δ_{LOBLEF}	[0, 40]	3
	δ_{LAMT}	[0, 60]	3
C_{10}	α	[-2.5, 42.5]	19
	δ_{REL}	[-30, 30]	3
	δ_{RAMT}	[0, 60]	3
C_{11}	α	[-2.5, 42.5]	19
	δ_{ROBLEF}	[0, 40]	3
	δ_{RAMT}	[0, 60]	3
C_{12}	α	[-2.5, 90]	29
	β	[-30, 30]	7
	δ_{LSSD}	[0, 60]	4
C_{13}	α	[-2.5, 45]	20
	β	[-10, 10]	3
	δ_{RIBLEF}	[0, 40]	2
C_{14}	α	[-2.5, 45]	20
	β	[-10, 10]	3
	δ_{RIBLEF}	[0, 40]	2
	δ_{ROBLEF}	[-40, 40]	5
	M	[0.3, 1.2]	4
C_{15}	α	[-2.5, 90]	28
	δ_{RSSD}	[0, 60]	4
	δ_{REL}	[-30, 30]	5
	M	[0.3, 2.16]	7
C_{16}	α	[-2.5, 90]	29
	β	[-30, 30]	7
	δ_{RAMT}	[0, 60]	5
C_{17}	α	[-2.5, 90]	29
	β	[-30, 30]	7
	δ_{RSSD}	[0, 60]	4
C_{18}	α	[0, 30]	13
C_{19}	M	[0.6, 2.2]	6

5

Project Definition

This chapter describes the definition of this research project. A clear definition of the project is given in section 5.1 where the research objective but also the research questions are presented. Followed by the chosen approach to design the upset recovery controller presented in section 5.2. In chapter 5.3 the experimental setup and expected results are described. Finally chapter 5.4 shows the design of the proof of concept and a spin demonstration flight.

5.1. Research Objective and Questions

This project investigates an innovative method that makes recovery of an aircraft possible from critical/upset condition in order to reduce the number of LOC accidents. Flight control systems require a more advanced upset recovery method which is able to recover from extremely high angles of attack far away from the boundary of the safe flight envelope. A method consisting of maximum aircraft control effectiveness is focusing instead of only aircraft states also on the maximum control authority of an aircraft in critical/upset flight conditions.

Therefore, the objective of the research project is to contribute to the development of an upset recovery controller for a highly maneuverable over-actuated fighter aircraft which is capable of recovering from any loss of control situation, by designing an advanced recovery flight control system which uses maximum control effectiveness for recovering the ICE aircraft.

This main objective of the research project can be divided into sub-objectives:

1. To design a proof of concept which uses maximum control effectiveness to reduce p, q, r for an aircraft in spin condition.
2. To develop a controller which is able to aim for maximum control effectiveness at every flight condition.
3. To establish a recovery strategy which shows highest recovery performance.
4. To develop a post-stall controller which is able to recover flight attitudes, velocity, and altitude.

With the above mentioned main project objective and corresponding sub-objectives, together with a comprehensive literature review into aircraft upset and recovery, nonlinear aircraft dynamics, and maximum control effectiveness the following research questions are formulated:

1. How to design an upset recovery method based on maximum control effectiveness for a high-performance over-actuated aircraft which is capable of recovering from any loss of control situation?
 - (a) Can the method be constructed for any aircraft upset condition?
 - (b) Which aircraft states and inputs determine the performance of upset recovery?
 - (c) Which upset recovery strategy is applicable in every upset condition?
2. How to determine the maximum control effectiveness of an aircraft?

- (a) Which aircraft states and inputs have influence on the control effectiveness?
- (b) Which multidimensional optimization method is able obtain optimal control authority?

A method based on maximum control effectiveness is new in the field of upset recovery for aviation. No previous upset recovery investigation was focusing on aerodynamic capabilities of an aircraft.

5.2. Upset Recovery Using Maximum Control Effectiveness and Incremental Control Design

Based on the literature review in chapters 2 and 3 and the research objective defined in section 5.1, an approach to use an incremental upset recovery controller which approximates the maximum control effectiveness at each condition to return the aircraft to the safe flight envelope has been chosen.

As can be read in chapter 2, existing upset recovery techniques fail to have a solution for the complete spectrum of upset conditions. Furthermore, it can be said that existing techniques are true in the fundamental basis but little effort has been made to understand possible non-linear effects that may occur during upset. Only the conditions in which reduction of the aerodynamic angles is described assuming that the aircraft is not in stall conditions. By using the existing techniques, a new strategy has been developed that is complete and comprehensive. This strategy is considered to be complete and can be used in aviation in general. This strategy will describe a step-by-step plan what the commanded states of the aircraft should be to return from an upset to the safe flight envelope.

To ensure a good performance of the upset recovery controller, the recovery strategy used to return the aircraft back to the safe flight envelope as soon as possible in addition to the requirement of the right sequence of steps to recover, will be providing good control inputs to the aircraft. This step consists of translating the error in the state to the required (direction of the) moment to correct the state of the aircraft. Traditional methods fail to make for every state a good translation of the error between the required state x_c and the current state x_0 , to the required inputs to minimize this error. That is because these methods often rely on gain scheduling, for determining the correct gains are often no guidelines.

The INDI principle does only require little gain scheduling to properly translate the error [38]. INDI uses the properties of the system together with nonlinear dynamic inversion by using body angular accelerations [38]. This body angular acceleration feedback eliminates sensitive to model mismatch, that certainly occurs close to or in upset conditions. The principle of elimination of model mismatch increases robustness compared with conventional nonlinear dynamic inversion. As a result, there was decided to translate the error determined by the upset recovery strategy with fundamental basis of the idea behind INDI to guarantee robust control inputs. Flight controllers based on INDI have proven to work well in nonlinear flight control [38–40].

At the moment the current flight condition of the aircraft is recognized and the approach to the problem is determined by the recovery strategy, the recognition of the situation must be translated into corresponding control efforts. These efforts consist of choosing the right deflections for the control effectors. The goal will always be to achieve maximum control effectiveness. There are different methods to derive an optimal solution. In section 3.4 two categories of optimization algorithms are described in basic form, these are the gradient search algorithm and stochastic search algorithm. The gradient search algorithm was chosen because of the higher computational efficiency. If the number of control effectors that need to be optimized increases, the algorithm can be reduced to only one iteration per time step. This is different for the random search method, with this method a high performance and at the same time achieving a minimum number of iterations is difficult.

The subsystems introduced above make the upset recovery controller a complete system. All these different steps must be carried out in order to reach a decision for the control effector deflections. These steps have to be carried out for each individual time step, and thus will be repeated multiple times. The general control flow is depicted in Fig. 5.1. The three different parts discussed in this section can be seen in the figure, these are represented as a block. These blocks contain functions that are calculated by means of the current state of the aircraft and control effector deflections.

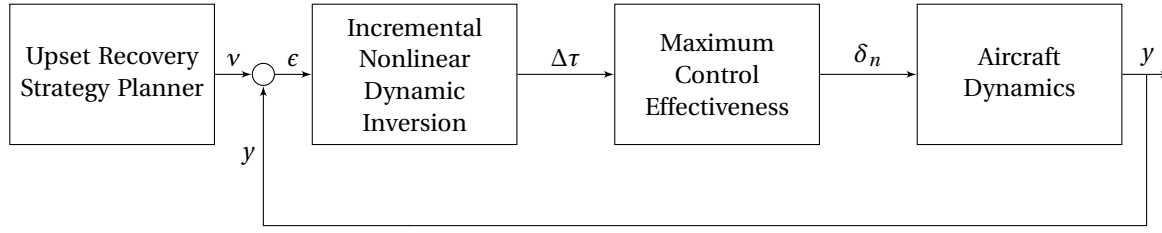


Figure 5.1: Control flow diagram for the upset recovery controller

5.3. Experimental Setup and Analysis of Results

On the basis of an experimental setup, the proposed upset recovery controller will be tested and validated in order to be able to give an answer to the research questions. The experimental setup will be based on simulations, these simulations will be carried out in a Matlab/Simulink simulation framework by using the high-fidelity aerodynamic model of the ICE aircraft that is provided by Lockheed Martin [29]. This wind tunnel tested aerodynamic database consist of 108 submodels that together construct the six main aerodynamic force and moment coefficients.

In Matlab Simulink, the proposed controller will be developed using Simulink blocks and Matlab functions. Within Matlab Simulink, Matlab function blocks make it possible to use Matlab programming language instead of predefined Simulink blocks which makes the Simulink model in the end clear and solid. The theory that has been decided on in section 5.2 will be implemented in order to construct a new methodology for upset recovery. For the upset recovery controller, direct control commands are given for each individual control effector on the aircraft model. For flying into an upset condition in order to test the upset recovery controller, incremental nonlinear control allocation (INCA) will be used. This will be tested in predefined (upset) flight conditions to compare performance for different upset maneuvers.

These tests for different flight conditions will yield results that are required to validate the controller on validity. During testing and validation, the following variables will be considered:

- Time histories of all aircraft states.
- Time histories of control effector deflections δ_n and incremental control deflections $\Delta\delta_n$.
- Time histories of commanded states from upset recovery strategy.
- Time histories of the commanded pseudo-control input τ_c .
- Time histories of active/inactive selected control effectors.

5.4. Proof of Concept

In this section a proof of concept will be described and corresponding results will be shown. Because the combination of an upset recovery strategy and maximum control effectiveness of a given aircraft is new in the field of upset recovery in aviation, first it will be shown using a simplified concept that this combination gives sufficient reason for further research. The proof of concept is constructed on the same fundamental idea as described in section 5.2 and the accompanying supporting theory. Nevertheless, the concept is significantly different to the proposed design. This section shows how the concept is structured and what the working principle is.

5.4.1. Proof of Concept Design

The proof of concept is purely based on reducing body angular rates, a compact selection of control effectors, and iterating for maximum control effectiveness in local incremental control deflection range. First there will be checked what the current flight conditions are of the aircraft. Then the condition is selected in which the aircraft is located. This condition is needed to determine what the maximum control effectiveness will be. Active control effectors are chosen in advance that are used to execute the recovery strategy. By using random search, two possible control effector deflections will be chosen based on the maximum increment in each time step. All these possibilities are collected in a matrix. This matrix contains all possible iterations for

which the control effectiveness will be calculated, this matrix scales with factor 2^n . The maximum calculated control effectiveness from all possible iterations has been selected as control input for the control effectors. The global overview of control flows for the proof of concept is shown in Fig. 5.2.

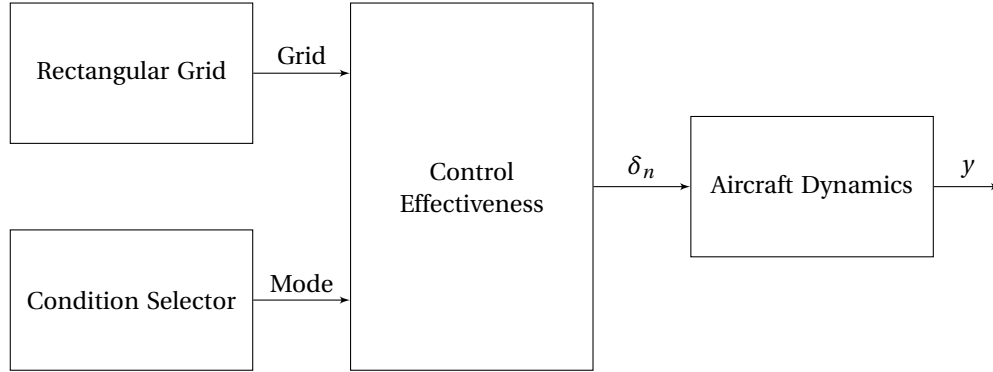


Figure 5.2: Control flow diagram for the proof of concept upset recovery controller

The exact content of these blocks is explained below and examples are given where necessary.

- **Rectangular Grid:** In this component potential control effector deflections are selected for the next time step. For the proof of concept the simple form of random search algorithm is applied. This random search algorithm selects two possible maximum incremental control deflection for each active control effector based on current control effector deflections, this algorithm scales with 2^n . The output is defined as a rectangular grid containing all possible control effector settings for the current time step. For the proof of concept only three control effectors are selected: left elevon, right elevon, and yaw multi-axis thrust vectoring.
- **Condition Selector:** In this component the upset recovery strategy is installed. Because the performance of the upset recovery controller can best be observed during a severe upset conditions, there is chosen for the developed spin as demonstration upset condition. The developed spin is a typical upset motion that can not be recovered with prescribed upset recovery techniques. That is why the proof of concept is mainly focusing on reducing body angular rates. The output of this block is a number that represents the current mode of the aircraft.
- **Control Effectiveness:** In this component the maximum control effectiveness is derived given the current state and the potential control effector deflections. In order to calculate the control effectiveness, the information of the components discussed above is required. The output of the control effectiveness is a vector containing all the direct control inputs for all control effectors. By means of the rectangular grid all options are iterated in only one time step.

5.4.2. Spin Recovery Demonstration

In this section the upset recovery controller proof of concept is demonstrated, in order to show its ability in severe flight conditions for the ICE aircraft. The demonstration flight in this section will consist of a pitch-up input followed by full roll and full yaw input. This will eventually lead to departure from the safe flight envelope to a fully developed spin. From the moment the aircraft rotates about 360 deg/s, the algorithm will be started to make recovery possible. Note that the following demonstration is only to show the proof of concept. Little time has been spent on applying optimization techniques or designing sophisticated recovery strategies, which means that the final performance is likely to improve.

The points in the time histories that can be identified during the demonstration flight are dictated in Table 5.1. In Fig. 5.3 to Fig. 5.5 the most important states are shown that show the performance of the upset recovery controller. Figure 5.3 shows the angular rates q and r . From 12 seconds onwards a steep increase in yaw angular rate can be observed. At the maximum peak value of the yaw rate, a yaw rate of 375 deg/s is obtained. From 19 seconds onwards the upset recovery algorithm is activated with the result a steep decrease in angular yaw rate. For the pitch rate q unsteady dynamics are the result of high aerodynamic angles. Those aerodynamic angles are shown in Fig. 5.4. In Fig. 5.4 high fluctuations in angle of attack α and sideslip

Table 5.1: Flight conditions during yaw spin demonstration

Time [s]	Flight condition
[0 - 8]	Steady flight
[8 - 12]	Full pitch-up control
[12 - 19]	Full roll and yaw control
[19 - 24]	Upset recovery
[24 - 40]	Recover attitude and airspeed

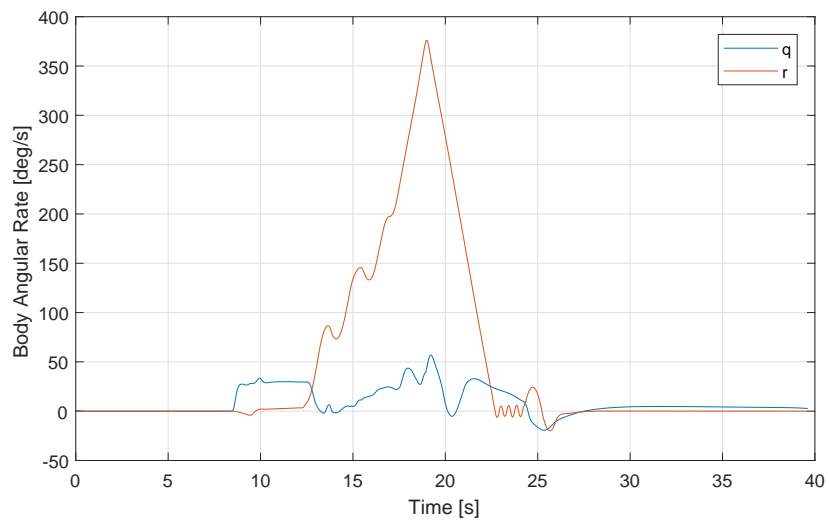
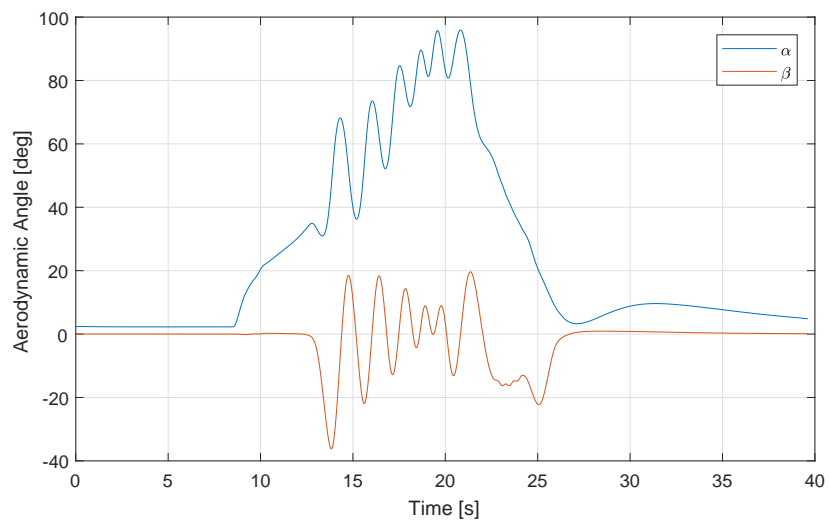
Figure 5.3: Body angular rates q and r during yaw spin demonstration

Figure 5.4: Aerodynamic angles during yaw spin demonstration

angle β are present. These fluctuations indicate that the aircraft is exceeding the safe flight envelope. From 19 seconds onwards where the upset recovery is activated, an increase in sideslip angle is the result of fast opposite yaw control by the yaw thrust vectoring. Furthermore it can be observed that the fluctuations in angle of attack after 19 seconds damps out and decreases rapidly. What is striking is that the maximum value of the angle of attack approaches 96 deg. This can be explained with Fig. 5.5 where the airspeed is displayed. In Fig. 5.5 a steep drop in airspeed is the result of applying full pitch-up control from 8 seconds onwards.

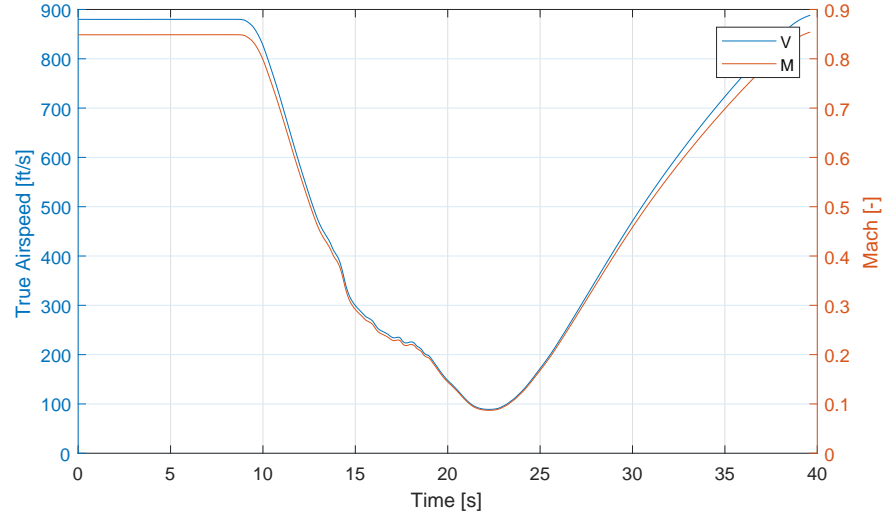


Figure 5.5: Airspeed and Mach number during yaw spin demonstration

At around 16 seconds oscillations in airspeed can be detected. After activating the upset recovery controller, these oscillations damp out. The striking maximum value in angle of attack of 96 deg can be explained with section 2.3 that states that in a fully developed spin the trajectory is approximately vertical. Furthermore it can be noticed that Mach is approaching minimums with even values below 0.1 Mach.

6

Upset Recovery Controller Design

In order to test the maximum control effectiveness concept in upset conditions, a new flight control system is designed for the ICE aircraft. The all-encompassing strategy designed by extending existing upset strategies for civil aviation, is the origin of the design. This all-encompassing strategy is applied to angular body rate control, the innermost loop of the flight control system using the INDI control methodology. Different outer loops are implemented for different phases in flight. Pseudo control inputs determine next control effector deflections based on gradient optimization.

This chapter presents the final design of the upset recovery controller. The design of the inner loop for body rate control and outer control loop is elaborated on in section 6.1. Choosing the most optimal set of control effectors is described in section 6.3. Most optimal control effectors deflections are determined in section 6.4 that describes the methodology and algorithms used. Sections 6.5 and 6.6 show the implementation of actuator dynamics compensation and fault tolerant control capabilities. If a pitch down moment cannot be generated and control effectors are saturated, section 6.7 describes the procedure to roll around the velocity vector. Followed by section 6.8 which describes low altitude anti ground collision control. Finally, section 6.9 presents the design of the entire flight control system implemented to complete the upset recovery controller.

6.1. Upset Recovery Strategy Planner

The brain behind the upset recovery controller is the strategy planner, from this plan the final individual control effector deflections are determined which should return the aircraft back to nominal flight conditions. The strategy that will be used has already been described in chapter 2, and functions as an inner and outer control loop.

The most crucial part of the planner is described in the first predefined steps of section 2.5, where Fig. 2.1 describes the steps to recover from an aircraft upset condition to a nominal flight condition within the flight envelope. These steps are first to reduce angular rates (p, q, r) followed by recovering the aerodynamic angles (α, β). The implementation of these two control loops for angular rates and aerodynamic angles is performed using inner and outer control loops described in section 6.1.1 and 6.1.2 respectively.

Reducing states to acceptable levels is an unclear specified level on which a control strategy as described before is unable to operate. Clear limits are needed to determine whether a given flight condition is inside or outside the safe flight envelope. This is primarily important to judge whether an aircraft is close to departure into upset, but also to determine whether current flight conditions can be considered as safe. Currently, no flight envelope is specified for the ICE aircraft and the proposed safe envelope from literature on upset recovery guidelines does not apply to high-performance aircraft. For this reason, Table 6.1 presents aircraft dependent data which is determined for describing the flight envelope parameters of the inner and outer control loop.

6.1.1. Angular Rate Control Loop

In the inner control loop of the upset recovery strategy planner, the INDI control methodology from chapter 3 has been implemented. This inner loop controls the body angular rates of the aircraft (p, q, r) by calculating the required control moment. Equation (6.1) shows the general rotational dynamics equation rewritten for a

Table 6.1: Envelope limits of inner and outer control loop parameters

State	Envelope limit	Unit
p	90	deg/s
q	90	deg/s
r	90	deg/s
α	20	deg
β	20	deg

nonlinear control effector model $\Phi(x, \delta)$.

$$\dot{\omega} = I^{-1}(\tau - \omega \times I\omega) = I^{-1}\Phi(x, \delta) + I^{-1}(\tau_a - \omega \times I\omega) \quad (6.1)$$

where

$$\tau = \tau_a + \tau_\delta = \tau_a + \Phi(x, \delta) \quad (6.2)$$

In order to calculate the rotational dynamics for each time step, Eq. (6.1) is locally linearized at current state x_0 and current control effector position δ_0 as a first-order Taylor expansion equation. When controlling in particular rotational dynamics the first-order Taylor expansion becomes Eq. (6.3).

$$\dot{\omega} \approx \dot{\omega}_0 + \frac{\partial}{\partial \omega} [I^{-1}\Phi(x, \delta) + I^{-1}(\tau_a - \omega \times I\omega)](\omega - \omega_0) + \frac{\partial}{\partial \delta} [I^{-1}\Phi(x, \delta) + I^{-1}(\tau_a - \omega \times I\omega)](\delta - \delta_0) \quad (6.3)$$

According to the time scale separation principle elaborated in chapter 3, the second term on the right hand side of Eq. (6.3) can be neglected. This time scale separation principle states that body angular rates and attitude angles changes could be neglected for small times steps if a moment acts on an aircraft [25, 35, 38]. In Eq. (6.3) the changes of the control input dependent term δ has notably faster dynamics compared to the state change ω . Therefore the second term on the right hand side in Eq. (6.3) is small enough to be neglected with high sampling rates. The third term containing δ changes significantly faster than ω in one time step, therefore the influence of δ is expected to be higher.

This statement of time scale separation and the determination of the partial derivative results into Eq. (6.4) which is written in terms of control input changes $\Delta\delta$ in incremental form.

$$\dot{\omega} = \dot{\omega}_0 + I^{-1} \nabla_\delta \Phi(x_0, \delta_0) \Delta\delta \quad (6.4)$$

Equation (6.4) can be rewritten by defining the virtual input as body angular acceleration $v(x) = \dot{\omega}$, which results into the following INDI problem formulation

$$I[v(x) - \dot{\omega}_0] = \nabla_\delta \Phi(x_0, \delta_0) \Delta\delta = \Delta\tau_\delta \quad (6.5)$$

where as earlier defined in chapter 3 is $\Delta\tau_\delta$ the pseudo control input command. This pseudo control input command defines the required increment in moment generated by control effectors, given the current state x_0 and current control effector deflections δ_0 . The output of Eq. (6.5) is essential in a further calculation for calculating the direction (positive or negative) in control effector deflection optimization described in section 6.4.

6.1.2. Aerodynamic Angle Control Loop

After correctly defining the inner most control loop which is fundamental for elaborating the INDI problem, outer control loops can be determined on the basis of kinematic inversion. After reducing body angular rates p, q, r is the next step to minimize aerodynamic angles to acceptable states and introduce any attitude angle that is required while recovering altitude and attitude. In order to reduce these angles, the kinematic relationships between those angles and body angular rates are required. A total of three different outer loops are designed: ϕ, α, β .

Roll Angle Inversion Loop A dynamic inversion loop need to be designed to have a clear definition of the relationship between roll angle and body angular rates. The kinematic relationship is given in Eq. (6.6).

$$\begin{bmatrix} p \\ q \\ r \end{bmatrix} = \begin{bmatrix} 1 & 0 & -\sin\theta \\ 0 & \cos\phi & \sin\phi\cos\theta \\ 0 & -\sin\phi & \cos\phi\cos\theta \end{bmatrix} \begin{bmatrix} \dot{\phi} \\ \dot{\theta} \\ \dot{\psi} \end{bmatrix} \quad (6.6)$$

Which results into the following equation (Eq. (6.7)).

$$p = \dot{\phi} - \dot{\psi} \sin \theta \quad (6.7)$$

Angle of Attack Inversion Loop Similarly, a dynamic inversion loop is designed for α . The dynamic equation can be described by

$$\alpha = \arcsin \frac{w}{V} \quad (6.8)$$

where the first derivative of Eq. (6.8) is

$$\dot{\alpha} = \frac{V\dot{w} - w\dot{V}}{V^2\sqrt{1 - \left(\frac{w}{V}\right)^2}} = \frac{\dot{w}}{\sqrt{u^2 + v^2}} - \frac{w\dot{V}}{V\sqrt{u^2 + v^2}} \quad (6.9)$$

where the following flight dynamics equations may be applied

$$\begin{bmatrix} \ddot{u} \\ \ddot{v} \\ \ddot{w} \end{bmatrix} = \frac{1}{m} \begin{bmatrix} X \\ Y \\ Z \end{bmatrix} - \begin{bmatrix} qw - rv \\ ru - pw \\ pv - qu \end{bmatrix} + g \begin{bmatrix} \sin \theta \\ \sin \phi \cos \theta \\ \cos \phi \cos \theta \end{bmatrix} \quad (6.10)$$

where the first term on the right hand side of Eq. (6.10) is the body acceleration in X, Y, Z which can be rewritten into A_x, A_y, A_z . When substituting Eq. (6.10) into Eq. (6.9) results in Eq. (6.11).

$$\dot{\alpha} = \frac{1}{\sqrt{u^2 + v^2}} \left[\frac{-uw}{V^2} (A_x - g \sin \theta) - \frac{vw}{V^2} (A_y + g \sin \phi \cos \theta) + \left(1 - \frac{w^2}{V^2}\right) (A_z + g \cos \phi \cos \theta) \right] + \begin{bmatrix} \frac{-v}{\sqrt{u^2 + v^2}} & \frac{u}{\sqrt{u^2 + v^2}} & 0 \end{bmatrix} \begin{bmatrix} p \\ q \\ r \end{bmatrix} \quad (6.11)$$

When the virtual control input of α is applied on the outer control loop for the input q , the angle of attack dynamic inversion law is given by Eq. (6.12).

$$q = \left(v_\alpha - \frac{1}{\sqrt{u^2 + v^2}} \left(\frac{-uw}{V^2} (A_x - g \sin \theta) - \frac{vw}{V^2} (A_y + g \sin \phi \cos \theta) + \left(1 - \frac{w^2}{V^2}\right) (A_z + g \cos \phi \cos \theta) - vp \right) \right) \cdot \left(\frac{u}{\sqrt{u^2 + v^2}} \right)^{-1} \quad (6.12)$$

Sideslip Inversion Loop Finally the sideslip dynamic inversion is integrated in the outer control loop to compensate for large sideslip angles in upset conditions. This loop is an outer control loop for controlling the yaw rate. The sideslip angle β is given by

$$\beta = \arcsin \frac{v}{V} \quad (6.13)$$

where the first derivative of Eq. (6.13) is

$$\dot{\beta} = \frac{V\dot{v} - v\dot{V}}{V^2\sqrt{1 - \left(\frac{v}{V}\right)^2}} = \frac{\dot{v}}{\sqrt{u^2 + w^2}} - \frac{v\dot{V}}{V\sqrt{u^2 + w^2}} \quad (6.14)$$

When substituting Eq. (6.10) into Eq. (6.14) results in

$$\dot{\beta} = \frac{1}{\sqrt{u^2 + w^2}} \left[\frac{-uv}{V^2} (A_x - g \sin \theta) + \left(1 - \frac{v^2}{V^2}\right) (A_y + g \sin \phi \cos \theta) - \frac{vw}{V^2} (A_z + g \cos \phi \cos \theta) \right] + \begin{bmatrix} \frac{w}{\sqrt{u^2 + w^2}} & 0 & \frac{-u}{\sqrt{u^2 + w^2}} \end{bmatrix} \begin{bmatrix} p \\ q \\ r \end{bmatrix} \quad (6.15)$$

When the virtual control input of β is applied on the outer control loop for the input r , the sideslip dynamic inversion law is given by Eq. (6.16).

$$r = \left(v_\beta - \frac{1}{\sqrt{u^2 + w^2}} \left(\frac{-uw}{V^2} (A_x - g \sin \theta) + \left(1 - \frac{v^2}{V^2} \right) (A_y + g \sin \phi \cos \theta) - \frac{vw}{V^2} (A_z + g \cos \phi \cos \theta) - wp \right) \right) \cdot \left(\frac{-u}{\sqrt{u^2 + w^2}} \right)^{-1} \quad (6.16)$$

6.2. Multivariate Simplex B-Splines Jacobian

In chapter 3 and section 6.1 is stated that an INDI problem formulation requires the Jacobian of the control effectiveness matrix. Furthermore section 6.1.1 describes the detailed implementation of the inner angular rate control loop and dynamic inversion. The Jacobian of the control effectiveness matrix $\nabla_\delta \Phi(x, \delta_0)$ contains the derivatives of the control moments coefficients with respect to control effector inputs $\Delta\delta$. Since the control effector inputs contains aerodynamic and propulsion inputs, Jacobian models are separately constructed for aerodynamic and propulsion inputs in section 6.2.1 and 6.2.2 respectively.

6.2.1. Aerodynamic Multivariate Simplex B-Splines Jacobian

In the final design of the upset recovery controller, the aerodynamic part of the Jacobian control effectiveness matrix is derived from a 0th-order multivariate simplex spline-based aerodynamic model identified from a high-fidelity aerodynamic database of the Lockheed Martin ICE aircraft [44]. The total number of spline functions to aerodynamic moment for this model is 108. This spline model maintains the aerodynamic structure including nonlinear aerodynamics as stated in Eq. (6.17).

$$\begin{aligned} C_i = & C_{i_1}(\alpha, M) + C_{i_2}(\alpha, \beta, M) + C_{i_3}(\alpha, \beta, \delta_{LIBLEF}) + C_{i_4}(\alpha, \beta, \delta_{LIBLEF}, \delta_{OBLEF}, M) \\ & + C_{i_5}(\alpha, \delta_{LSSD}, \delta_{LEL}, M) + C_{i_6}(\alpha, \delta_{LSSD}, \delta_{RSSD}, \delta_{PF}, M) + C_{i_7}(\alpha, \beta, \delta_{LAMT}) \\ & + C_{i_8}(\alpha, \delta_{LEL}, \delta_{LAMT}) + C_{i_9}(\alpha, \delta_{LOBLEF}, \delta_{LAMT}) + C_{i_{10}}(\alpha, \delta_{REL}, \delta_{RAMT}) \\ & + C_{i_{11}}(\alpha, \delta_{ROBLEF}, \delta_{RAMT}) + C_{i_{12}}(\alpha, \beta, \delta_{LSSD}) + C_{i_{13}}(\alpha, \beta, \delta_{RIBLEF}) \\ & + C_{i_{14}}(\alpha, \beta, \delta_{RIBLEF}, \delta_{ROBLEF}, M) + C_{i_{15}}(\alpha, \delta_{RSSD}, \delta_{REL}, M) + C_{i_{16}}(\alpha, \beta, \delta_{RAMT}) \\ & + C_{i_{17}}(\alpha, \beta, \delta_{RSSD}) + C_{i_{18}}(\alpha, M) + C_{i_{19}}(\alpha, M) \end{aligned} \quad (6.17)$$

Equation (6.17) is defined for a six degree of freedom problem where $i = \{X, Y, Z, l, m, n\}$. Calculating the dynamic inversion of the inner loop based on body angular rates only requires the Jacobian of three moment coefficients l, m, n . Using the simplex model the partial derivatives of the aerodynamic force and moment coefficients C with respect to δ are calculated, in Eq. (6.18) the control effectiveness Jacobian matrix is defined.

$$\frac{\partial \Phi(x, \delta)}{\partial \delta} = \begin{bmatrix} \frac{\partial C_l(x, \delta)}{\partial \delta_1} & \frac{\partial C_l(x, \delta)}{\partial \delta_2} & \dots & \frac{\partial C_l(x, \delta)}{\partial \delta_c} \\ \frac{\partial C_m(x, \delta)}{\partial \delta_1} & \frac{\partial C_m(x, \delta)}{\partial \delta_2} & \dots & \frac{\partial C_m(x, \delta)}{\partial \delta_c} \\ \frac{\partial C_n(x, \delta)}{\partial \delta_1} & \frac{\partial C_n(x, \delta)}{\partial \delta_2} & \dots & \frac{\partial C_n(x, \delta)}{\partial \delta_c} \end{bmatrix} \quad (6.18)$$

In Eq. (6.18), c is defined as the total number of control effectors.

6.2.2. Multi-Axis Thrust Vectoring Jacobian

Besides the aerodynamic part of the moment coefficients Jacobian, there are propulsion Jacobian terms generated by the multi-axis thrust vectoring. Analytically the thrust vectoring model equation is given by

$$\tau_T = T d_{c.g.} \begin{bmatrix} 0 \\ -\sin(\delta_{TVP}) \\ -\cos(\delta_{TVP}) \tan(\delta_{TVY}) \end{bmatrix} \quad (6.19)$$

where τ_T indicates moments generated by the multi-axis thrust vectoring, T thrust force, $d_{c.g.}$ the distance between the multi-axis thrust vectoring and the center of gravity (C.G.), and δ_{TVP} and δ_{TVY} thrust vectoring deflection angles for pitch and yaw respectively. From Eq. (6.19), Jacobian terms providing the directional

derivative of the moments generated by thrust vectoring are shown in Eq. (6.20).

$$\nabla_{\delta} \tau_T (\delta_{TVP}, \delta_{TVY}) = T d_{c.g.} \begin{bmatrix} 0 & 0 \\ -\cos(\delta_{TVP}) & 0 \\ \sin(\delta_{TVP}) \tan(\delta_{TVY}) & -\frac{\cos(\delta_{TVP})}{\cos^2(\delta_{TVY})} \end{bmatrix} \quad (6.20)$$

From Eq. (6.20) it both can be seen that the control effectiveness is highly dependent on the thrust setting of the aircraft, and a higher thrust force results in a higher thrust control effectiveness.

6.3. Control Effector Selection

Section 6.2 described the Jacobian model of the control effectiveness matrix. In order to determine which control effector is most effective at a given flight condition, this Jacobian model provides useful information. For each individual control effector, there are three moment derivatives. Based on the largest control effectiveness derivative for each control effector, the corresponding moment will be optimized by that particular control effector. This complete algorithm for selecting control effectors is shown in algorithm 3.

Algorithm 3: Control effector selection

Data: Control effectiveness Jacobian J_d
 $J_d = \text{abs}(J_d)$;
 $[, id] = \text{sort}(J_d)$;
 $[n, m] = \text{size}(J_d)$;
 $d_{on} = \text{zeros}(n, m)$;
for $i = 1 : m$ **do**
 $d_{on}(id(1, i), i) = i$;
end
Result: Control effector effectiveness selection d_{on}

6.4. Control Effectiveness Optimization

Now that all the details of the system are known, finally the upset recovery controller can be optimized. The optimization is performed per individual control effector installed on the aircraft. The data from section 6.1 in which the pseudo-control input is calculated, section 6.2 that defines the control effectiveness Jacobian, and section 6.3 for control effector selection completes the required information for control effector optimization.

This section elaborates on the decision for next time step control effector inputs. It is essential to translate the pseudo-control input which is determined by the commanded states, in a correct way to the corresponding control effector inputs that makes recovery of an aircraft possible. A direction of optimization for each control effector individually is determined based on: as first the individual value of the control effectiveness Jacobian corresponding to one moment and one control effector described in section 6.2, and second the pseudo-control input of section 6.1. Based on the pseudo-control input shown in Eq. (6.21) which is the required control effector induced incremental moment, and the control effectiveness Jacobian, Eq. (6.21) can be rewritten into Eq. (6.22).

$$I [\nu(x) - \dot{\omega}_0] = \nabla_{\delta} \Phi(x, \delta_0) \Delta\delta = \Delta\tau_{\delta} \quad (6.21)$$

$$\Delta\delta = \nabla_{\delta} \Phi(x, \delta_0)^{-1} \Delta\tau_{\delta} \quad (6.22)$$

Equation (6.22) provides the change in control effector deflections. Based on the sign whether it is positive or negative a maximum deflection increment is added or subtracted from the current control effector deflection. This equation uses the gradient of control effectiveness to all control effectors in order to optimize control effector deflections by means of calculating deflection increments. This control input increment is dependent on effector position and rate constraints. Control effector position and rate constraints are formulated in Eq. (6.23) and Eq. (6.24) respectively.

$$\delta_{min} \leq \delta \leq \delta_{max} \quad (6.23)$$

$$|\dot{\delta}| \leq \dot{\delta}_{max} \quad (6.24)$$

In discrete-time simulation environments, rate constraints determine the maximum effector position increment for each time step Δt as can be seen in Eq. (6.25).

$$\Delta\delta_{max} = \dot{\delta}_{max}\Delta t \quad (6.25)$$

Using Eq. (6.25), Eq. (6.23) can be rewritten as Eq. (6.26) where incremental position constraints are taken into account in order to define a lower and upper incremental deflection constraint for the current control effector position.

$$\delta_l \leq \delta \leq \delta_u \quad (6.26)$$

with [30]

$$\delta_l = \max(-\dot{\delta}_{max}\Delta t, \delta_{min} - \delta_0) \quad (6.27)$$

$$\delta_u = \min(\dot{\delta}_{max}\Delta t, \delta_{max} - \delta_0) \quad (6.28)$$

where δ_l and δ_u selects the most restrictive constraint.

The relations defined in Eq. (6.27) and Eq. (6.28) defines the local search space for maximum control effectiveness optimization. The entire algorithm describing the proces of optimizing next time step control effector deflections can be seen in algorithm 4. Where d_{pcons} is a two column vector with lower and upper effector position constraints, d_{rcons} a vector with effector rate constraints, d_0 the current control effector position, J_d the control effectiveness Jacobian defined in section 6.2, d_{on} the control effector effectiveness selection described in section 6.3, and d_τ the pseudo-control input of section 6.1.

Algorithm 4: Control effectiveness optimization

Data: Effector position constraints d_{pcons} , effector rate constraints d_{rcons} , current control input d_0 , control effectiveness Jacobian J_d , control effector effectiveness selection d_{on} , time step dt , pseudo-control input d_τ

```

m = length(d0);
d_dir = zeros(m,1);
for i = 1 : 3 do
    for j = d_on(i,:) do
        if j > 0 then
            d_dir(j) = (J_d(i,j)^(-1)) d_tau(i);
        end
    end
end
end
idx_n = d_dir < 0;
idx_p = d_dir > 0;
;
u_max = min(d_rcons*dt, d_pcons(:,1) - d_0);
u_min = max(-d_rcons*dt, d_pcons(:,2) - d_0);
;
d_ci = zeros(m,1);
d_ci(idx_n) = u_min(idx_n);
d_ci(idx_p) = u_max(idx_p);
;
d_c = d_0 + d_ci;

```

Result: Commanded control input d_c

6.5. Actuator Dynamics Compensation

Actuator dynamics compensation is included in order to improve tracking performance and make use of the full capabilities of the control effectors. Section 3.3 described the general problem formulation for commanded/desired control inputs for the aircraft. The following compensation scheme has been used in order to take actuator dynamics into account (Fig. 6.1). Where δ_c represents the commanded control effector deflections by the control effectiveness optimization, δ_0 the current control deflections, δ_e the error between

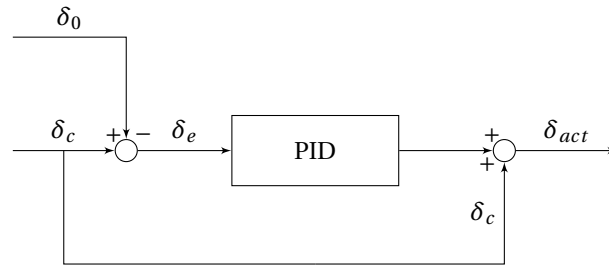


Figure 6.1: Actuator dynamics compensation scheme

the commanded and current control effector deflection, and δ_{act} the actual control input to the control effectors of the aircraft. The effect of actuator dynamics is solved by using feedback and feedforward control on the actuator input channel. By propagating the error and the current actuator position, actuator dynamics are taken into account. For the low- and high-bandwidth actuator transfer functions, the proportional gain is set to 5.5 and 2.5 respectively.

Figure 6.2 gives a performance example of a high-bandwidth transfer function control effector, which is deflected from 0 degrees to maximum deflection of 30 degrees taking into account rate constraint of 150 deg/s. The second order transfer function is described in Eq. (4.2).

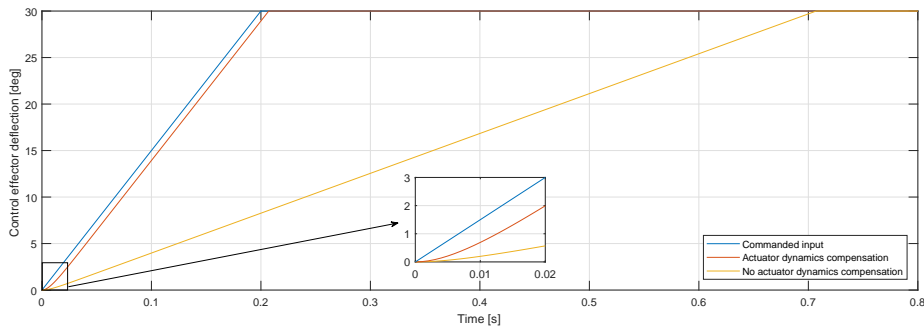


Figure 6.2: Actuator dynamics compensation high-bandwidth transfer function

6.6. Fault Tolerant Control Capabilities

In the event of failure of one or more parts of the aircraft, there is a chance the aircraft will fail completely if the system is highly model dependent. Preferably, the aircraft can continue the intended operation at a reduced level of control authority rather than failing completely. In order to continue operating at a sufficient level in the presence of errors, the system must be fault-tolerant.

In section 2.2 different causes are described in which unsafe flight conditions can arise among which aircraft failure. The failure of parts of the flight control will lead to anomalies such as control effectors that are stuck at a certain deflection angle and reduce aircraft control authority. The reduced capabilities of control effectors affect the model of the aircraft. Being less dependent on the model of the aircraft will lead to a more fault tolerant system.

Section 3.1 described an introduction to the nonlinear system at hand. Furthermore, it was described how the general equation of nonlinear dynamics could be rewritten in form of incremental nonlinear dynamic inversion (Eq. (3.10)). INDI increases robustness due to the principle of elimination of model mismatch by providing body angular acceleration feedback to the controller. The principle of INDI is implemented in the upset recovery system, which makes the system fault-tolerant at the same time.

6.7. Control Effector Saturation

There are particular aircraft upset conditions in which an aircraft is unable to generate a nose-down moment in order to mitigate the situation, for example in a (deep) stall condition. Turning around the velocity vector is provided as a solution to prevent the stall from getting severe [11]. Also in manuals describing aircraft upset

recovery strategies, rolling the aircraft to a bank angle starts a nose-down motion is prescribed. Nose-down elevator will ensure that the angle of attack α remains as low as possible which makes aileron control effective [4, 14, 19].

Despite the fact that some (military) aircraft in dangerous flight conditions still have full to little control authority over the aircraft, the solution of rolling around the velocity vector is included. In the event a nose-down motion can not be generated with the current selection of control effectors, all control effectors are saturated with a maximum possible deflection for each individual control effector. This functionality is controlled by means of algorithm 5.

Algorithm 5: Control effector saturation

Data: Effector position constraints d_{pcons} , effector rate constraints d_{rcons} , commanded control input d_c , control effector effectiveness selection d_{on}

$[n, m] = \text{size}(d_{on})$;

$d_s = \text{zeros}(n, m)$;

for $i = 1 : n$ **do**

for $j = 1 : m$ **do**

if $d_{on}(i, j) > 0$ **then**

if $d_c(d_{on}(i, j)) == d_{pcons}(d_{on}(i, j), 1) || d_c(d_{on}(i, j)) == d_{pcons}(d_{on}(i, j), 2)$ **then**

$d_s(i, j) = 1$;

end

end

end

$idx_d = d_{on}(i, :) > 0$;

$idx_s = d_s(i, :) > 0$;

if $idx_d == idx_s$ **then**

$d_{sat}(i) = 1$;

end

end

Result: Control effector saturation d_{sat}

6.8. Low Altitude Control

During an aircraft upset it is important to keep an eye on the altitude of the aircraft. Airspeed and altitude are important states of the aircraft between which energy can be exchanged. During or after an aircraft upset, altitude can be exchanged for speed to reach the desired speed faster. However, this is not always achievable and it may be that altitude is so low that immediate action is necessary. Still the first priority is to reduce the angular rates p, q, r , but the pitch command may need to be manipulated to avoid collision with the ground.

In the second phase of recovery is reducing angle of attack α applied as pitch command. However, this strategy does not take into account any low altitude flight conditions. Therefore an additional variable to the pitch command needs to be included. Equation (6.29) displays the flightpath angle, which is the angle between the flight path vector and the local atmosphere.

$$\gamma = \theta - \alpha \quad (6.29)$$

This additional flightpath angle only needs to be included for low altitude flight conditions. The following equation completes the definition

$$q_{add} = \cos(\phi) \left(\gamma_{des} - \gamma_{des} \cdot \min \left(1, \frac{h}{h_{des}} \right) - \gamma \right) \quad (6.30)$$

where γ_{des} is the desired flightpath angle, h altitude, and h_{des} the desired altitude. This additional term will be included in the pitch command in the second phase of recovery.

6.9. Upset Recovery Controller Design Overview

After describing the various components in the upset recovery controller, this section provides a global overview of the various information flows and subsystems. What is striking is that no external control inputs enter the

Simulation and Results

This chapter evaluates the performance of the complete upset recovery system compared to current flight control systems and reviews individual subsystems and their functionality. Results are based on a real-time simulation setup using the high-fidelity aerodynamic model of the ICE aircraft developed by Lockheed Martin as described in chapter 4 and the flight control system for upset recovery described in chapter 6. Simulations shown in this chapter present the performance of the newly designed aircraft upset recovery system, in particular controlled states of the aircraft. These aircraft parameters are compared to the INCA flight controller currently installed for allocating individual control effector deflections in nominal flight conditions.

INCA captures nonlinearities and interactions of control effectors in a real-time control allocation flight control system by using an incremental reformulation of the control allocation problem [28]. This flight control system relies on body angular accelerations in order to reduce model dependencies. Important to mention is that all control effector deflections are initialized with 0 degrees, except if the simulation starts from steady trimmed flight to ensure a fair comparison. To make the comparison, the INCA is used together with the angular body rate controller described in [28] without external control inputs.

Section 7.1 describes the simulation equipment used for presenting the results. In section 7.2 several critical motions are described such as deep stall and developed spin. Followed by external caused upset such as environmental and mission dependent causes in section 7.3. Fault tolerant capabilities are shown in section 7.4. Next to that, section 7.5 simulates low altitude stall conditions with and without low altitude pitch command modification. Finally, section 7.6 shows the added value of compensating for actuator dynamics. Results not included in this chapter can be seen in appendix B which shows additional results.

7.1. Simulation Equipment

Simulations shown in this chapter are performed in a Matlab/Simulink framework using aerodynamic wind tunnel data from the high-fidelity ICE aircraft which is described in chapter 4. The controller design described in chapter 6 is fully implemented into Matlab Simulink, mainly using Matlab function blocks that makes describing input-output relations written in Matlab programming environment possible. To simulate the dynamic system, aircraft states are computed at predefined time steps over a specified time span. Computations are solved using a fourth-order Runge-Kutta solver with a fixed sampling rate of 100 Hz. The simulations are executed on a 64-bit computer environment with two Intel(R) Core(TM) i3-2370M CPU @ 2.40 GHz processors and 4.0 Gb RAM.

In all the simulations equal gains are used for inner and outer control loops, exact values are listed in Table 7.1. These gains are selected based on best overall performance. Therefore there may exist a gain which makes faster recovery possible for a given upset condition. For each separate set of simulations, initial flight conditions are discussed beforehand. This chapter only describes the first two phases of recovery, consisting of reducing body angular rates and recovering aerodynamic angles. Simulating subsequent phases such as attitude recovery is unnecessary and mitigates the clear results of the upset recovery controller. Simulation parameters separated from the ICE aircraft model include a 1976 COESA-extended U.S. Standard Atmosphere and a discrete wind gust model to simulate external environmental upset causes.

Table 7.1: Gains used during simulation of upset recovery controller

	Proportional
p	3.5
q	6.5
r	2.5
α	4.0
β	2.0

7.2. Critical Upset Motions

There are very specific aircraft motions that are characterized by flying outside the safe flight envelope. In section 2.3 an introduction has been given to these particular motions. These motions in generally could happen to every aircraft, but do not necessarily lead to dangerous conditions for every aircraft. The reason for this could be that the aircraft is very maneuverable or certain flight conditions are not considered to be dangerous. For this reason, only the critical upset motions are simulated in which high angles of attack combined with potential oscillations can be observed. Therefore, no critical upset motions that mainly consist of oscillations around the roll, pitch, or yaw axis are simulated. Section 7.2.1 shows simulations and results for several deep stall conditions, and section 7.2.2 shows simulations and results for two different types of spin.

7.2.1. Deep Stall

The first set of simulations consist of initial conditions that are specified as deep stall. In general deep stall is defined as an upset condition in which the aircraft is unable to generate a nose-down moment. For aircraft without thrust vectoring this might be true, however the simulation aircraft that is being used is equipped with thrust vectoring and therefore it is always possible to generate a nose-down moment with a running engine. Nevertheless, simulating this upset condition provides interesting results. Two different deep stall upset are simulated, the first with a relatively low speed and high angle of attack and the second describes a deep stall upset condition initialized with a 90 degree angle of attack at zero airspeed.

Deep Stall at Low Airspeed A deep stall at low speed can be mitigated by minimizing aerodynamic angles as soon as possible and aiming for trim velocity to prevent the upset motion from entry into a second upset. The first deep stall upset is initialized with the following most important flight parameters: $h = 24,900$ ft, $V = 304$ ft/s, $\theta = 90$ deg, and $\alpha = 81$ deg. A comparison in body angular rate responses between the current INCA flight control system and the upset recovery flight control system are shown in Fig. 7.1. As can be seen in Fig. 7.1, the INCA control systems shows slow body angular rates compared to the upset recovery system. INCA is focused on reducing the angular rates of each axis to zero, but ignores the aerodynamic angles. This results in an uncontrolled angle of attack as can be seen in Fig. 7.2, where the angle of attack is constantly above 50 degrees for the first 5 seconds of simulation. The upset recovery system, however, shows increases in angular body rates, mainly for the pitch command. The rapid increase in pitch rate results in a decrease in angle of attack. As described in chapter 6, body angular rates are reduced until they are within the nominal flight conditions of the envelope. This limit is specified as a hard limit at 90 deg/s for the 3 different body rates. Therefore, in the time range [0.5 - 1] seconds a fast oscillation can be seen in pitch rate because the pitch rate should be within the envelope. At the same time as the pitch rate increases, there is also an increase in the roll rate. Despite the commanded zero roll rate, there are small fluctuations obtained. This is mainly due to the aerodynamic coupling of particular control effectors that could be used for both pitch and roll control inputs. After about three seconds all body angular rates are reduced to values within the envelope and both angle of attack and sideslip angle are minimized to acceptable levels within the safe flight envelope. Finally the time histories of the 13 different control effector deflections together with the thrust setting applied by the upset recovery controller can be seen in Fig. B.1 in appendix B. Quick responses are the result of reducing aerodynamic angles in the first 3 seconds followed by constant control inputs after three seconds when the aircraft is stabilized.

Deep Stall at Zero Airspeed Military aircraft might encounter situations in which object avoidance or fast rotations at low speed are necessary. Those maneuvers may end-up in an upset condition at high pitch angle and angle of attack at relatively low airspeed or even zero airspeed. This second deep stall upset is initialized with the following most important flight parameters: $h = 20,000$ ft, $V = 10$ ft/s, $\theta = 90$ deg, and $\alpha = 89$ deg.

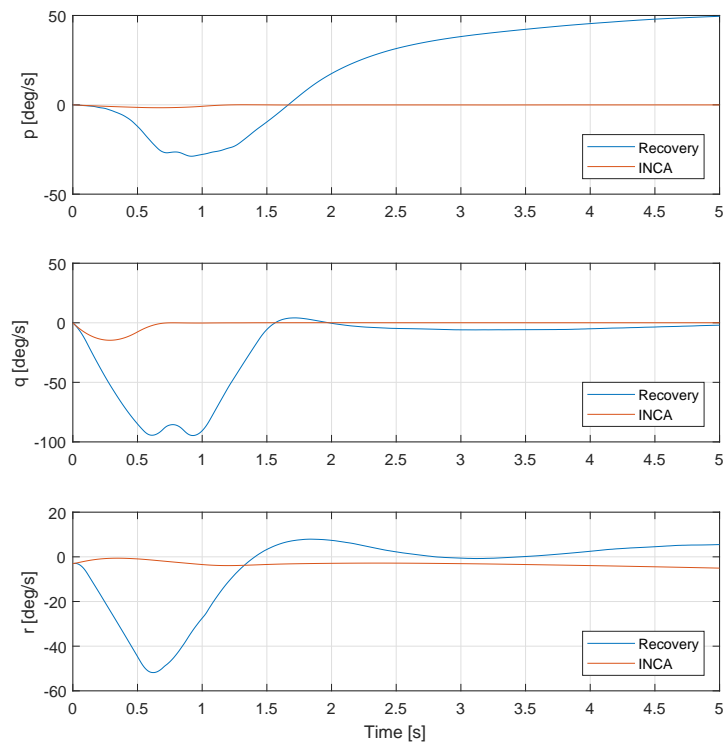


Figure 7.1: Body angular rates in a deep stall upset at low airspeed

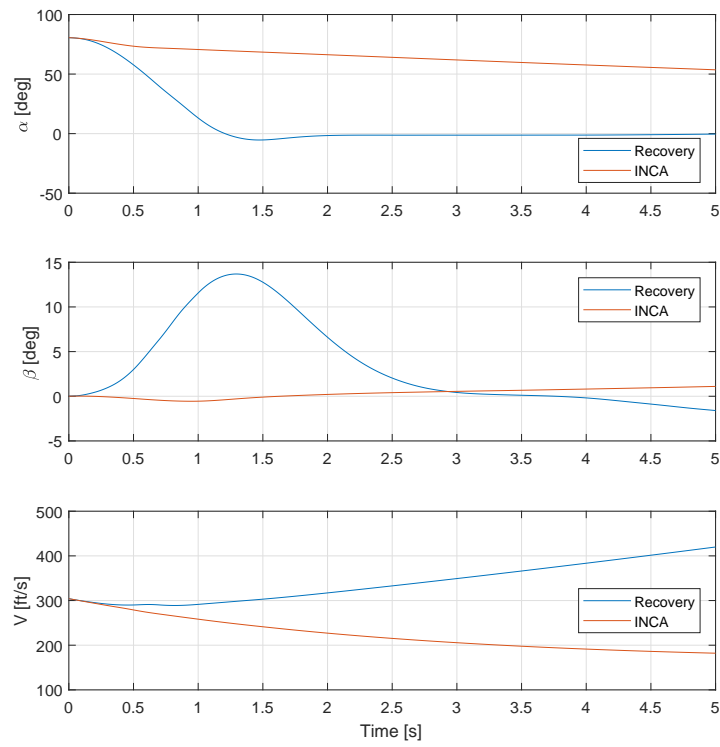


Figure 7.2: Aerodynamic angles and airspeed in a deep stall upset at low airspeed

This upset condition is simulated in this section where Fig. 7.3 and Fig. 7.4 show body angular rate and aerodynamic angles responses respectively. INCA control system again is aiming for minimizing angular body

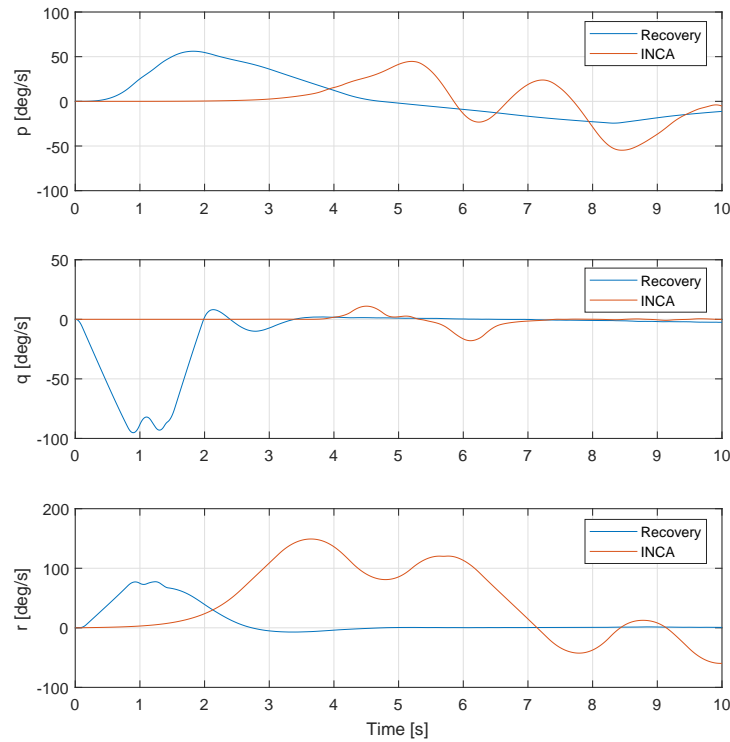


Figure 7.3: Body angular rates in a deep stall upset at zero airspeed

rates, this time with the consequence of making aircraft even more unstable and entering a second upset. This is a typical LOC condition in which an incorrect strategy has been applied and high aerodynamic angles are obtained. After 10 seconds the aircraft is still not able to fully recover. The upset recovery system on the other hand, reduces the angle of attack as quickly as possible by keeping the same time in the flight envelope for all three angular body rates. This results in a rapid decrease of angle of attack and a stable aircraft within 4 seconds. Only small oscillations in sideslip angle can be seen compared with the INCA controller which reaches 80 degrees sideslip angle. Finally the time histories of the 13 different control effector deflections together with the thrust setting applied by the upset recovery controller can be seen in Fig. B.2 in appendix B. Control effectors responsible for generating a pitch down moment (δ_{TVP} , δ_{PF}) in order to reduce the angle of attack deflect to maximum control effectiveness in the first second.

7.2.2. Spin

The second set of simulations consist of initial conditions that are specified as a spin. Spin in general is defined as a condition in which high angular rates are obtained while flying at high angles of attack. This section will describe two types of spin including the simulated aircraft response. The first in the category spin is rotation in yaw direction, the spin which is most common and well known. Second is a spin in pitch direction that rarely occurs but is considered to be a dangerous one.

Yaw Spin Spin in general is associated with a high yaw rate combined with a low velocity of which the vector is pointing downward. In order to simulate performance results the following most important flight parameters are defined: $h = 24,000$ ft, $V = 184$ ft/s, $\alpha = 86$ deg, and $r = 500$ deg/s. A comparison in body angular rate and aerodynamic angle responses between the current INCA flight control system and the upset recovery flight control system are shown in Fig. 7.5 and Fig. 7.6 respectively. First point to notice is the faster reducing yaw rate by the upset recovery system. In about 4.5 seconds the aircraft is fully recovered from the

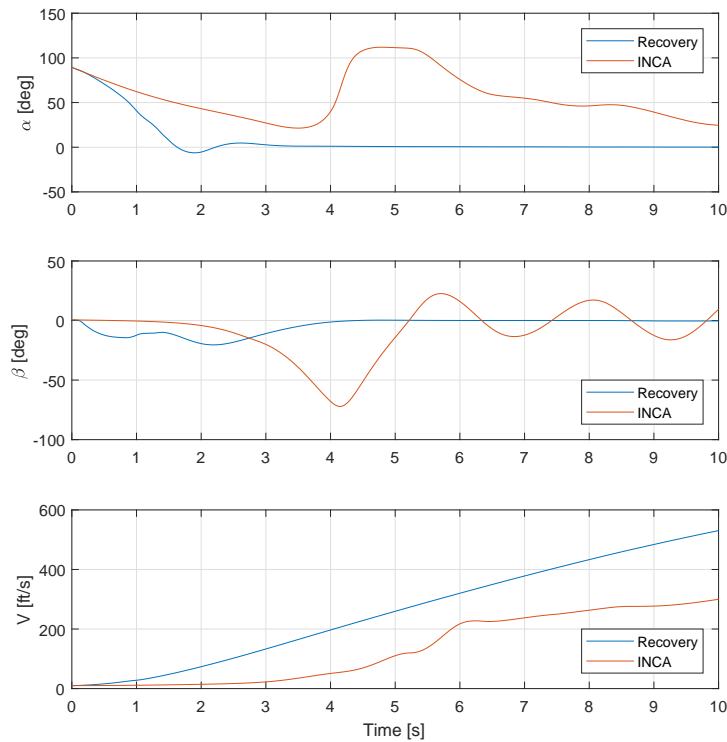


Figure 7.4: Aerodynamic angles and airspeed in a deep stall upset at zero airspeed

spinning motion, 1 second faster compared to the INCA flight control system. This fast result is mainly due to the difference in control effector optimization and actuator dynamics compensation. The pitch rate is also minimized faster and more stable, until the moment that all angular rates are within the flight envelope. The sudden increase in pitch rate is caused by the reduction of the high angle of attack. Important to point out is the smaller oscillation in sideslip angle for the upset recovery system due to faster reduction of the yaw rate. At the end it can be concluded that the upset recovery system is able to recover the aircraft to acceptable flight conditions about 2 seconds faster compared to INCA flight control system which is not optimized for upset recovery. Time histories of the 13 different control effector deflections together with the thrust setting applied by the upset recovery controller can be seen in Fig. B.3 in appendix B. Control effectors responsible for generating a yaw moment (δ_{TVY} , δ_{amt} , δ_{ssd}) to counteract the high yaw rate deflect to maximum control effectiveness from start.

Pitch Spin This set of simulation consist of a high pitch rate causing a spin in pitch direction. This maneuver is typically associated with the aircraft falling out of the sky, resulting in a high pitch rate. There is a direct relationship between pitch and angle of attack which makes this upset motion hard to recover. High and rapid fluctuations in angle of attack make aerodynamic control effectors ineffective, therefore pitch thrust vectoring is highly necessary. In order to simulate performance results the following most important flight parameters are defined: $h = 22,500$ ft, $V = 162$ ft/s, $\alpha = 88$ deg, and $q = 716$ deg/s. A comparison in body angular rate and aerodynamic angle responses between the current INCA flight control system and the upset recovery flight control system are shown in Fig. 7.7 and Fig. 7.8 respectively. INCA is able to reduce pitch rate more quickly with the consequence of increased roll and yaw rate up to 300 deg/s. Due to unstable body rate dynamics, sideslip angle β shows oscillations reaching values over 60 degrees. Followed by a constant angle of attack α of about -160 degrees, which means that the aircraft is orientated flying backwards with respect to the velocity vector. These flight conditions are highly unstable. As can be seen from these figures, the INCA flight control system is unable to deal with high fluctuation in angles of attack combined with high angular body rates. Using the upset recovery system a stable reduction in pitch rate can be obtained while keeping the other angular body rates at minimum levels. It is worth highlighting that the pitch rate response shows small

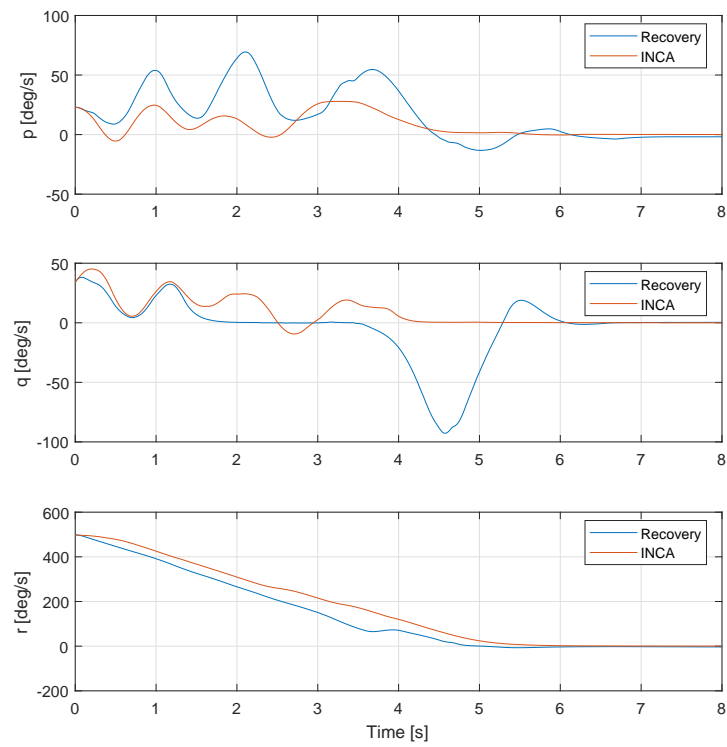


Figure 7.5: Body angular rates in a yaw spin upset

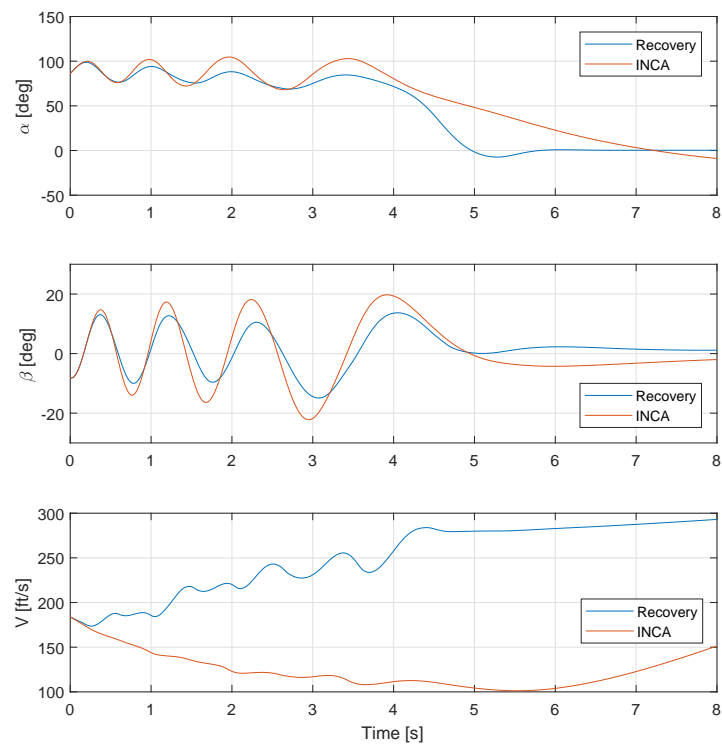


Figure 7.6: Aerodynamic angles and airspeed in a yaw spin upset

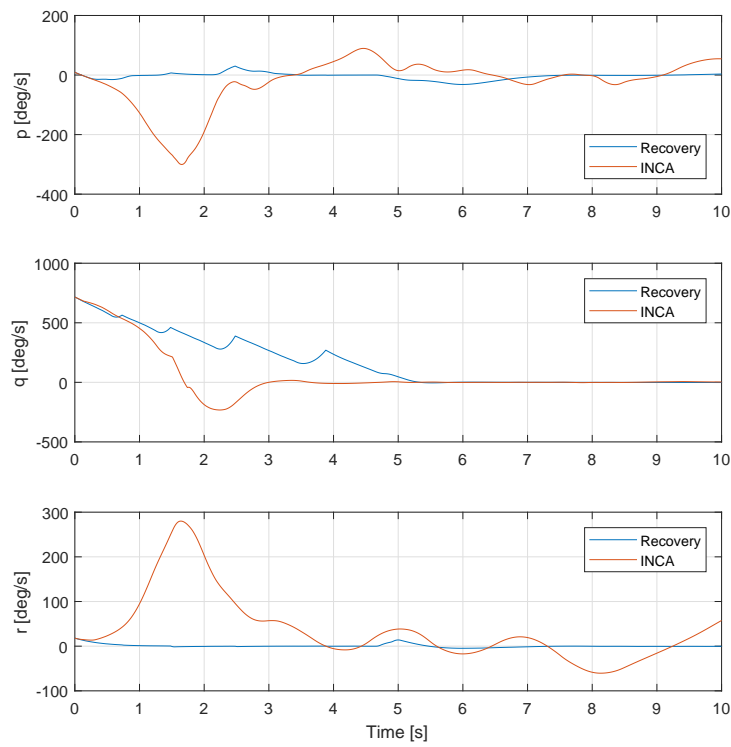


Figure 7.7: Body angular rates in a pitch spin upset

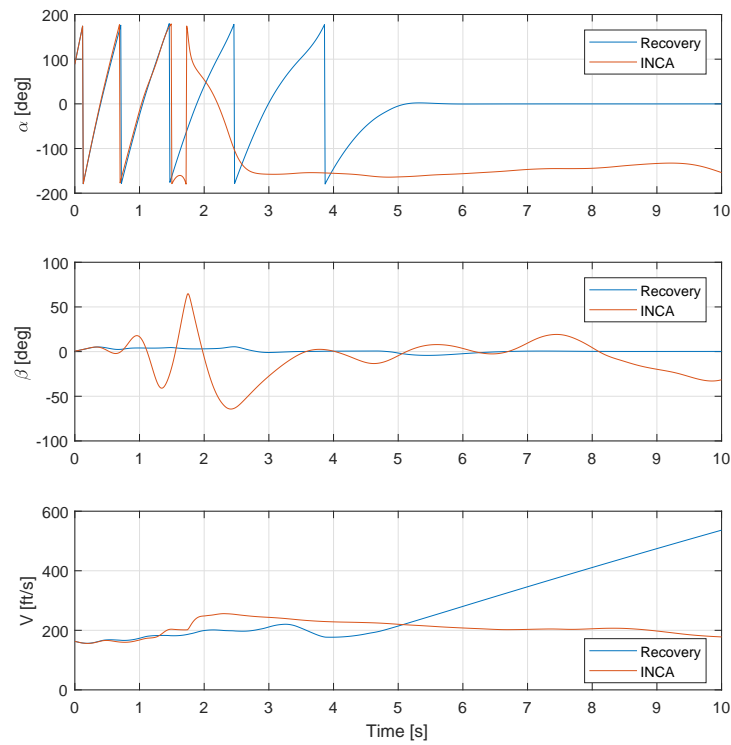


Figure 7.8: Aerodynamic angles and airspeed in a pitch spin upset

interruptions at times where angle of attack is close to 180 degrees. Control effectors become less effective at such high angles of attack which results in performance degradation. Sideslip angle remains at low angles of about 0 degrees. Largest performance increase can be seen while focusing on the angle of attack. At the start of the simulation, equal results are obtained while reducing body angular rates compared to INCA. After reducing body angular rates, the upset recovery system aims at minimizing aerodynamic angles one of them angle of attack. Instead of keep on reducing the pitch rate, small pitch rate commands are used to force angle of attack to 0 degrees. From this point on the aircraft is considered to be recovered. Within 5 seconds the aircraft is recovered to safe flight conditions within the flight envelope. Figure B.4 in appendix B shows time histories of the 13 different control effector deflections together with the thrust setting applied by the upset recovery controller. In particular pitch thrust vectoring but also both elevons help to decrease the pitch rate as fast as possible. Where previously the elevons are used to minimize the roll rate, these are now used to minimize the pitch rate. This choice is determined by the control effector selection which determines for each time step where the largest increase in control effectiveness could be realized.

7.3. External Caused Aircraft Upsets

As described before in chapter 2.2, causes of upset can be separated into four different categories. In this section two practical problems an aircraft might encountered during flight operations that could end up in upset are simulated. The first category to be simulated is aircraft upset due to environmental causes (section 7.3.1). The second category of interest is aircraft upset due to mission dependent causes (section 7.3.2).

7.3.1. Environmental Caused Upset

The first set of external caused aircraft upsets finds its origin in an environmental reason. Strong gusts or upward moving air produced by for example mountain wave, thunderstorms, or micro-bursts lead in certain circumstances to severe situations. These different types of turbulence cause large variations in airspeed and the aircraft might be out of control for some time. These variations in wind speed affect the aerodynamic angles of an aircraft. A strong gust is simulated by a strong vertical wind of 1,000 ft/s in the body frame that builds up as a standard cosine shape initialized at 3.0 seconds. For the simulation of results, the following data is known about the gust encountered by the aircraft to make a performance comparison between both flight control systems.

$$V_{gust} = \begin{cases} 0, & x < 0. \\ \frac{V_{amp}}{2} \left(1 - \cos\left(\frac{\pi x}{d_{gust}}\right) \right), & 0 < x < d_{gust}. \\ V_{amp}, & x > 0. \end{cases} \quad (7.1)$$

where V_{amp} is the gust amplitude, d_{gust} is the gust length, x is the distance traveled, and V_{gust} is the resultant wind velocity in the body axis frame. Gust amplitude is set to 1,000 ft/s and gust length equal to 1,000 ft initialized at 3.0 seconds. The following important flight parameters are used: $h = 20,000$ ft and $V = 880$ ft/s. A comparison in body angular rate and aerodynamic angle responses between the current INCA flight control system and the upset recovery flight control system are shown in Fig. 7.9 and Fig. 7.10 respectively. INCA starts minimizing body angular rates to zero while at the same time the sideslip angle increases until it reaches a maximum value of 75 degrees. From that point on INCA is not able to keep angles at low rates and loses control over the aircraft. In this particular example the clear main differences in control methodology appear. Using the upset recovery strategy implemented, aerodynamic angles are reduced while keeping angular body rates within the flight envelope. Figure B.5 in appendix B shows time histories of the 13 different control effector deflections together with the thrust setting applied by the upset recovery controller. Only small increments in control effector deflections can be noticed.

7.3.2. Mission Dependent Caused Upset

For military aircraft there are external factors that may occur with higher probability, as described in section 2.2. Impact of a missile has direct impact on the dynamics of an aircraft, a combination of external moments due to the pressure explosion results in spinning motions. To simulate the impact of a missile on the aircraft, an external moment is applied on the roll and pitch axis at time 3.0 seconds. A step input provides the additional moment on the axes for a fixed time period of 0.1 seconds to ensure that it approximates an impulse moment input. Properties known about the close explosion impact are described in Table 7.2. The following important flight parameters are used: $h = 20,000$ ft and $V = 880$ ft/s. A comparison in body angular rate and aerodynamic angle responses between the current INCA flight control system and the upset recovery flight

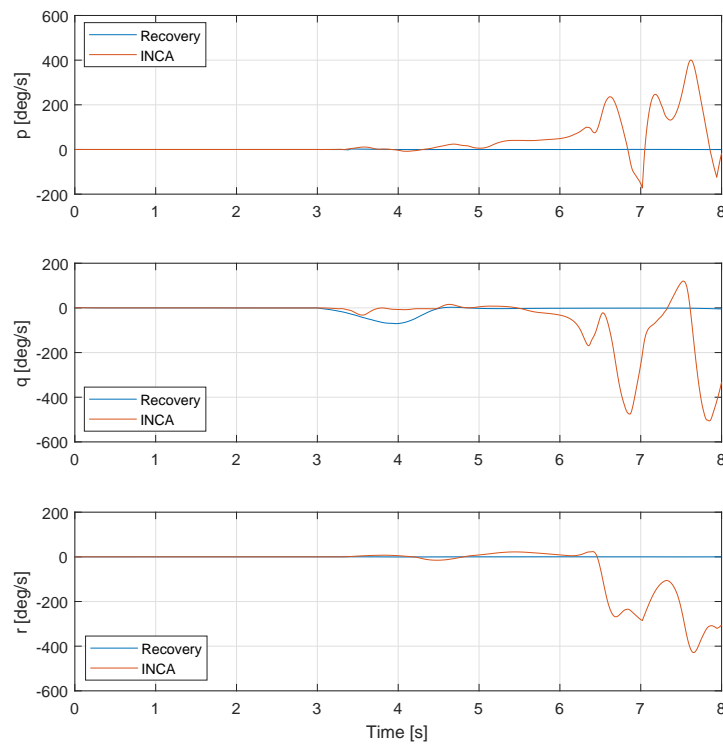


Figure 7.9: Body angular rates while encountering a 1,000 ft/s wind gust

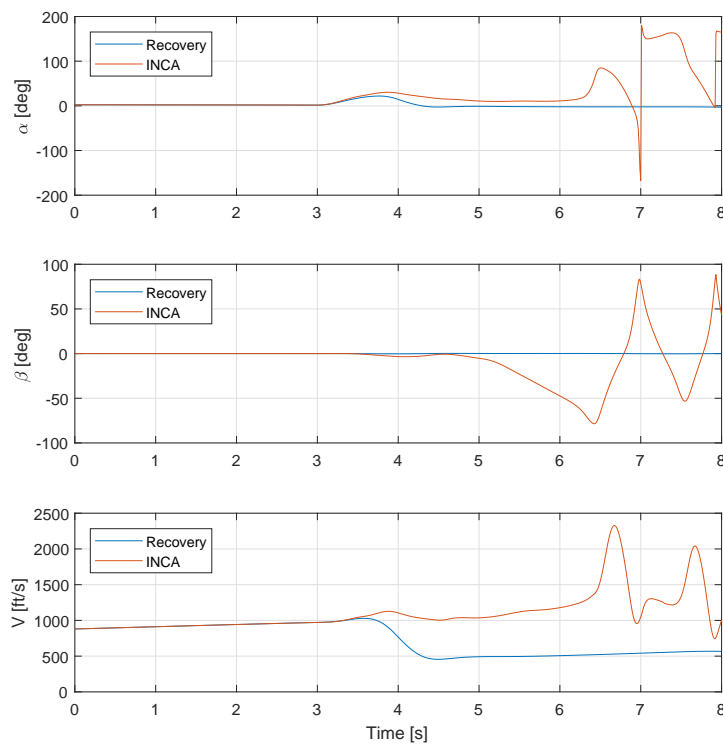


Figure 7.10: Aerodynamic angles and airspeed while encountering a 1,000 ft/s wind gust

Table 7.2: Close explosion moment properties of missile impact

Axis	lbf ft	Nm
l	6.6e6	8.9e6
m	-1.0e7	-1.4e7
n	0	0

Table 7.3: Fault tolerant close explosion moment properties of missile impact

Axis	lbf ft	Nm
l	5.0e6	6.8e6
m	-9.5e6	-1.3e7
n	0	0

control system are shown in Fig. 7.11 and Fig. 7.12 respectively. Due to the impulse in moment, angular body

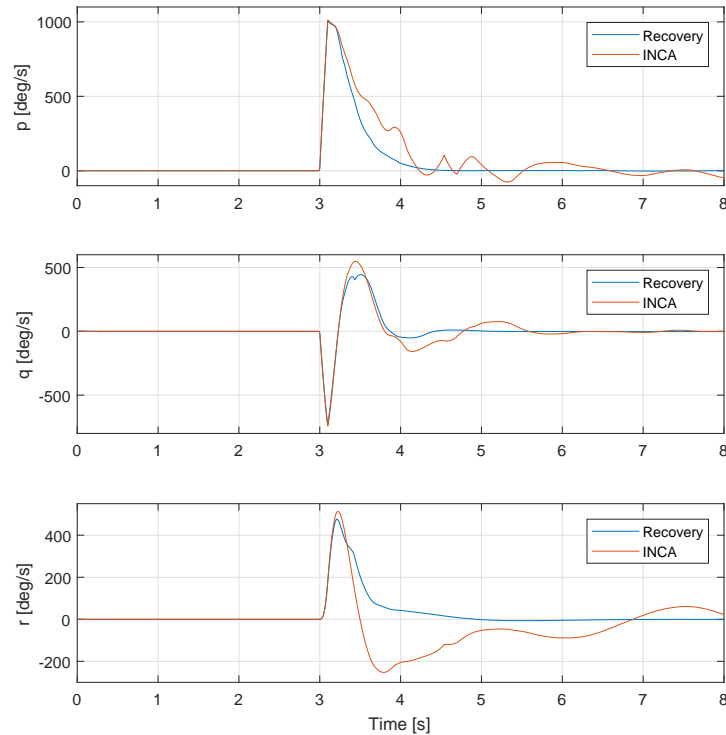


Figure 7.11: Body angular rates while being hit by missile

rates of 1000, 500, and 500 are achieved for respective roll, pitch, and yaw. The simulation of the upset recovery system achieves slightly smaller body angular rates compared to INCA. The system stabilizes relatively quickly, all rates are minimized within just 1 second. INCA system encounters many more problems with reducing body angular rates. This problem is mainly because of the high aerodynamic angles, in particular angle of attack which reaches values of 180 degrees. Followed by highly unstable sideslip angles that reach up to 90 degrees. The upset motion is still not completely stable after 8 seconds due to the sideslip angle which is not directly compensated by control loops. Figure B.6 in appendix B shows time histories of the 13 different control effector deflections together with the thrust setting applied by the upset recovery controller. Mainly thrust vectoring, pitch flap, and both elevons are compensating for increased moments in roll and pitch encountered during the simulation.

7.4. Fault Tolerant Control Capabilities

Aircraft failure could be one of the reasons to end up in upset conditions. In order to be able to provide a reduced level of control authority, chapter 6 describes the part of the controller which makes the upset recovery system fault tolerant. In order to simulate fault tolerant capabilities, again the missile impact simulation is used. At time 3.0 seconds a rotational moment described in Table 7.3 for a fixed time period of 0.1 seconds is applied. Again the same flight parameters are used: $h = 20,000$ ft and $V = 880$ ft/s. A comparison in body

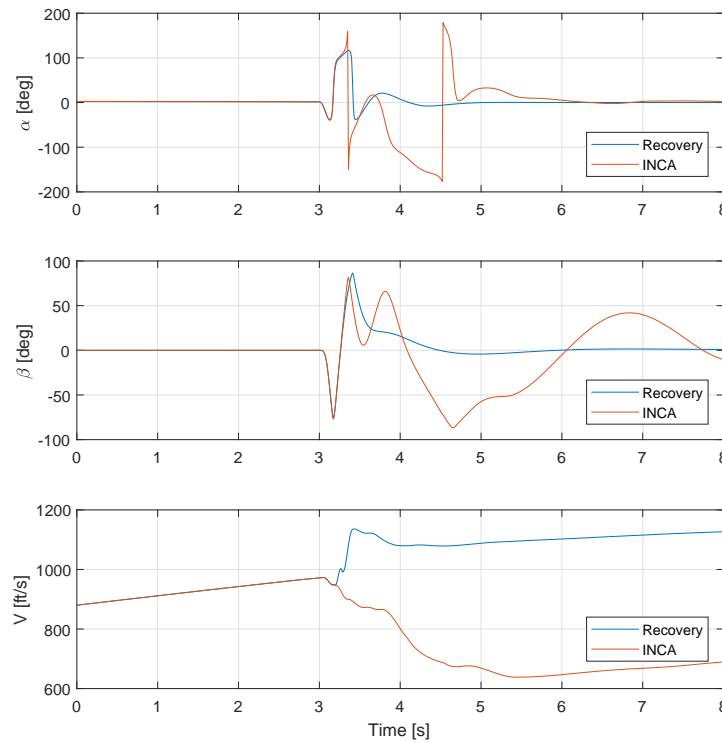


Figure 7.12: Aerodynamic angles and airspeed while being hit by missile

angular rate and aerodynamic angle responses between the current INCA flight control system and the upset recovery flight control system are shown in Fig. 7.13 and Fig. 7.14 respectively. The first entry in the legend indicated with "Recovery" shows the performance of the upset recovery system with full control authority. Followed by the second entry indicated as "Recovery FT" shows fault tolerant capabilities where control effectors have been fixed at a certain deflection. For the INCA controller all control effectors have full control capabilities indicated with "INCA". For "Recovery FT" all control effectors at the leading and trailing edge of the left wing are fixed at a zero control deflection ($\delta_{LIBLEF}, \delta_{LOBLEF}, \delta_{LAMT}, \delta_{LEL}$) after impact. What can be seen in Fig. 7.13 and Fig. 7.14 is that the upset recovery system is capable of recovering the aircraft within 6 seconds both for failure and nominal case. More oscillations reaching higher values can be observed for the failure case, mainly due to the reduced control authority in roll and pitch direction. Compared to INCA, the upset recovery shows improved performance while having reduced control authority in failure case. INCA control is not able to stabilize the aircraft within 10 seconds due to highly oscillating unstable aerodynamic angles. Figure B.7 and Fig. B.8 in appendix B show time histories of the 13 different control effector deflections together with the thrust setting applied by the upset recovery controller for the non failure and failure case respectively. Figure B.7 show large control inputs for $\delta_{LEL}, \delta_{REL}, \delta_{PF}$, and δ_{TVP} . Figure B.8 which shows the failure case, displays equal results for δ_{PF} and larger control inputs for δ_{REL} . What can be seen is that the function of deactivated control effectors that are stuck at zero degrees are taken over by other control effectors. Mainly thrust vectoring, pitch flap, and right elevon show maximum control effector inputs.

7.5. Low Altitude Control

The next set of simulations consist of low altitude simulations. At this low altitude, a stall condition is simulated that may occur during landing. When strong gusts appear during landing of the aircraft, for example due to micro-burst or turbulence, the airspeed but also the angle of attack may change rapidly. Although the main objective of the upset recovery system is to recover important aircraft states to the safe flight envelope such as angular body rates p, q, r and aerodynamic angles α, β , collision with the ground should be prevented at all times. Section 6.8 describes how the pitch command has been manipulated with a desired flightpath

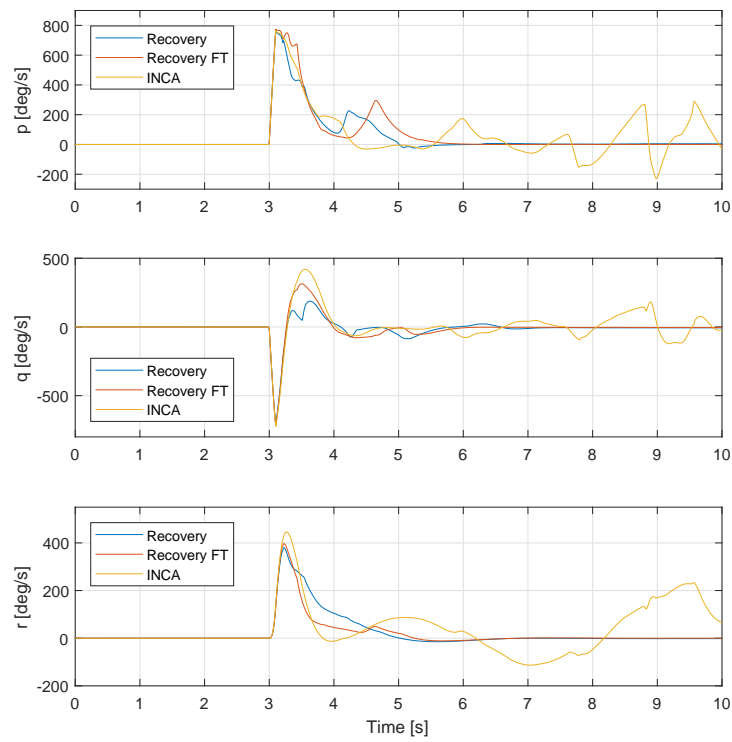


Figure 7.13: Body angular rates while being hit by missile, left wing control effector failure for "Recovery FT"

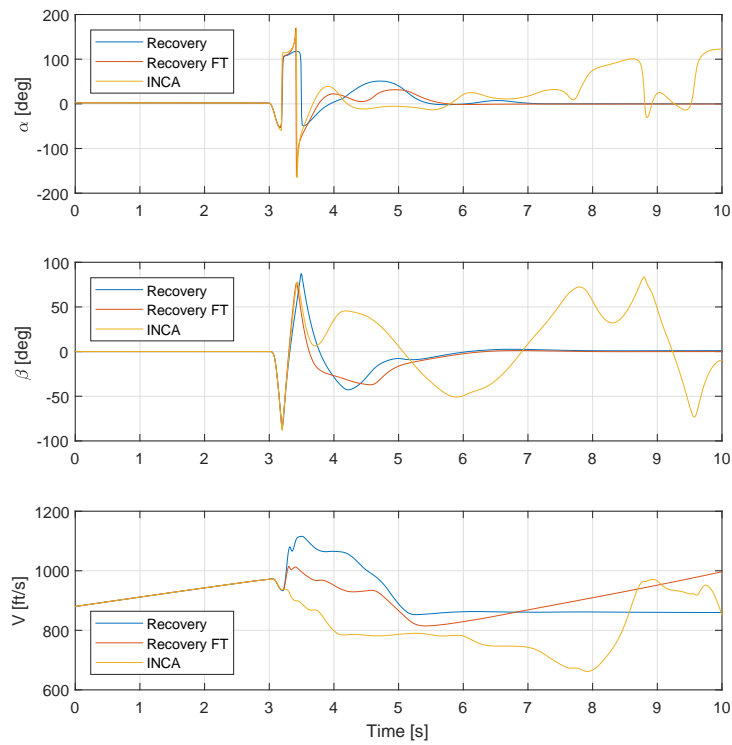


Figure 7.14: Aerodynamic angles and airspeed while being hit by missile, left wing control effector failure for "Recovery FT"

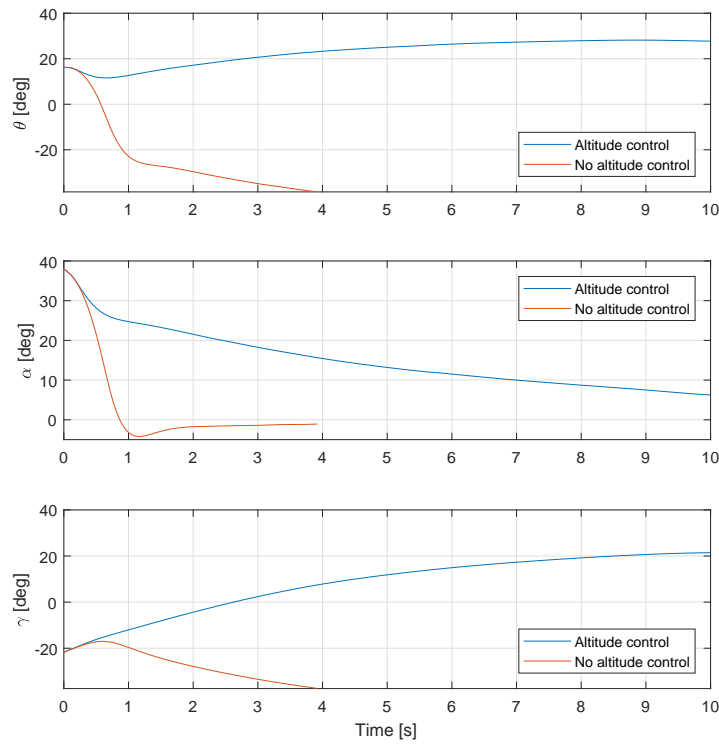


Figure 7.15: Pitch angle, angle of attack, and flightpath angle in stall condition near ground

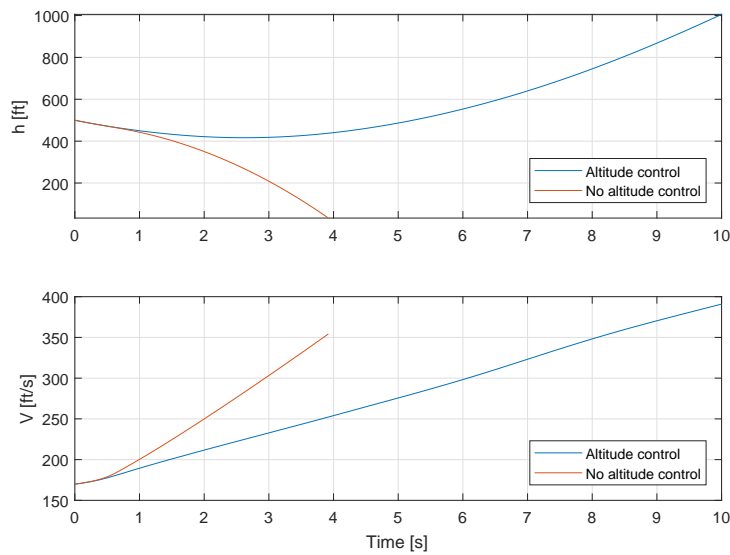


Figure 7.16: Altitude and airspeed in stall condition near ground

angle. The following flight parameters are used during the simulation: $h = 500$ ft, $V = 170$ ft/s, $\theta = 16$ deg, and $\alpha = 38$ deg. According to the given initial flight parameters, flightpath angle γ is negative and therefore the velocity vector is pointing -22 degrees with respect to the horizon. A comparison in flight conditions between the upset recovery flight control system with and without altitude control are shown in Fig. 7.15 and Fig. 7.16. In the first figure, Fig. 7.15, the pitch angle θ , angle of attack α , and flightpath angle γ are displayed. Without

taking into account the current altitude of the aircraft, the angle of attack is quickly reduced. In this upset condition, this reduction in angle of attack is accompanied by a negative pitch and flight path angle. As a result, the airspeed increases rapidly, the altitude decreases, and within 4 seconds there is impact with the ground. By taking the altitude into account during the second phase of recovery, the pitch angle increases, the angle of attack slowly decreases, and the desired flightpath angle is obtained. As a result, the flight path angle has been changed from negative to positive by 2.5 seconds and the aircraft descends to 416 ft, which is an altitude drop of 84 ft (26 m). Figure B.9 in appendix B shows time histories of the 13 different control effector deflections together with the thrust setting applied by the upset recovery controller. Small control effector deflections for δ_{TVP} and δ_{PF} can be noticed which stabilize to a final deflection.

7.6. Actuator Dynamics Compensation

This section describes the added value of compensating for actuator dynamics. To make use of the full capabilities of the control effectors, feedback and feedforward control on the actuator input channel is implemented to improve tracking performance. Figure 7.17 shows the responses in yaw rate between the upset recovery system with actuator dynamics compensation, without compensation, and INCA. Results are initialized with the following flight parameters: $h = 24,000$ ft, $V = 184$ ft/s, $\alpha = 86$ deg, and $r = 500$ deg/s. Significant

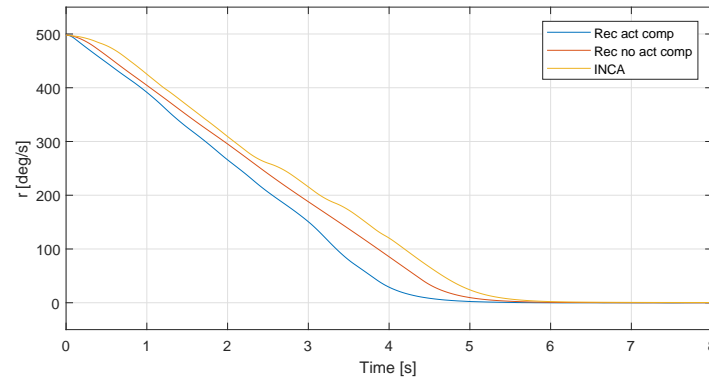
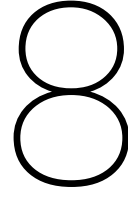


Figure 7.17: Performance comparison between having/not having actuator dynamics compensation and INCA

differences can be observed between the yaw rate responses. It can be seen that adding actuator dynamics compensation to the system reduces the time to zero yaw rate from 5.3 seconds to 4.7 seconds, which is a percentage improvement of 11%. With regard to the INCA system to full reduction, which takes 5.6 seconds, there is an improvement of 0.9 seconds.



Conclusions and Recommendations

Recent statistics have shown that loss of control is the largest contributor of fatal accidents in aviation for commercial and military aircraft. Adequate upset recovery controllers are necessary in order to increase safety and reduce the number of fatal accidents in aviation. Not to undermine the efforts described in literature, flight control systems require a more advanced upset recovery method which is able to recover from extremely high angles of attack and angular rates far away from the safe flight envelope. In those extreme flight conditions, aircraft encounter nonlinear influences such as kinematic coupling, oscillatory or divergent aircraft responses and reduced control capabilities. Neglecting these effects results in underutilization of aircraft control capabilities and maneuverability in aircraft upset conditions. Only the full use of control effector potentials combined with an adequate upset recovery strategy will be able to recover an aircraft from any aircraft upset. Therefore a novel method is introduced that combines maximum aircraft capabilities with a sophisticated upset recovery strategy to control key aircraft states to an acceptable level during off-nominal flight conditions that are specified as loss of control.

In this thesis research project an innovative method for aircraft upset recovery has been implemented that is able from the general essence of recovery to return from any aircraft upset condition to safe flight conditions. This methodology for upset recovery performs accurate, efficient, and robust recovery maneuvers and is suitable for real-time implementation in already existing flight control systems of high performance over-actuated aircraft. The concept is based on the INDI principle which determines incremental control induced moments based on commanded inner loop, outer control loops, and current dynamics of the system. The innermost body angular acceleration control loop which is simultaneously implemented in the first phase of the upset recovery control strategy, reduces model dependency and makes the system robust against mismatch of the aerodynamic model. Using these control induced moments individual control effectors deflections are optimized based on a control effectiveness Jacobian model that takes into account aerodynamic interactions and non-linearities between control effectors, furthermore this concept does not require further details of an aerodynamic model. Individual control effectors are optimized by means of focusing on maximum control effectiveness of the aircraft based on the current state of the aircraft.

Current approaches for preventing and recovering from aircraft upset are too narrow specified in order to recover from a wide range of different upset conditions and assume that the aircraft is not stalled. To ensure the availability of an adequate plan for every upset condition, a new upset recovery strategy has been developed. This strategy focuses on the method of reducing angular rates p , q , r until recovered in the safe flight envelope, followed by recovering aerodynamic angles α and β . This control strategy acts as an inner and outer control loop for the INDI control methodology. INDI calculated a pseudo control input command that defines the required increment in moment generated by control effectors, given the current state and current control effector deflections. This pseudo control input is fundamental in determining the heading of optimization of future control effector deflections for highest aircraft control effectiveness.

Control effectiveness optimization is executed by determining which control effector is most effective at a given flight condition. The aircraft control effectiveness Jacobian model provides useful information about aerodynamic control effector model and thrust vectoring model. Largest control derivatives with respect to

the moment coefficients for l, m, n determine the most effective control effectors for a particular to be controlled moment. The pseudo control input together with the knowledge about control effectiveness Jacobian model determines next time step control effector inputs based on maximum increment of control effector deflection keeping in mind control effector positions and rate constraints. This commanded control effector input is subjected to actuator dynamic compensation in order to provide the correct desired control inputs to the aircraft. By propagating the error and the current control effector position, actuator dynamics are taken into account.

The performance of the aircraft upset recovery controller in upset conditions was assessed and compared to INCA which is designed for nominal flight control and uses the entire aircraft control effectiveness Jacobian for mapping commanded control effector deflections by an incremental nonlinear control allocator. Simulations were executed using the ICE aircraft of Lockheed Martin that consist of a high-fidelity simulation aerodynamic model gathered by wind tunnel tests. Both flight control systems were exposed to different aircraft upset conditions. A division is made between the critical upset motion itself and externally created upset conditions that show a more practical implementation of the aircraft upset recovery system.

The recovery capabilities of the upset recovery system and INCA are compared by simulating several deep stall situations, fully developed spins, a strong gust situation, a missile impact upset condition, and low altitude condition. The performance of the flight control systems is based on body angular rates and aerodynamic angles which monitor the fundamental states of an aircraft to identify upset. In all simulated aircraft upset condition the performance of the upset recovery system was considerably faster and more reliable compared to INCA in terms of recovering angular body rates and aerodynamic angles. The main reason for this performance increase is due to the difference in control methodology. Where INCA is only focusing on reducing body angular rates to zero and fully neglecting severe aerodynamic angles that might result in departure into a second upset, is the upset recovery system first also focusing on reducing the angular body rates to acceptable levels within the flight envelope followed by fast reduction of aerodynamic angles such that the aircraft accommodate nominal flight conditions more quickly.

Results from simulations showed significant improvements in terms of recovering the aircraft en returning to the safe flight envelope. In deep stall conditions, angular rates and aerodynamic angles are recovered within 3.0 seconds to stable flight conditions even though the angle of attack was initiated at values larger than 80 degrees. The same is true for fully developed spins, where the upset recovery controller is stabilized after 5.0 seconds from a 500 deg/s yaw spin, shows the INCA controller still unstable responses after 7.0 seconds of simulation time. For the spin in pitch direction the differences are clearly emphasized, where both flight controllers show difficulties in reducing angular body rates due to highly a fluctuating angle of attack, is the upset recovery system able to recover within just 6.0 seconds while INCA shows loss of control and ends up at a constant angle of attack of -160 degrees. While simulating strong gust conditions with gust amplitude of 1,000 ft/s, is the INCA controller again in loss of control mode while the upset recovery system shows minimal changes in angular body rates which hardly can be recognized. Simulating missile impact results into an extremely fast recovery by the upset recovery system within just 1.0 second, where INCA requires more than 5.0 seconds to get close to stable flight dynamics and aerodynamic angles. Finally there are additional features simulated equipped on the upset recovery controller. The first feature is fault tolerant capabilities and second low altitude recovery control. Fault tolerant capabilities were tested for a missile impact situation where all left wing leading and trailing edge control effectors are deactivated after impact. Larger fluctuations in body angular rates were observed but the final performance approximates the performance of the upset recovery controller with full control over control effectors. Low altitude recovery control was tested and the comparison was made between compensating term in control command at low altitude. The inclusion of low altitude control shows a significantly higher survivability, where the aircraft only drops 84 ft (26 m) in altitude at a flight path angle of -22 deg, altitude of 500 ft, and a speed of 170 ft/s.

Regarding to future research, there are recommendations that will greatly improve the functionality of the upset recovery system. First of all, there is a need for a comprehensive aerodynamic database with wind tunnel test data specified for aircraft states and aerodynamic angles for off-nominal flight conditions. Currently, for some control effectors aerodynamic data up to 90 deg angle of attack is available. By extending the number of data points to the entire range of possible angles of attack, more nonlinear effects will be included in the data which results into more realistic aircraft responses. Second of all, including structural limitations of the

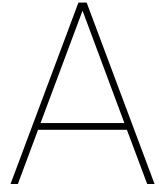
aircraft to the upset recovery controller will increase the applicability of the method. At the moment no data is available on structural limits of the ICE aircraft, which means that angular body rates and angular body accelerations are unlimited. Adding any limits will increase the survivability of the aircraft and pilot itself. This simply could be added to the upset recovery system through an additional inner control loop. Third of all, no clear envelope has been defined for the ICE simulation aircraft. Because of this reason, hard limits are set for the angular body rates of 90 deg/s. In order to guarantee a higher survivability, an envelope estimation method could make a better estimate of the envelope. Based on this envelope, a condition specific boundary can be given for each upset in which safe angular body rates can be guaranteed. Fourth of all, the necessity of implementing a control effector fault identification algorithm. Current fault tolerant performance is promising, however these performances can be even more overwhelming with the availability of the health status of effectors. For every effector fault condition, a new gain setting can be realized for tuning the upset recovery system. This will greatly increase the survivability of effector faults in upset conditions.

Bibliography

- [1] C.M. Belcastro. Loss of control prevention and recovery: Onboard guidance, control, and systems technologies. *AIAA Guidance, Navigation, and Control Conference 2012*, 2012. doi: 10.2514/6.2012-4762.
- [2] Boeing. Statistical summary of commercial jet aircraft accidents: Worldwide operations, 1959-2015. *Boeing Commercial Airplane*, Seattle, WA, 2016.
- [3] J.M. Brandon. Dynamic stall effects and applications to high performance aircraft. *Special Course on Aircraft Dynamics at High Angles of Attack: Experiments and Modeling*, (AGARD Report No. 776):2-1 – 2-15, Apr 1995.
- [4] D. Carbaugh, L. Rockliff, and B. Vandal. *Airplane Upset Recovery Training Aid Revision 2*. ICAO, Oct 2008.
- [5] B. Chang, H.G. Kwatny, E.R. Ballouz, and D.C. Hartman. Aircraft trim recovery from highly nonlinear upset conditions. *2016 AIAA Guidance, Navigation, and Control Conference*, 2016. doi: 10.2514/6.2016-0880.
- [6] L.G. Crespo, S.P. Kenny, D.E. Cox, and D.G. Murri. Analysis of control strategies for aircraft flight upset recovery. *AIAA Guidance, Navigation, and Control Conference 2012*, 2012. doi: 10.2514/6.2012-5026.
- [7] D.B. Doman and M.W. Oppenheimer. Improving control allocation accuracy for nonlinear aircraft dynamics. *AIAA Guidance, Navigation, and Control Conference and Exhibit*, 2002. doi: 10.2514/6.2002-4667.
- [8] J.E.T. Dongmo. Aircraft loss - of - control recovery using feedback linearization and high order sliding mode control. *AIAA Guidance, Navigation, and Control Conference 2012*, 2012. doi: 10.2514/6.2012-4548.
- [9] J.E.T. Dongmo. Aircraft loss - of - control recovery using feedback linearization and high order sliding mode control. *AIAA Guidance, Navigation, and Control Conference 2012*, 2012. doi: 10.2514/6.2012-4548.
- [10] J.E.T. Dongmo. Aircraft loss - of - control recovery using optimal high order sliding mode control with discontinuous high order observers. *AIAA Guidance, Navigation, and Control Conference 2012*, 2012. doi: 10.2514/6.2012-4545.
- [11] J.E.T. Dongmo and H.G. Kwatny. *Aircraft Loss-of-control Prevention and Recovery: A Hybrid Control Strategy*. PhD thesis, Drexel University, 2010.
- [12] K.M. Dorsett and D.R. Mehl. *Innovative Control Effectors (ICE)*. Lockheed Martin Tactical Aircraft Systems, 1996.
- [13] B.C. Dutoi, N.D. Richards, N. Gandhi, D.G. Ward, and J.R. Leonard. Hybrid robust control and reinforcement learning for optimal upset recovery. *AIAA Guidance, Navigation and Control Conference and Exhibit*, 2008. doi: 10.2514/6.2008-6502.
- [14] R. Eagles. *Guidance Material and Best Practices for the Implementation of Upset Prevention and Recovery Training*. Safety and Flight Operations, International Air Transport Association, June 2015.
- [15] J.A.A. Engelbrecht, S.J. Pauck, and I.K. Peddle. A multi-mode upset recovery flight control system for large transport aircraft. *AIAA Guidance, Navigation, and Control (GNC) Conference*, 2013. doi: 10.2514/6.2013-5172.
- [16] J.V. Foster, K. Cunningham, C.M. Fremaux, G.H. Shah, E.C. Stewart, R.A. Rivers, J.E. Wilborn, and W. Gato. Dynamics modeling and simulation of large transport airplanes in upset conditions. *Collection of Technical Papers - AIAA Guidance, Navigation, and Control Conference*, 2:826-838, 2005. doi: 10.2514/6.2005-5933.

- [17] M. Heller, R. David, and J. Holmberg. Falling leaf motion suppression in the f/a-18 hornet with revised flight control software. *AIAA Paper*, pages 5281–5291, 2004. doi: 10.2514/6.2004-542.
- [18] ICAO. *Doc 9803 AN/761 "Line Operations Safety Audit (LOSA)".* 1 edition, 2002.
- [19] ICAO. *Doc 10011 AN/506 "Manual on Aeroplane Upset Prevention and Recovery Training".* 1 edition, 2014.
- [20] D. Kim, G. Oh, Y. Seo, and Y. Kim. Reinforcement learning-based optimal flat spin recovery for unmanned aerial vehicle. *Journal of Guidance, Control, and Dynamics*, 40(4):1074–1081, 2017. doi: 10.2514/1.G001739.
- [21] R. Kristiansen and Hagen D. Modelling of actuator dynamics for spacecraft attitude control. *Journal of Guidance, Control, and Dynamics*, 32(3):1022–1025, 2009. doi: 10.2514/1.42574.
- [22] P.A. Kumar, P.K. Raghavendra, T. Sahai, and N. Ananthkrishnan. Spin recovery of an aircraft using nonlinear dynamic inversion techniques. *AIAA Paper*, pages 101–110, 2004. doi: 10.2514/6.2004-378.
- [23] H.G. Kwatny and H. Kim. Variable structure regulation of partially linearizable dynamics. *Systems and Control Letters*, 15(1):67 – 80, 1990. doi: 10.1016/0167-6911(90)90046-W.
- [24] H.G. Kwatny, J.E.T. Dongmo, B. Chang, G. Bajpai, M. Yasar, and C. Belcastro. Nonlinear analysis of aircraft loss of control. *Journal of Guidance, Control, and Dynamics*, 36(1):149–162, 2013. doi: 10.2514/1.56948.
- [25] T.J.J. Lombaerts, G.H.N. Looye, Q.P. Chu, and J.A. Mulder. Pseudo control hedging and its application for safe flight envelope protection. *AIAA Guidance, Navigation, and Control Conference*, 2010. doi: 10.2514/6.2010-8280.
- [26] Y. Luo, A. Serrani, S. Yurkovich, M.W. Oppenheimer, and D.B. Doman. Model predictive dynamic control allocation with actuator dynamics. In *Proceedings of the 2004 American Control Conference*, volume 2, pages 1695–1700, June 2004.
- [27] Y. Luo, A. Serrani, S. Yurkovich, M.W. Oppenheimer, and D.B. Doman. Model-predictive dynamic control allocation scheme for reentry vehicles. *Journal of Guidance, Control, and Dynamics*, 30(1):100–113, Jan 2007. ISSN 0731-5090. doi: 10.2514/1.25473.
- [28] I. Matamoros and C.C. de Visser. Incremental nonlinear control allocation for a tailless aircraft with innovative control effectors. *AIAA Guidance, Navigation, and Control Conference*, 2018, 2018. doi: 10.2514/6.2018-1116.
- [29] M.A. Niestroy, K.M. Dorsett, and K. Markstein. A tailless fighter aircraft model for control-related research and development. *AIAA Modeling and Simulation Technologies Conference*, 2017, 2017. doi: 10.2514/6.2017-1757.
- [30] M.W. Oppenheimer and D.B. Doman. Methods for compensating for control allocator and actuator interactions. *Journal of Guidance, Control, and Dynamics*, 27(5):922–927, 2004. doi: 10.2514/1.7004.
- [31] M.W. Oppenheimer, D.B. Doman, and M.A. Bolender. *The Control Handbook, Second Edition: Control System Applications (chap. 8)*. Electrical Engineering Handbook. CRC Press, Dec 2010.
- [32] P.K. Raghavendra, T. Sahai, P. Ashwani Kumar, M. Chauhan, and N. Ananthkrishnan. Aircraft spin recovery, with and without thrust vectoring, using nonlinear dynamic inversion. *Journal of Aircraft*, 42(6): 1492–1503, 2005. doi: 10.2514/1.12252.
- [33] H. Ranter. *Airliner Accident Statistics 2006*. Aviation Safety Network, 2007.
- [34] D.M.K.K.V. Rao and N.K. Sinha. Aircraft spin recovery using a sliding-mode controller. *Journal of Guidance, Control, and Dynamics*, 33(5):1675–1678, 2010. doi: 10.2514/1.50186.
- [35] J. Reiner, G.J. Balas, and W.L. Garrard. Flight control design using robust dynamic inversion and time-scale separation. *Automatica*, 32(11):1493–1504, 1996. doi: 10.1016/S0005-1098(96)00101-X.

- [36] A. Sabanovic. Variable structure systems with sliding modes in motion control - a survey. *IEEE Transactions on Industrial Informatics*, 7(2):212–223, 2011. doi: 10.1109/TII.2011.2123907.
- [37] S. Schuet, T.J.J. Lombaerts, J. Kaneshige, K. Shish, and V. Stepanyan. Stall recovery guidance using fast model predictive control. *AIAA Guidance, Navigation, and Control Conference, 2017*, 2017. doi: 10.2514/6.2017-1513.
- [38] S. Sieberling, Q.P. Chu, and J.A. Mulder. Robust flight control using incremental nonlinear dynamic inversion and angular acceleration prediction. *Journal of Guidance, Control, and Dynamics*, 33(6):1732–1742, 2010. doi: 10.2514/1.49978.
- [39] P. Simplício, M.D. Pavel, E. van Kampen, and Q.P. Chu. An acceleration measurements-based approach for helicopter nonlinear flight control using Incremental Nonlinear Dynamic Inversion. *Control Engineering Practice*, 21(8):1065 – 1077, 2013. doi: {10.1016/j.conengprac.2013.03.009}.
- [40] E.J.J. Smeur, Q.P. Chu, and G.C.H.E. de Croon. Adaptive incremental nonlinear dynamic inversion for attitude control of micro air vehicles. *Journal of Guidance, Control, and Dynamics*, 39(3):450–461, Dec 2015. doi: 10.2514/1.G001490.
- [41] R.F. Stengel and W.B. Nixon. Stalling characteristics of a general aviation aircraft. *Journal of Aircraft*, 19(6):425–434, 1982. doi: 10.2514/3.57412.
- [42] G.D. Sweriduk, P.K. Menont, and M.L. Steinberg. Design of a pilot-activated recovery system using genetic search methods. *1999 Guidance, Navigation, and Control Conference and Exhibit*, pages 1–10, 1999. doi: 10.2514/6.1999-4082.
- [43] (USAF) US Air Force. *Manual on Aeroplane Upset Prevention and Recovery Training*. MIL-S-83691A, 1972.
- [44] I. van der Peijl, C.C. de Visser, and M. A. Niestroy. Physical splines for aerodynamic modelling of innovative control effectors. Unpublished thesis, 2017.
- [45] J.E. Wilborn and J.V. Foster. Defining commercial transport loss-of-control: A quantitative approach. *Collection of Technical Papers - AIAA Atmospheric Flight Mechanics Conference*, 1:205–215, 2004. doi: 10.2514/6.2004-4811.
- [46] W. Zhang and H. Chen. Aircraft loss-of-control recovery strategy using high order sliding: Mode control based on optimal trim condition. *16th AIAA Aviation Technology, Integration, and Operations Conference*, pages 1–15, 2016. doi: 10.2514/6.2016-3919.
- [47] Y. Zhao and J.J. Zhu. Aircraft loss-of-control arrest autopilot using trajectory linearization control. *Proceedings of the American Control Conference*, 2016-July:1602–1607, 2016. doi: 10.1109/ACC.2016.7525145.



Conference Paper

Upset Recovery Controller Based on Maximum Control Effectiveness for a High-Performance Over-Actuated Aircraft

D.J. van Oorspronk*

Delft University of Technology, Delft, 2600GB, The Netherlands

Current flight control systems fail to recover to safe flight conditions in off-nominal flight conditions and require a more advanced upset recovery methodology which is able to provide full control authority. Existing upset recovery methods are focused on fast recovery taking into account the current flight conditions while neglecting nonlinear effects. This paper implements a new approach for upset recovery which aims for maximum control effectiveness of control effectors given the flight conditions by means of incremental nonlinear dynamic inversion. A recovery control strategy based on reducing angular body rates and aerodynamic angles generates inner and outer loop commands. Pseudo control inputs defined as required moment increments are derived using a nonlinear Jacobian model of the control effectors. This pseudo control input and Jacobian determine the direction of control effector effectiveness gradient optimization. The upset recovery system is implemented on the Innovative Control Effectors (ICE) aircraft, a high performance over-actuated aircraft with 13 highly nonlinear, interacting and coupled control effectors. Real-time simulation results show that the upset recovery system is fault tolerant, considerably faster, and more reliable compared to nominal flight control in terms of recovering angular body rates and aerodynamic angles, and is applicable in every aircraft upset condition.

Nomenclature

A_x, A_y, A_z	=	Specific forces in body frame
C	=	Dimensionless aerodynamic coefficients
g	=	Gravitational acceleration
I	=	Aircraft inertia
l, m, n	=	Aerodynamic moments in body frame
M	=	Mach number
p, q, r	=	Pitch, roll, and yaw angular rate

*MSc student, Control and Simulation Division, Faculty of Aerospace Engineering, Kluyverweg 1, 2629HS Delft, The Netherlands, dennisvanoorspronk@gmail.com, AIAA Member.

T	= Thrust force
u, v, w	= Airspeed components in body frame
V	= Airspeed
X, Y, Z	= Aerodynamic forces in body frame
α	= Angle of attack
β	= Sideslip angle
δ	= Control effector deflection
ω	= Body angular rates
τ	= Aerodynamic moments
ϕ, θ, ψ	= Roll, pitch, and yaw angle

I. Introduction

Recent statistics show that loss of control (LOC) is the largest contributor of fatal accidents in aviation for commercial and military aircraft [1–5]. In order to increase safety and reduce the number of fatal accidents in aviation, LOC requires more in-depth research. In general LOC is associated with flying outside the save flight envelope, where pilots encounter nonlinear influences such as kinematic coupling, oscillatory or divergent aircraft responses and experience reduced capabilities to control the aircraft [2, 6, 7]. Also high angular rates and displacements together with the lack to maintain aircraft attitude can be expected [2]. Despite the improvements made to reduce aircraft accidents, some factors are still not fully described and well understood [7].

Although modern commercial and military aircraft are equipped with autonomous envelope protection in order to keep the aircraft in the safe envelope, aircraft still end-up in critical regions (upset) due to pilot inputs, aircraft failures, or environmental causes. For these occurrences of flying outside the save envelope where aircraft are not capable of responding to pilot inputs as in nominal flight conditions, upset recovery is essential for preventing a fatal incident. In this context recovery is defined as the capability to control key aircraft states to an acceptable level during off-nominal flight conditions that are specified as LOC [7].

Traditionally, flight control systems have been developed for nominal flight conditions. Since aircraft upsets occur outside the safe nominal flight envelope, development of effective algorithms for off-nominal flight conditions is crucial. Guidance laws that recover the aircraft are investigated, by using a pilot-activated recovery system based on genetic search [8], linear quadratic regulator state feedback controller [9], sliding mode controller [10–12], high order sliding mode controller [13–16], and nonlinear dynamic inversion [17, 18]. Other systems are limited to incomplete pilot recovery guidelines by using reinforcement learning systems [19, 20] or online model predictive control [21]. In order reduce the number of LOC accidents, it is vital to enhance current flight control systems with algorithms that cope with

off-nominal conditions where nonlinear dynamics and uncertainties are present [22].

Flight control systems require a more advanced upset recovery methodology which is able to recover from extreme angles of attack far away from the safe flight envelope. Current methods are more focused on how to recover as fast as possible taking only into account the current states of the aircraft, while neglecting nonlinear aircraft dynamics, control effector nonlinearities, and control effector interactions. However, in off-nominal conditions and full control effector deflections, usage of linear models is of limited value [23, 24]. A new designed method implementing maximum aircraft control effectiveness, is focusing on maximum control authority of an aircraft in critical/upset flight conditions while taking into account nonlinearities.

This paper implements a methodology for designing an aircraft upset recovery system which is able to recover from any type of aircraft upset condition for a high performance over-actuated aircraft. Currently no adequate method in the field of upset recovery is available. Based on maximum control effectiveness of control effectors given the flight condition, key aircraft states are controlled to an acceptable condition within the safe flight envelope. By means of a reformulation of nonlinear dynamics in incremental form, known as incremental nonlinear dynamic inversion (INDI), a pseudo control input defined as the required moment increment generated by control effectors is derived using a nonlinear Jacobian model of the control effectors. This pseudo control input is fundamental in determining the heading of gradient optimization of future control effector deflections for highest aircraft control effectiveness. Inner and outer control loops for determining a pseudo control input are derived from an all-encompassing upset recovery strategy sequence necessary for quick recovery.

The paper is structured as follows. First a description of aircraft upset is given in section II. Next to that incremental nonlinear dynamics are derived from the general equation for nonlinear dynamics in section III. A brief description of the Innovative Control Effectors (ICE) aircraft and corresponding aerodynamic model will be given in section IV. Section V describes the concept of the final design followed by results and simulations that are provided in section VI. Finally, conclusions are drawn and recommendations are presented in section VII.

II. Aircraft Upset Conditions

Aircraft upset can be defined as an undesired aircraft state which is characterized by unintentional exceeding parameters usually experienced during normal operations [25–27]. Defining specific values for aircraft approaching upset condition vary among aircraft specification. However, for airplane upset recovery training programs the following values have been used [25].

- Nose up pitch attitude larger than 25 degrees.
- Nose down pitch attitude smaller than 10 degrees.
- Bank angle larger than 45 degrees.
- Within the above mentioned flight conditions, but at a reasonable low airspeed for current flight parameters.

However, these values are specified for civil aviation and therefore can not be applied to aircraft in general. The remainder of this section discusses the possible causes of aircraft upset in section II.A, followed by critical motions in section II.B that can be caused by these causes, and finally a new upset recovery strategy is defined in section II.C.

A. Causes of Aircraft Upsets

For commercial aircraft, aircraft upset is not a common occurrence. Despite this fact, incidents of this type still occur. This section describes the four most common aircraft upsets. First of all, attention is paid to environmental causes of aircraft upset. A significant number of aircraft upsets are caused by environmental factors where aircraft often have no influence on [25].

- **Turbulence** Turbulent air contains large variations in flow velocity over a short distance. The main causes of turbulence are windshear, jet streams, and wind obstructions.
 - **Clear air turbulence (CAT)** can be encountered at any altitude but is known as high-level turbulence (usually above 15,000 ft.). CAT is mainly caused by jet streams.
 - **Mountain Wave** belongs to the category wind obstruction. In case of severe turbulence it may cause large variations in airspeed and the aircraft might be out of control for some time.
 - **Windshear** is defined as wind variations at low altitude which may cause hazards during take-off and approach. These wind variations are caused by local meteorological conditions.
 - **Thunderstorms** produce strong gusts and high precipitation. Due to accelerating airflow within the storm, large changes in windspeed could occur.
 - **Micro-burst** is defined as a concentrated, more powerful downdraft (downward moving column of air). Micro-bursts occur in convective weather conditions. Still micro-burst accidents occur from which cannot be successfully escaped with known techniques.
- **Wake Turbulence** is the dominant cause of aircraft upset by environmental conditions. Due to high pressure air on the lower wing surface and low pressure air on the upper wing surface, air flows from the lower to the upper surface. This phenomenon creates a pair of counter rotating vortices. Those vortices are generally very strong dependent on mainly the weight of the aircraft. Other aircraft flying into the vortices encounter usually induced roll and pitch moments.
- **Aircraft Icing** causes large aerodynamic performance degradation due to disturbed flow around the airfoil. These adverse effects vary with location and reduced aircraft handling.

Second of all, upset causes due to aircraft (sub component) failure. Over the years, aircraft designs become better and better and are equipped with more safety systems than before. This is required by the ever-improved certification process of aircraft.

The third category is aircraft upset due to pilot control inputs or unawareness. Sensory input can lead to misconception

in the case of low visibility or extreme flight conditions.

Finally there are particular aircraft upset conditions where military aircraft have to deal with more often than commercial aircraft, one of those examples is an in-air missile attack. An impact from such a missile has dramatic impact on the current flight condition of the aircraft depending on the power of the missile warhead and impact location. High angular rates and control effector failures can be expected.

B. Aircraft Critical Motions

Various events can contribute to LOC during the flight mission, these events may depend on the type of mission but may also depend on meteorological, aircraft failure, or pilot induced causes. Investigation of aircraft LOC shows that in flight LOC is much more complicated than just the failure of components and other known factors [5]. Analysis shows that in flight LOC is the consequence of maneuverability near the boundary of the safe flight envelope [13]. Close to the envelope limits smaller control authority due to flight parameters can be expected. The following aircraft critical motions are described.

- **Stall:** An aircraft is in stall conditions if the angle of attack α exceeds the stall angle [13, 25]. The stall angle is the maximum angle at which the wings ability to produce lift is equal to the weight and the aircraft is able to maintain steady flight [28, 29]. Wings can stall at any airspeed and any altitude.
- **Departure:** Defined as the post-stall flight condition which accelerates entry into deep stall, spin, or post-stall gyration. Departure is the aircraft motion that indicates the transition from controlled flight into uncontrolled flight conditions. Departure is characterized by sudden uncommanded aircraft motions [30].
- **Deep stall:** In deep stall conditions the aircraft is unable to generate a nose-down moment. In order to prevent the deep stall from getting worse, turning around the velocity vector is advised [13].
- **Wing rock:** An aircraft is in wing rock mode if dominant oscillation in the roll axis are detected [31]. The motion is characterized by instability of the Dutch roll mode [13].
- **Spin:** A high yaw rate r at angles of attack α above stall angle. Additional body rates may cause oscillation in pitch q and roll p . In the severe case of a fully developed spin, the trajectory is approximately vertical and no major changes in the spin are observed [30].
- **Falling leaf:** The interchange of both aerodynamic and kinematic effects which causes a continuous motion about all three moment axes is called the falling leaf mode [32]. In the case of a falling leaf maneuver the aircraft is wings-level stalled and is forced into a spin motion. At the moment the spin develops, the spin is reversed by opposite rudder such that the spin starts developing in opposite direction.

C. Aircraft Upset Recovery Strategy

To ensure a higher chance of survival for a recovery controller, the controller must have an adequate plan for each flight condition. Setting up a correct strategy plan is therefore essential. Current upset recovery strategies described in [25, 27, 33] are limited to describing recommended procedures for nose-high and nose-low upsets that assume the aircraft is not stalled. These procedures cover only part of the potentially critical motions.

A well defined upset recovery strategy is designed for the entire set of upset conditions, taking into account aerodynamic angles that exceed stall angle. Based upon recommended recovery procedures and multi-mode upset recovery strategy [34], a new strategy is designed. Critical motions are divided into two categories, the first of which consists of high body angular rate critical motions and the second category includes high aerodynamic angles. It is important to first reduce high body angular rates followed by reducing high and unstable aerodynamic angles. The following sequence of actions are defined as aircraft upset recovery strategy, in which the numbers 1, 2, and 3 mainly determine the performance of recovery.

- 1) Start upset recovery
- 2) Reduce angular rates p, q, r
- 3) Recover aerodynamic angles α, β
- 4) Recover attitude angles ϕ, γ
- 5) Recover altitude h and airspeed V
- 6) Normal flight control

This entire upset recovery strategy is visualized in Fig. 1. Rounded square boxes represent the action required, diamonds contain the question if certain flight conditions are satisfied.

III. Incremental Nonlinear Dynamics

In this paper the general equation for nonlinear dynamics is reformulated by writing the equation in incremental form and applying the time scale separation principle. Incremental nonlinear dynamics has been implemented and proven to work in many aerospace applications [35–37]. Section III.A describes the reformulation of the general dynamics into incremental form, followed by section III.B which describes the formulation of control effector constraints into incremental form.

A. Nonlinear Dynamic System

In general, dynamics of an aircraft in upset/critical conditions can be described as Eq. (1).

$$\dot{x}(t) = f(x) + g(x)\tau \quad (1)$$

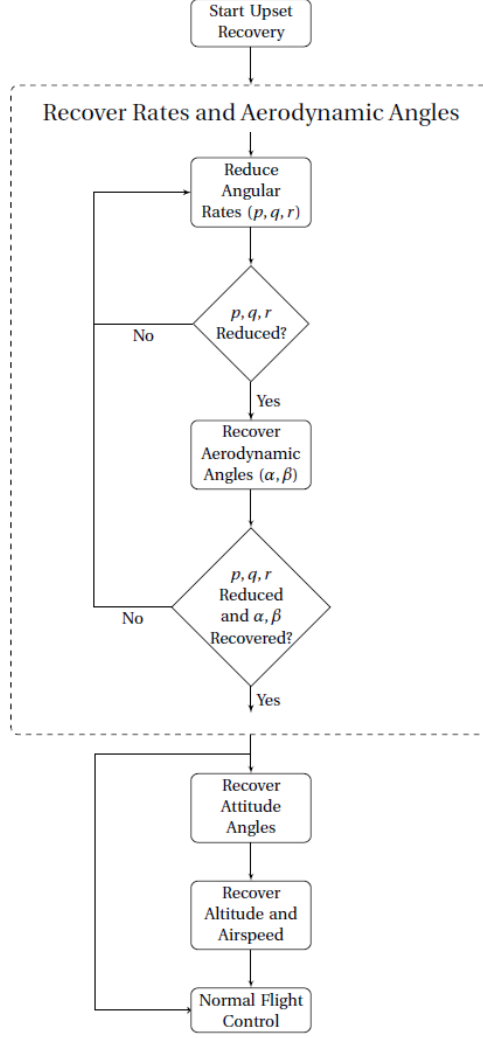


Figure 1 Upset recovery strategy

where $x \in \mathbb{R}^n$ is the state vector containing n scalars, $g(x)$ is control effectiveness, $\tau \in \mathbb{R}^m$ containing the input vector of size m . In Eq. (1) the state equation is only influenced externally by the input vector τ . This τ is often defined as (aerodynamic) moments generated. Equation (2) shows the separation of the largest moment contributors.

$$\tau = \tau_a + \tau_\delta \quad (2)$$

Where τ_a consist of moments generated only by the airframe, and τ_δ of moments generated by control effectors. Model τ_δ for nonlinear functions can be expressed as $\Phi(x, \delta)$ for nonlinear mapping. Here, $\delta \in \mathbb{R}^c$ describes c control effector deflections/positions. For conventional aircraft configurations where control effectors are far apart from each other, the influence of interactions between control effectors is small and can be assumed as separable. However, if multiple control effectors are installed close together, the influence of the interactions will be larger [38]. Equation (2) can be

rewritten for a nonlinear mapping of (aerodynamic) moments generated by the control effectors, this rewritten equation is shown in Eq. (3).

$$\tau = \tau_a + \Phi(x, \delta) \quad (3)$$

By using this aerodynamic control vector formulation the general aircraft dynamics of Eq. (1) can be rewritten as

$$\dot{x} = [f(x) + g(x)\tau_a] + g(x)\Phi(x, \delta) = F(x) + g(x)\Phi(x, \delta) \quad (4)$$

where $F(x)$ contains all the effects that are not generated by the control effectors.

If the flight control system works in a discrete-time scheme, dynamic equations as written in general form in Eq. (4) can be locally linearized at time steps around current state x_0 and control effector position δ_0 as a first-order Taylor expansion equation:

$$\dot{x} \approx \dot{x}_0 + \frac{\partial}{\partial x} [F(x) + g(x)\Phi(x, \delta)](x - x_0) + \frac{\partial}{\partial \delta} [F(x) + g(x)\Phi(x, \delta)](\delta - \delta_0) \quad (5)$$

The time scale separation principle states that if a moment acts on an aircraft, this mainly causes angular rate changes and attitude angles remain roughly the same for small time steps [35, 39, 40]. For Eq. (5) time scale separation may be used since the derivative of the state vector \dot{x} have notably faster dynamics compared to the state itself x . Therefore the second term on the right-hand side of Eq. (5) is small enough to be neglected with high sampling rates. The third term on the right-hand side containing δ changes significantly faster than x in one time step, therefore the influence of δ is expected to be higher. Applying the time scale separation principle to Eq. (5) results into Eq. (6).

$$\dot{x} \approx \dot{x}_0 + \frac{\partial}{\partial \delta} [F(x) + g(x)\Phi(x, \delta)](\delta - \delta_0) \approx \dot{x}_0 + g(x_0) \frac{\partial \Phi(x_0, \delta_0)}{\partial \delta} \Delta \delta \quad (6)$$

Where $g(x)\partial\Phi(x_0, \delta_0)/\partial\delta$ in Eq. (6) represents the control effectiveness Jacobian function that contains (non)linear behavior of control effectors.

Setting the virtual control input $v(x) = \dot{x}$, Eq. (6) can be simplified to

$$v(x) = \dot{x} \approx \dot{x}_0 + g(x_0) \frac{\partial \Phi(x_0, \delta_0)}{\partial \delta} \Delta \delta \quad (7)$$

For a general problem of this form with three moments to be controlled in the equation, the time derivative of the state vector x_0 contains body angular accelerations. These body angular accelerations are sometimes not immediately measurable therefore state estimation methods can be used to obtain those parameters. The system can be linearized by

rewriting Eq. (7) into Eq. (8).

$$\Delta\delta = \left[\frac{\partial\Phi(x_0, \delta_0)}{\partial\delta} \right]^{-1} g(x_0)^{-1} [v(x) - \dot{x}_0] \quad (8)$$

Where $g(x)\partial\Phi(x_0, \delta_0)/\partial\delta$ is the control effectiveness Jacobian and $g(x_0)^{-1}[v(x) - \dot{x}_0]$ the pseudo-control input command. The response between the virtual input $v(x)$ and x is linearized using this control law. The approach in Eq. (8) is also known as INDI which uses the properties of the system together with nonlinear dynamic inversion by using body angular accelerations [35–37]. This body angular acceleration feedback eliminates sensitivity to model mismatch, that certainly occurs close to or in upset conditions. The principle of elimination of model mismatch increases robustness compared with conventional nonlinear dynamic inversion. Furthermore no or little gain scheduling is required in comparison with other nonlinear dynamic inversion methods [35].

B. Incremental Effector Constraints

By rewriting the general nonlinear dynamics of a system in increments, there is also a necessity for a new formulation of control effectors constraints. Control effectors have constraints on deflection angles and deflection rates which in discrete-time are formulated into local constraints due to the deflection rate limits. Due to these constraints, unlimited position increments can not be achieved. Effector position and rate constraints are formulated in Eq. (9) and Eq. (10) respectively.

$$\delta_{min} \leq \delta \leq \delta_{max} \quad (9)$$

$$|\dot{\delta}| \leq \dot{\delta}_{max} \quad (10)$$

In discrete-time environments, rate constraints determine the maximum effector position increment for each time step Δt as can be seen in Eq. (11) [24].

$$\Delta\delta_{max} = \dot{\delta}_{max}\Delta t \quad (11)$$

Using Eq. (11), Eq. (9) can be rewritten as Eq. (12) where incremental position constraints are taken into account in order to define a lower and upper incremental deflection constraint for the current effector position.

$$\delta_l \leq \delta \leq \delta_u \quad (12)$$

with [24]

$$\delta_l = \max(-\dot{\delta}_{max}\Delta t, \delta_{min} - \delta_0) \quad (13)$$

$$\delta_u = \min(\dot{\delta}_{max}\Delta t, \delta_{max} - \delta_0) \quad (14)$$

where δ_l and δ_u selects the most restrictive constraint.

The relations defined in Eq. (13) and Eq. (14) defines at the same time the local search space for maximum control effectiveness optimization.

IV. Innovative Control Effectors Aircraft

The upset recovery flight control system was implemented and tested on Lockheed Martin's Innovative Control Effectors (ICE) simulation aircraft, a highly maneuverable tailless aircraft with unconventional innovative control effectors. The ICE simulation aircraft operates on an extensive high-fidelity aerodynamic model consisting of data for unconventional high aerodynamic angles that are defined as off-nominal flight conditions. A general introduction to the ICE program is provided in section IV.A, next to that the aerodynamic model of the aircraft is described in section IV.B.

A. Innovative Control Effectors

The ICE program was introduced in 1993 in order to investigate innovative methods for aircraft control and stabilization of high performance, low signature fighters over the entire flight envelope. Low signature technologies have led to limitations in the design of a high performance fighter. These low signature related discussion together with a higher requirement for maneuverability are a guideline for devising new concepts for innovative control for fighter aircraft. Two different fighter concepts were introduced. The first one is a land based fighter aircraft developed for the US Air Force which is 65 degrees sweep angle delta wing. The second fighter was designed as a carrier based fighter aircraft which has a 42 degrees leading edge sweep canard-delta wing especially designed for navy purposes.

After evaluating several novel fighter concepts, a control suite consisting of 13 control effectors showed best performance. Besides the conventional control effectors such as elevons, pitch flaps, and multi-axis thrust vectoring, new concepts have also been applied to the design. Control concepts applied were the all moving wing tip (AMT), spoiler slot deflector (SSD), and differential leading edge flap (DLEF). Figure 2 shows the land based baseline configuration that has been used for results and simulations equipped with the control effectors mentioned, where Fig. 3 displays the corresponding planform. Table 1 shows all 13 different control effectors. Maximum position and rate limits are given together with sign convention for what is considered to be a positive deflection. There are three different conventions: Trailing edge up (TEU), trailing edge down (TED), or leading edge down (LED). When the project was initialized back in the mid 1990s, the main part of the research was focused on the aerodynamics of the various control effectors and therefore no actuator dynamics are taken into account [42]. Dynamics of the control effectors are modeled as second-order transfer functions for low and high-bandwidth in Eq. (15) and Eq. (16) respectively. The last column in

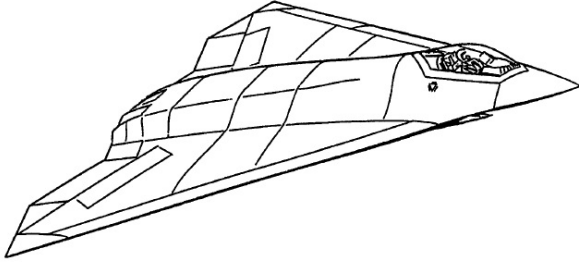


Figure 2 Land based baseline configuration [41]

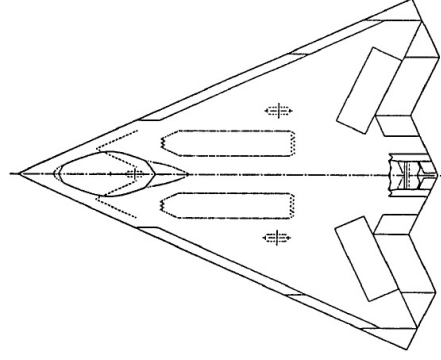


Figure 3 Land based configuration plan-form [41]

Table 1 shows the second order dynamics of each control effector indicated with H_l and H_h .

$$H_l = \frac{1800}{s^2 + 118s + 1800} \quad (15)$$

$$H_h = \frac{4000}{s^2 + 140s + 4000} \quad (16)$$

Table 1 Control effectors overview of the ICE aircraft, sign convention, position and rate limits, abbreviations, and effector dynamics [41, 42].

Control effector	Positive deflection	Position limits [deg]	Rate limits [deg/s]	Abbreviation	Effector dynamics
All moving tips	TED	[0, 60]	150	LAMT, RAMT	H_h
Inboard leading edge flaps	LED	[0, 40]	40	LIBLEF, RIBLEF	H_l
Outboard leading edge flaps	LED	[-40, 40]	40	LOBLEF, ROBLEF	H_l
Elevons	TED	[-30, 30]	150	LEL, REL	H_h
Pitch thrust vectoring	$\dot{q} > 0$	[-15, 15]	150	TVP	H_h
Yaw thrust vectoring	$\dot{p} > 0$	[-15, 15]	150	TVY	H_h
Pitch flaps	TED	[-30, 30]	150	PF	H_h
Spoiler slot deflectors	TEU	[0,60]	150	LSSD, RSSD	H_h

B. Aerodynamic Model of Innovative Control Effector Aircraft

The aerodynamic model of the ICE aircraft that has been used contains nonlinear effects of control effectors, dynamic derivatives, coupling effects between control effectors, aeroelastic effects, and hinge moment derivatives [42]. This aerodynamic model consists of measured data from wind tunnel testing and numerical simulations in which angles of attack in the range [-4, 90] deg, Mach numbers ranging from [0.1, 2.16], and sideslip angles ranging from [-30, 30] have been measured.

This model contains of six different coefficients that represent the aerodynamic force and moment coefficients. There are three main force coefficients defined where the axial component is indicated by C_X , the side component by C_Y , and the normal component by C_Z . The same is done for the moment coefficients where the roll component is indicated by C_l , the pitch component by C_m , and finally the yaw component by C_n . These six main aerodynamic coefficients are further subdivided into sixteen to eighteen sub coefficients. All these aerodynamic sub coefficient represent a state or control effector of the aircraft and are function of aircraft states at the current flight condition. Aerodynamic flexibility factors included in the model will be neglected and are not part of the simulation model. Dimensionless coefficients where $i = \{X, Y, Z, l, m, n\}$ are provided as a summation of nonlinear sub coefficients that depend on current aircraft and control effector state:

$$\begin{aligned}
C_i = & C_{i1}(\alpha, M) + C_{i2}(\alpha, \beta, M) + C_{i3}(\alpha, \beta, \delta_{LIBLEF}) + C_{i4}(\alpha, \beta, \delta_{LIBLEF}, \delta_{OBLEF}, M) \\
& + C_{i5}(\alpha, \delta_{LSSD}, \delta_{LEL}, M) + C_{i6}(\alpha, \delta_{LSSD}, \delta_{RSSD}, \delta_{PF}, M) + C_{i7}(\alpha, \beta, \delta_{LAMT}) \\
& + C_{i8}(\alpha, \delta_{LEL}, \delta_{LAMT}) + C_{i9}(\alpha, \delta_{LOBLEF}, \delta_{LAMT}) + C_{i10}(\alpha, \delta_{REL}, \delta_{RAMT}) \\
& + C_{i11}(\alpha, \delta_{ROBLEF}, \delta_{RAMT}) + C_{i12}(\alpha, \beta, \delta_{LSSD}) + C_{i13}(\alpha, \beta, \delta_{RIBLEF}) \\
& + C_{i14}(\alpha, \beta, \delta_{RIBLEF}, \delta_{ROBLEF}, M) + C_{i15}(\alpha, \delta_{RSSD}, \delta_{REL}, M) + C_{i16}(\alpha, \beta, \delta_{RAMT}) \\
& + C_{i17}(\alpha, \beta, \delta_{RSSD}) + C_{i18}(\alpha, M) + C_{i19}(\alpha, M)
\end{aligned} \tag{17}$$

V. Upset Recovery Controller Design

In order to test the maximum control effectiveness concept for upset recovery, a new flight control system is designed for the ICE aircraft. The all-encompassing strategy from section II designed by extending existing upset strategies for civil aviation, is the origin of the design which is described in section V.A. This all-encompassing strategy is applied to angular body rate control, the innermost loop of the flight control system using the INDI methodology. Different outer loops are implemented for different phases in flight. Pseudo control inputs determine next control effector deflections based on gradient optimization in section V.C. The complete upset recovery controller design is described in section V.E.

A. Upset Recovery Strategy Planner

The brain behind the upset recovery controller is the strategy planner, from this plan the final individual control effector deflections are determined which should return the aircraft back to nominal flight conditions. The most crucial part of the planner is described in the first predefined steps. These steps are first to reduce angular rates (p, q, r) followed by recovering the aerodynamic angles (α, β). The implementation of these two control loops for angular rates and aerodynamic angles is performed using inner and outer control loops.

Reducing states to acceptable levels is an unclear specified level on which a control strategy as described before

is unable to operate. Clear limits are needed to determine whether a given flight condition is inside or outside the safe flight envelope. This is primarily important to judge whether an aircraft is close to departure into upset, but also to determine whether current flight conditions can be considered as safe. Currently, no flight envelope is specified for the ICE aircraft and the proposed safe envelope from literature on upset recovery guidelines does not apply to high-performance aircraft. For this reason, Table 2 presents aircraft dependent data which is determined for describing the flight envelope parameters of the inner and outer control loop.

Table 2 Envelope limits of inner and outer control loop parameters

State	Envelope limit	Unit
p	90	deg/s
q	90	deg/s
r	90	deg/s
α	20	deg
β	20	deg

In the inner control loop of the upset recovery strategy planner, the INDI control methodology has been implemented. This inner loop controls the body angular rates of the aircraft (p, q, r) by calculating the required control moment. Equation (18) shows the general rotational dynamics equation rewritten for a nonlinear control effector model $\Phi(x, \delta)$.

$$\dot{\omega} = I^{-1}(\tau - \omega \times I\omega) = I^{-1}\Phi(x, \delta) + I^{-1}(\tau_a - \omega \times I\omega) \quad (18)$$

where τ is rewritten in Eq 3. In order to calculate the rotational dynamics for each time step, Eq. (18) is locally linearized at current state x_0 and current control effector position δ_0 as a first-order Taylor expansion equation. When controlling in particular rotational dynamics the first-order Taylor expansion becomes

$$\dot{\omega} \approx \dot{\omega}_0 + \frac{\partial}{\partial \omega} [I^{-1}\Phi(x, \delta) + I^{-1}(\tau_a - \omega \times I\omega)](\omega - \omega_0) + \frac{\partial}{\partial \delta} [I^{-1}\Phi(x, \delta) + I^{-1}(\tau_a - \omega \times I\omega)](\delta - \delta_0) \quad (19)$$

Using the time scale separation principle as stated in section III, the second term on the right hand side in Eq. (19) is small enough to be neglected with high sampling rates. This results into Eq. (20) which is written in terms of control input changes $\Delta\delta$ in incremental form.

$$\dot{\omega} = \dot{\omega}_0 + I^{-1} \nabla_{\delta} \Phi(x_0, \delta_0) \Delta\delta \quad (20)$$

Equation (20) can be rewritten by defining the virtual input as body angular acceleration $v(x) = \dot{\omega}$, which results into the following INDI problem formulation

$$I [v(x) - \dot{\omega}_0] = \nabla_{\delta} \Phi(x_0, \delta_0) \Delta\delta = \Delta\tau_{\delta} \quad (21)$$

Pseudo control input $\Delta\tau_\delta$ defines the required increment in moment generated by control effectors, given the current state x_0 and current control effector deflections δ_0 .

After correctly defining the inner most control loop which is fundamental for elaborating the INDI problem, outer control loops can be determined on the basis of kinematic inversion. After reducing body angular rates p, q, r , the next step is to minimize aerodynamic angles to acceptable levels. In order to reduce these angles, the kinematic relationships between those angles and body angular rates are required. A total of two different outer loops are designed: α and β .

A dynamic inversion loop needs to be designed to have a clear definition of the relationship between angle of attack and body angular rates. The dynamic equation can be described by

$$\alpha = \arcsin \frac{w}{V} \quad (22)$$

where the first derivative of Eq. (22) is

$$\dot{\alpha} = \frac{V\dot{w} - w\dot{V}}{V^2\sqrt{1 - \left(\frac{w}{V}\right)^2}} = \frac{\dot{w}}{\sqrt{u^2 + v^2}} - \frac{w\dot{V}}{V\sqrt{u^2 + v^2}} \quad (23)$$

where the following flight dynamics equations may be applied

$$\begin{bmatrix} \dot{u} \\ \dot{v} \\ \dot{w} \end{bmatrix} = \frac{1}{m} \begin{bmatrix} X \\ Y \\ Z \end{bmatrix} - \begin{bmatrix} qw - rv \\ ru - pw \\ pv - qu \end{bmatrix} + g \begin{bmatrix} \sin \theta \\ \sin \phi \cos \theta \\ \cos \phi \cos \theta \end{bmatrix} \quad (24)$$

where the first term on the right hand side of Eq. (24) is the body acceleration in X, Y, Z which can be rewritten into A_x, A_y, A_z . Substituting Eq. (24) into Eq. (23) results in

$$\dot{\alpha} = \frac{1}{\sqrt{u^2 + v^2}} \left[\frac{-uw}{V^2} (A_x - g \sin \theta) - \frac{vw}{V^2} (A_y + g \sin \phi \cos \theta) + \left(1 - \frac{w^2}{V^2}\right) (A_z + g \cos \phi \cos \theta) \right] + \begin{bmatrix} p \\ q \\ r \end{bmatrix} \begin{bmatrix} \frac{-v}{\sqrt{u^2 + v^2}} & \frac{u}{\sqrt{u^2 + v^2}} & 0 \end{bmatrix} \quad (25)$$

When the virtual control input of α is applied on the outer control loop for the input q , the angle of attack dynamic

inversion law is given by Eq. (26).

$$q = \left(v_\alpha - \frac{1}{\sqrt{u^2 + v^2}} \left(\frac{-uw}{V^2} (A_x - g \sin \theta) - \frac{vw}{V^2} (A_y + g \sin \phi \cos \theta) + \left(1 - \frac{w^2}{V^2} \right) (A_z + g \cos \phi \cos \theta) - vp \right) \right) \cdot \left(\frac{u}{\sqrt{u^2 + v^2}} \right)^{-1} \quad (26)$$

Finally the sideslip dynamic inversion is integrated in the outer control loop to compensate for large sideslip angles in upset conditions. This loop is an outer control loop for controlling the yaw rate. The sideslip angle β is given by

$$\beta = \arcsin \frac{v}{V} \quad (27)$$

where the first derivative of Eq. (27) is

$$\dot{\beta} = \frac{V\dot{v} - v\dot{V}}{V^2 \sqrt{1 - \left(\frac{v}{V}\right)^2}} = \frac{\dot{v}}{\sqrt{u^2 + w^2}} - \frac{v\dot{V}}{V\sqrt{u^2 + w^2}} \quad (28)$$

When substituting Eq. (24) into Eq. (28) results in

$$\dot{\beta} = \frac{1}{\sqrt{u^2 + w^2}} \left[\frac{-uv}{V^2} (A_x - g \sin \theta) + \left(1 - \frac{v^2}{V^2} \right) (A_y + g \sin \phi \cos \theta) - \frac{-vw}{V^2} (A_z + g \cos \phi \cos \theta) \right] + \begin{bmatrix} \frac{w}{\sqrt{u^2 + w^2}} & 0 & \frac{-u}{\sqrt{u^2 + w^2}} \end{bmatrix} \begin{bmatrix} p \\ q \\ r \end{bmatrix} \quad (29)$$

When the virtual control input of β is applied on the outer control loop for the input r , the sideslip dynamic inversion law is given by Eq. (30).

$$r = \left(v_\beta - \frac{1}{\sqrt{u^2 + w^2}} \left(\frac{-uv}{V^2} (A_x - g \sin \theta) + \left(1 - \frac{v^2}{V^2} \right) (A_y + g \sin \phi \cos \theta) - \frac{-vw}{V^2} (A_z + g \cos \phi \cos \theta) - wp \right) \right) \cdot \left(\frac{-u}{\sqrt{u^2 + w^2}} \right)^{-1} \quad (30)$$

B. Multivariate Jacobian

The aerodynamic part of the Jacobian control effectiveness matrix is derived from a 0th-order multivariate simplex spline-based aerodynamic model identified from a high-fidelity aerodynamic database of the Lockheed Martin ICE

aircraft [43]. The total number of spline functions to aerodynamic moment for this model is 108. This spline model maintains the aerodynamic structure including nonlinear aerodynamics as stated in Eq. (17). Equation (17) is defined for a six degree of freedom problem where $i = \{X, Y, Z, l, m, n\}$. Calculating the dynamic inversion of the inner loop based on body angular rates only requires the Jacobian of three moment coefficients l, m, n . Using the simplex model the partial derivatives of the aerodynamic moment coefficients C with respect to δ are calculated, in Eq. (31) the control effectiveness Jacobian matrix is defined.

$$\frac{\partial \Phi(x, \delta)}{\partial \delta} = \begin{bmatrix} \frac{\partial C_l(x, \delta)}{\partial \delta_1} & \frac{\partial C_l(x, \delta)}{\partial \delta_2} & \dots & \frac{\partial C_l(x, \delta)}{\partial \delta_c} \\ \frac{\partial C_m(x, \delta)}{\partial \delta_1} & \frac{\partial C_m(x, \delta)}{\partial \delta_2} & \dots & \frac{\partial C_m(x, \delta)}{\partial \delta_c} \\ \frac{\partial C_n(x, \delta)}{\partial \delta_1} & \frac{\partial C_n(x, \delta)}{\partial \delta_2} & \dots & \frac{\partial C_n(x, \delta)}{\partial \delta_c} \end{bmatrix} \quad (31)$$

In Eq. (31), c is defined as the total number of control effectors.

Besides the aerodynamic part of the moment coefficients Jacobian, there are propulsion Jacobian terms generated by the multi-axis thrust vectoring. Analytically the thrust vectoring model equation is given by

$$\tau_T = T d_{c.g.} \begin{bmatrix} 0 \\ -\sin(\delta_{TVP}) \\ -\cos(\delta_{TVP}) \tan(\delta_{TVY}) \end{bmatrix} \quad (32)$$

where τ_T indicates moments generated by the multi-axis thrust vectoring, T thrust force, $d_{c.g.}$ the distance between the multi-axis thrust vectoring and the center of gravity (C.G.), and δ_{TVP} and δ_{TVY} thrust vectoring deflection angles for pitch and yaw respectively. From Eq. (32), Jacobian terms providing the directional derivative of the moments generated by thrust vectoring are shown in Eq. (33).

$$\nabla_{\delta} \tau_T(\delta_{TVP}, \delta_{TVY}) = T d_{c.g.} \begin{bmatrix} 0 & 0 \\ -\cos(\delta_{TVP}) & 0 \\ \sin(\delta_{TVP}) \tan(\delta_{TVY}) & -\frac{\cos(\delta_{TVP})}{\cos^2(\delta_{TVY})} \end{bmatrix} \quad (33)$$

From Eq. (33) it both can be seen that the control effectiveness is highly dependent on the thrust setting of the aircraft, and a higher thrust force results in a higher thrust control effectiveness.

C. Control Effectiveness Optimization

For each individual control effector, there are three moment derivatives l, m, n calculated in the Jacobian model of the control effectiveness matrix. Based on the largest control effectiveness derivative for each control effector, the corresponding moment will be optimized by that particular control effector:

$$d_{on}(c) = \max(\text{abs}(J_d(:, c))) \quad (34)$$

where d_{on} is the control effector effectiveness selection, J_d the control effectiveness Jacobian, and c the number of control effectors (1:c).

It is essential to translate the pseudo-control input which is determined by the commanded states, in a correct way to the corresponding control effector inputs that makes recovery of an aircraft possible. A direction of optimization for each control effector individually is determined based on: as first the individual value of the control effectiveness Jacobian corresponding to one moment and one control effector, and second the pseudo-control input. Based on the pseudo-control input shown in Eq. (21) which is the required control effector induced incremental moment, and the control effectiveness Jacobian, Eq. (21) can be rewritten into Eq. (35).

$$\Delta\delta = \nabla_{\delta}\Phi(x, \delta_0)^{-1}\Delta\tau_{\delta} \quad (35)$$

Equation (35) provides the change in control effector deflections, based on one moment control effectiveness for one control effector. Based on the sign whether this value is positive or negative, a maximum allowed deflection increment is added (Eq. (14)) or subtracted (Eq. (13)) from the current control effector deflection. This discrete-time control input increment is dependent on effector position and rate constraints.

D. Actuator Dynamics Compensation

Actuator dynamics compensation is included in order to improve tracking performance and make use of the full capabilities of the control effectors. Feedforward and feedbackward control loops are designed according to Eq. (36).

$$\delta_{act} = \delta_c + K_P(\delta_c - \delta_0) + K_I \int (\delta_c - \delta_0)dt + K_D \frac{d(\delta_c - \delta_0)}{dt} \quad (36)$$

Where δ_{act} represents the actual control input to the control effectors of the aircraft, δ_c the commanded control effector deflections by the control effectiveness optimization, and δ_0 the current control deflections. For the low- and high-bandwidth actuator transfer functions, the proportional gain is set to 5.5 and 2.5 respectively.

E. Upset Recovery Controller Design Overview

After describing the various components in the upset recovery controller, this section provides a global overview of the various information flows and subsystems. What is striking is that no external control inputs enter the controller in addition to the necessary information of the current states of the aircraft, this makes the upset recovery methodology completely automatic. Figure 4 provides an overview of the design.

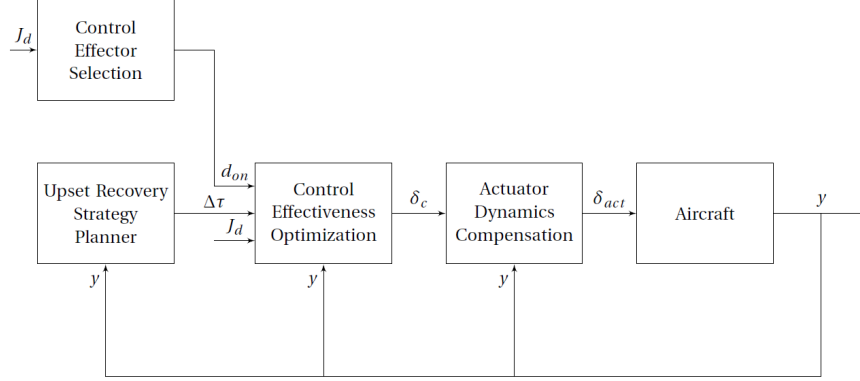


Figure 4 Upset recovery controller design overview

VI. Simulations and Results

This section evaluates the performance of the complete upset recovery system compared to incremental nonlinear control allocation (INCA) flight control system. Simulations shown in this section are performed in a Matlab/Simulink framework using aerodynamic wind tunnel data from the high-fidelity ICE aircraft developed by Lockheed Martin. Computations are solved using a fourth-order Runge-Kutta solver with a fixed sampling rate of 100 Hz. In all the simulations equal gains are used for inner and outer control loops, exact values are listed in Table 3. Important to mention is that all control effector deflections are initialized with 0 degrees, except if the simulation starts from steady trimmed flight to ensure a fair comparison. This section only describes the first two phases of recovery, consisting of reducing body angular rates and recovering aerodynamic angles. Simulating subsequent phases such as attitude recovery is unnecessary and mitigates the clear results of the upset recovery controller.

INCA captures nonlinearities and interactions of control effectors in a real-time control allocation flight control system by using an incremental reformulation of the control allocation problem [44]. This flight control system relies on body angular accelerations in order to reduce model dependencies. To make the comparison, the INCA control allocation method is used together with the angular body rate controller described in [44] without external control inputs. Simulations of deep stall and yaw spin are shown in section VI.A. Furthermore, section VI.B shows how the externally caused upsets (strong gust and missile impact) are recovered. Finally fault tolerant capabilities are simulated in section VI.C.

Table 3 Gains used during simulation of upset recovery controller

	Proportional
p	3.5
q	6.5
r	2.5
α	4.0
β	2.0

A. Critical Upset Motions

There are very specific aircraft motions that are characterized by flying outside the safe flight envelope. In section II an introduction has been given to these particular motions.

The first set of simulations consist of initial conditions that are specified as deep stall with almost zero airspeed. This deep stall upset is initialized with the following most important flight parameters: $h = 20,000$ ft, $V = 10$ ft/s, $\theta = 90$ deg, and $\alpha = 89$ deg. This upset condition is simulated in this section where Fig. 5 and Fig. 6 show body angular rate and aerodynamic angles responses respectively. INCA control system again is aiming for minimizing angular body

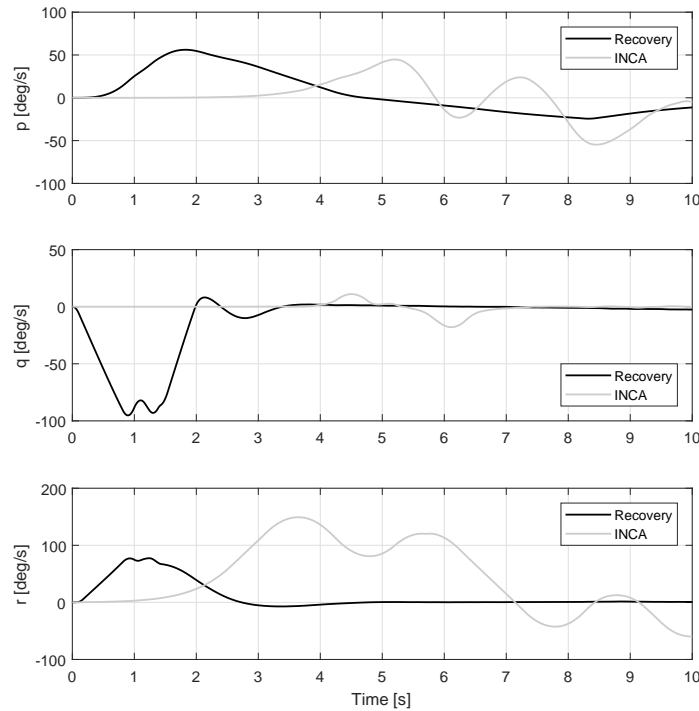


Figure 5 Body angular rates in a deep stall upset at zero airspeed

rates, this time with the consequence of making aircraft even more unstable and entering a second upset. This is a typical LOC condition in which an incorrect strategy has been applied and high aerodynamic angles are obtained. After

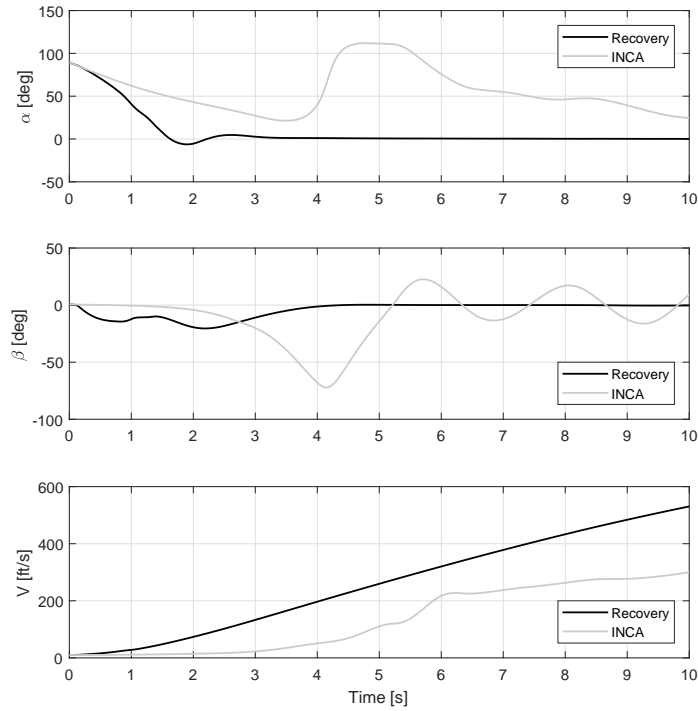


Figure 6 Aerodynamic angles in a deep stall upset at zero airspeed

10 seconds the aircraft is still not able to fully recover. The upset recovery system on the other hand, reduces the angle of attack as quickly as possible by keeping the same time in the flight envelope for all three angular body rates. This results in a rapid decrease of angle of attack and a stable aircraft within 4 seconds. Only small oscillations in sideslip angle can be seen compared with the INCA controller which reaches 80 degrees sideslip angle.

The second set of simulations consist of initial conditions that are specified as a spin. In order to simulate the resulting performance, the following most important flight parameters are defined: $h = 24,000$ ft, $V = 184$ ft/s, $\alpha = 86$ deg, and $r = 500$ deg/s. A comparison in body angular rate and aerodynamic angle responses between the current INCA flight control system and the upset recovery flight control system are shown in Fig. 7 and Fig. 8 respectively. First point to notice is the faster reducing yaw rate by the upset recovery system. In about 4.5 seconds the aircraft is fully recovered from the spinning motion, 1 second faster compared to the INCA flight control system. This fast result is mainly due to the difference in control effector optimization and actuator dynamics compensation. The pitch rate is also minimized faster and more stable, until the moment that all angular rates are within the flight envelope. The sudden increase in pitch rate is caused by the reduction of the high angle of attack. Important to point out is the smaller oscillation in sideslip angle for the upset recovery system due to faster reduction of the yaw rate. At the end it can be concluded that the upset recovery system is able to recover the aircraft to acceptable flight conditions about 2 seconds faster compared to INCA flight control system which is not optimized for upset recovery.

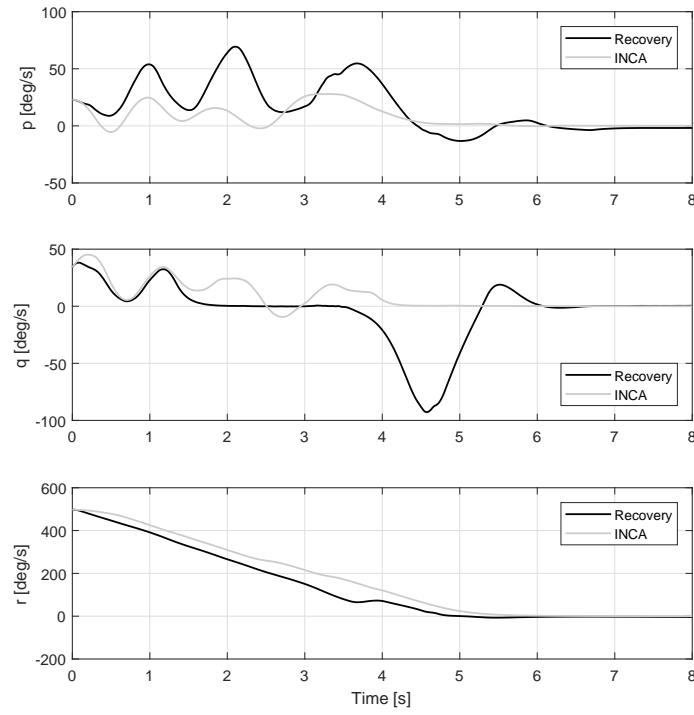


Figure 7 Body angular rates in a yaw spin upset

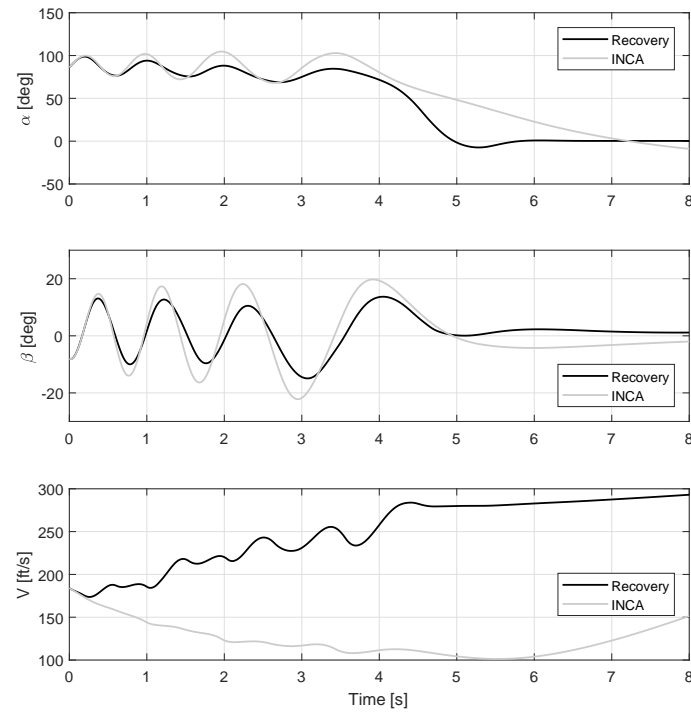


Figure 8 Aerodynamic angles in a yaw spin upset

B. External Caused Aircraft Upsets

Causes of upset can be separated into four different categories, one of them is mission dependent causes. Impact of a missile has direct impact on the dynamics of an aircraft, a combination of external moments due to pressure explosion results in spinning motions. To simulate the impact of a missile on the aircraft, an external moment is applied on the roll and pitch axis at time 3.0 seconds. A step input provides the additional moment on the axes for a fixed time period of 0.1 seconds to ensure that it approximates an impulse moment input. Properties known about the close explosion impact are described in Table 4. The following important flight parameters are used: $h = 20,000$ ft and $V = 880$ ft/s. A comparison

Table 4 Close explosion moment properties of missile impact

Axis	Lbf ft	Nm
l	6.6e6	8.9e6
m	-1.0e7	-1.4e7
n	0	0

in body angular rate and aerodynamic angle responses between the current INCA flight control system and the upset recovery flight control system are shown in Fig. 9 and Fig. 10 respectively. Due to the impulse in moment, angular

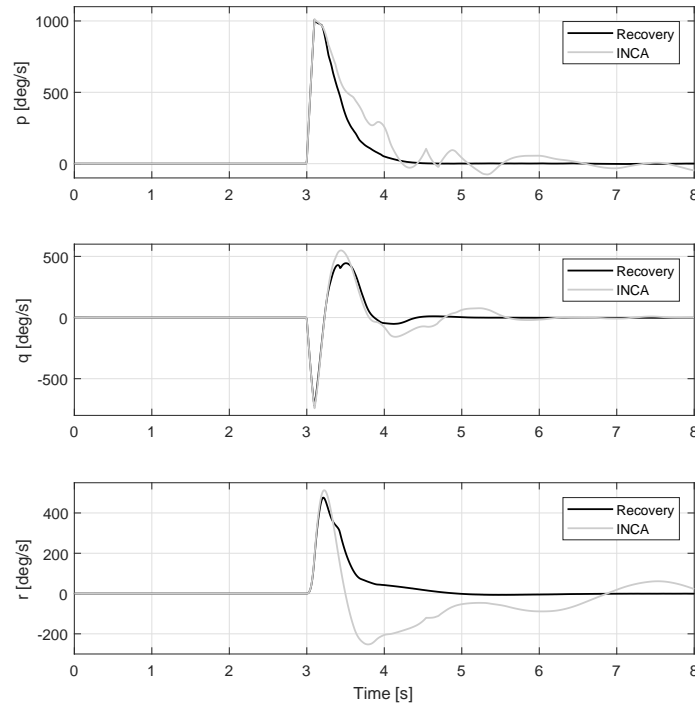


Figure 9 Body angular rates while being hit by missile

body rates of 1000, 500, and 500 are achieved for respective roll, pitch, and yaw. The simulation of the upset recovery system achieves slightly smaller body angular rates compared to INCA. The system stabilizes relatively quickly, all rates

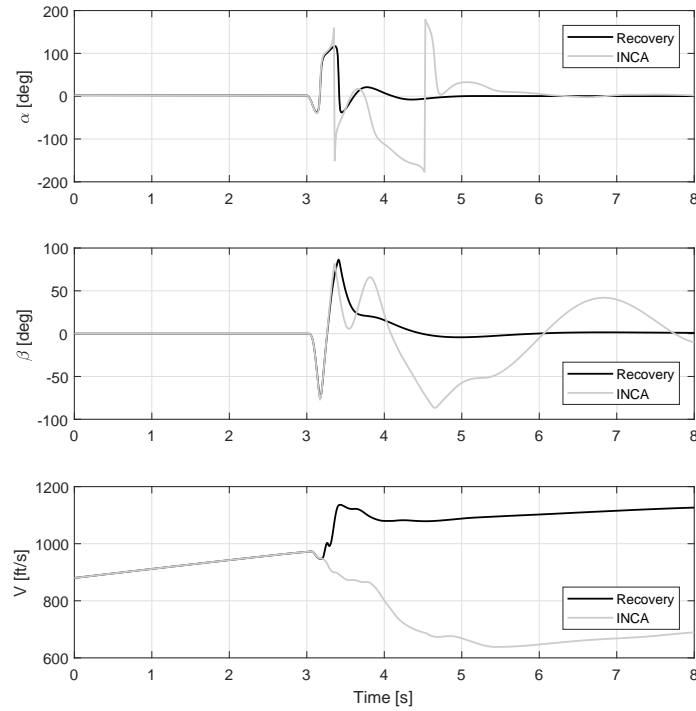


Figure 10 Aerodynamic angles while being hit by missile

are minimized within just 1 second. INCA system encounters many more problems with reducing body angular rates. This problem is mainly because of the high aerodynamic angles in particular angle of attack which reaches values of 180 degrees. Followed by highly unstable sideslip angles that reach up to 90 degrees. The upset motion is still not completely stable after 8 seconds due to the sideslip angle which is not directly compensated by control loops.

C. Fault Tolerant Control Capabilities

Aircraft failure could be one of the reasons to end up in upset conditions. In order to simulate fault tolerant capabilities, again the missile impact simulation is used. At time 3.0 seconds a rotational moment described in Table 5 for a fixed time period of 0.1 seconds is applied. Again the same flight parameters are used: $h = 20,000$ ft and $V = 880$

Table 5 Fault tolerant close explosion moment properties of missile impact

Axis	Lbf ft	Nm
l	5.0e6	6.8e6
m	-9.5e6	-1.3e7
n	0	0

ft/s. A comparison in body angular rate and aerodynamic angle responses between the current INCA flight control system and the upset recovery flight control system are shown in Fig. 11 and Fig. 12 respectively. The first entry in

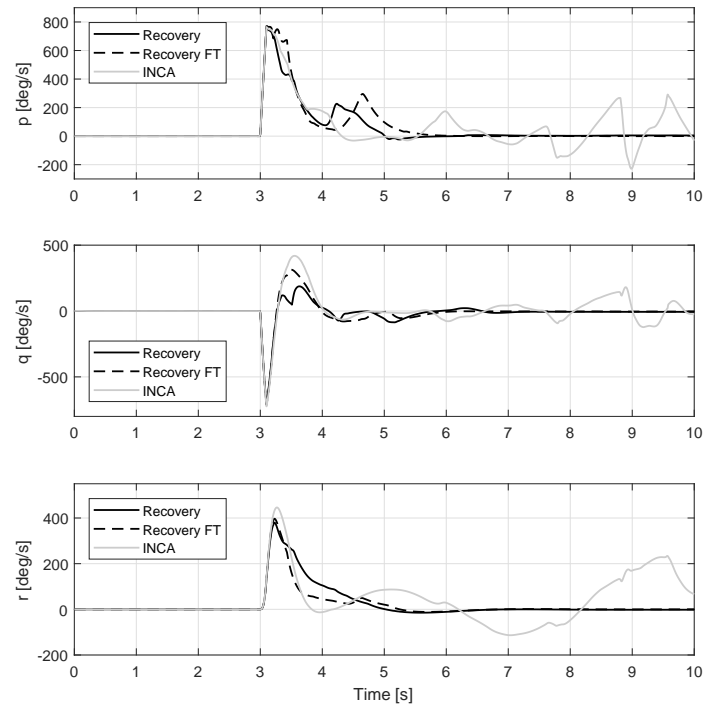


Figure 11 Body angular rates while being hit by missile and failure in left wing for "Recovery FT"

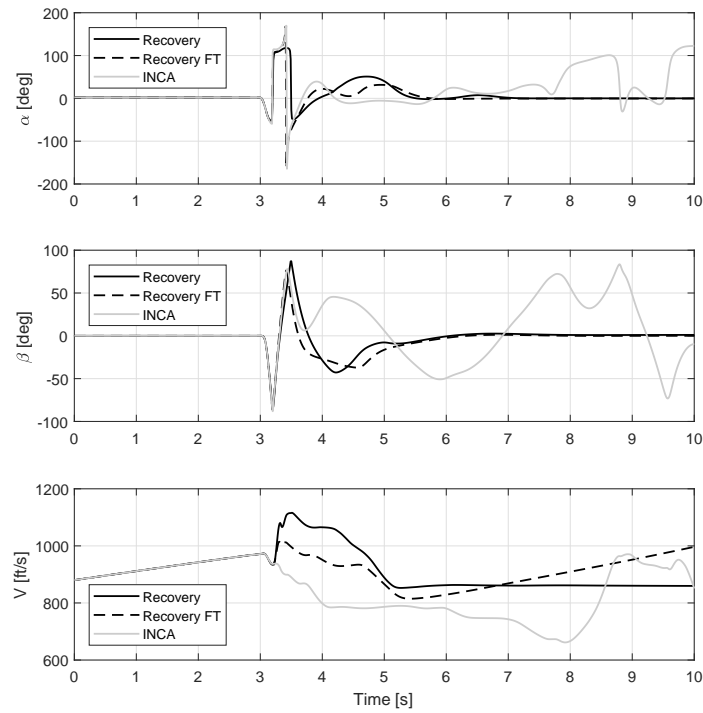


Figure 12 Aerodynamic angles while being hit by missile and failure in left wing for "Recovery FT"

the legend indicated with "Recovery" shows the performance of the upset recovery system with full control authority. Followed by the second entry indicated as "Recovery FT" shows fault tolerant capabilities where control effectors have been fixed at a certain deflection. For the INCA controller all control effectors have full control capabilities indicated with "INCA". For "Recovery FT" all control effectors at the leading and trailing edge of the left wing are fixed at a zero control deflection (δ_{LIBLEF} , δ_{LOBLEF} , δ_{LAMT} , δ_{LEL}) after impact. What can be seen in Fig. 11 and Fig. 12 is that the upset recovery system is capable of recovering the aircraft within 6 seconds both for failure and nominal case. More oscillations reaching higher values can be observed for the failure case, mainly due to the reduced control authority in roll and pitch direction. Compared to INCA, the upset recovery shows improved performance while having reduced control authority in failure case. INCA control is not able to stabilize the aircraft within 10 seconds due to highly oscillating unstable aerodynamic angles.

VII. Conclusions and Recommendations

Adequate upset recovery controllers are necessary in order to increase safety and reduce the number of fatal accidents in aviation. In those extreme flight conditions aircraft encounter nonlinear influences such as kinematic coupling, oscillatory or divergent aircraft responses and reduced control capabilities. Neglecting these effects results in underutilization of aircraft control capabilities and maneuverability in aircraft upset conditions. In this paper an innovative method for aircraft upset recovery has been implemented that is able from the general essence of recovery to return from any aircraft upset condition to safe flight conditions. This methodology for upset recovery performs accurate, efficient, and robust recovery maneuvers and is suitable for real-time implementation in already existing flight control systems of high performance over-actuated aircraft.

The concept is based on the INDI principle which determines incremental control induced moments based on commanded inner and outer control loops from the upset recovery planner and current dynamics of the system. The innermost body angular acceleration control loop which is simultaneously implemented in the first phase of the upset recovery control strategy, reduces model dependency, therefore introduces fault tolerant capabilities, and makes the system robust against mismatch of the aerodynamic model. Using these control induced moments individual control effectors deflections are optimized based on a control effectiveness Jacobian model that takes into account aerodynamic interactions and non-linearities between control effectors, furthermore this concept does not require further details of an aerodynamic model. Individual control effectors are optimized by means of focusing on maximum control effectiveness of the aircraft based on the current state of the aircraft.

The recovery capabilities of the upset recovery system and INCA are compared by simulating a deep stall situation, a fully developed spin, and a missile impact upset condition. The performance of the flight control systems is based on body angular rates and aerodynamic angles which monitor the fundamental states of an aircraft to identify upset. In all simulated aircraft upset condition the performance of the upset recovery system was considerably faster and more

reliable compared to INCA in terms of recovering angular body rates and aerodynamic angles. The main reason for this performance increase is due to the difference in control methodology. Where INCA is only focusing on reducing body angular rates to zero and fully neglecting severe aerodynamic angles that might result in departure into a second upset, is the upset recovery system first also focusing on reducing the angular body rates to acceptable levels within the flight envelope followed by fast reduction of aerodynamic angles such that the aircraft accommodates to nominal flight conditions more quickly.

Results from simulations showed significant improvements in terms of recovering the aircraft en returning to the safe flight envelope. In deep stall condition, angular rates and aerodynamic angles are recovered within 3.0 seconds to stable flight conditions even though the angle of attack was initiated at values larger than 80 degrees. The same is true for fully developed spins, where the upset recovery controller is stabilized after 5.0 seconds from a 500 deg/s yaw spin, shows the INCA controller still unstable responses after 7.0 seconds of simulation time. Simulating missile impact results into an extremely fast recovery by the upset recovery system within just 1.0 second, where INCA requires more than 5.0 seconds to get close to stable flight dynamics and aerodynamic angles. Finally, fault tolerant capabilities as an additional features is simulated. Fault tolerant capabilities were tested for a missile impact situation where all left wing leading and trailing edge control effectors are deactivated after impact. Larger fluctuations in body angular rates were observed but the final performance approximates the performance of the upset recovery controller with full control over control effectors.

References

- [1] Foster, J., Cunningham, K., Fremaux, C., Shah, G., Stewart, E., Rivers, R., Wilborn, J., and Gato, W., "Dynamics modeling and simulation of large transport airplanes in upset conditions," *Collection of Technical Papers - AIAA Guidance, Navigation, and Control Conference*, Vol. 2, 2005, pp. 826–838. doi:10.2514/6.2005-5933.
- [2] Wilborn, J., and Foster, J., "Defining commercial transport loss-of-control: A quantitative approach," *Collection of Technical Papers - AIAA Atmospheric Flight Mechanics Conference*, Vol. 1, 2004, pp. 205–215. doi:10.2514/6.2004-4811.
- [3] Ranter, H., *Airliner Accident Statistics 2006*, Aviation Safety Network, 2007.
- [4] Boeing, "Statistical Summary of Commercial Jet Aircraft Accidents: Worldwide Operations, 1959-2015," *Boeing Commercial Airplane*, Seattle, WA, 2016.
- [5] Belcastro, C., "Loss of control prevention and recovery: Onboard guidance, control, and systems technologies," *AIAA Guidance, Navigation, and Control Conference 2012*, 2012. doi:10.2514/6.2012-4762.
- [6] Kwatny, H., Dongmo, J., Chang, B., Bajpai, G., Yasar, M., and Belcastro, C., "Nonlinear analysis of aircraft loss of control," *Journal of Guidance, Control, and Dynamics*, Vol. 36, No. 1, 2013, pp. 149–162. doi:10.2514/1.56948.
- [7] Dongmo, J., "Aircraft loss - Of - Control recovery using feedback linearization and high order sliding mode control," *AIAA Guidance, Navigation, and Control Conference 2012*, 2012. doi:10.2514/6.2012-4548.

- [8] Sweriduk, G., Menont, P., and Steinberg, M., "Design of a pilot-activated recovery system using genetic search methods," *1999 Guidance, Navigation, and Control Conference and Exhibit*, 1999, pp. 1–10. doi:10.2514/6.1999-4082.
- [9] Chang, B., Kwatny, H., Ballouz, E., and Hartman, D., "Aircraft trim recovery from highly nonlinear upset conditions," *2016 AIAA Guidance, Navigation, and Control Conference*, 2016. doi:10.2514/6.2016-0880.
- [10] Rao, D., and Sinha, N., "Aircraft spin recovery using a sliding-mode controller," *Journal of Guidance, Control, and Dynamics*, Vol. 33, No. 5, 2010, pp. 1675–1678. doi:10.2514/1.50186.
- [11] Sabanovic, A., "Variable structure systems with sliding modes in motion control - A survey," *IEEE Transactions on Industrial Informatics*, Vol. 7, No. 2, 2011, pp. 212–223. doi:10.1109/TII.2011.2123907.
- [12] Zhao, Y., and Zhu, J., "Aircraft loss-of-control arrest autopilot using trajectory linearization control," *Proceedings of the American Control Conference*, Vol. 2016-July, 2016, pp. 1602–1607. doi:10.1109/ACC.2016.7525145.
- [13] Dongmo, J., and Kwatny, H., "Aircraft Loss-of-control Prevention and Recovery: A Hybrid Control Strategy," Ph.D. thesis, Drexel University, 2010.
- [14] Dongmo, J., "Aircraft loss - Of - Control recovery using feedback linearization and high order sliding mode control," *AIAA Guidance, Navigation, and Control Conference 2012*, 2012. doi:10.2514/6.2012-4548.
- [15] Zhang, W., and Chen, H., "Aircraft loss-of-control recovery strategy using high order sliding: Mode control based on optimal trim condition," *16th AIAA Aviation Technology, Integration, and Operations Conference*, 2016, pp. 1–15. doi:10.2514/6.2016-3919.
- [16] Dongmo, J., "Aircraft loss - Of - Control recovery using optimal high order sliding mode control with discontinuous high order observers," *AIAA Guidance, Navigation, and Control Conference 2012*, 2012. doi:10.2514/6.2012-4545.
- [17] Raghavendra, P., Sahai, T., Ashwani Kumar, P., Chauhan, M., and Ananthkrishnan, N., "Aircraft spin recovery, with and without thrust vectoring, using nonlinear dynamic inversion," *Journal of Aircraft*, Vol. 42, No. 6, 2005, pp. 1492–1503. doi:10.2514/1.12252.
- [18] Kumar, P., Raghavendra, P., Sahai, T., and Ananthkrishnan, N., "Spin recovery of an aircraft using nonlinear dynamic inversion techniques," *AIAA Paper*, 2004, pp. 101–110. doi:10.2514/6.2004-378.
- [19] Dutoi, B., Richards, N., Gandhi, N., Ward, D., and Leonard, J., "Hybrid robust control and reinforcement learning for optimal upset recovery," *AIAA Guidance, Navigation and Control Conference and Exhibit*, 2008. doi:10.2514/6.2008-6502.
- [20] Kim, D., Oh, G., Seo, Y., and Kim, Y., "Reinforcement learning-based optimal flat spin recovery for unmanned aerial vehicle," *Journal of Guidance, Control, and Dynamics*, Vol. 40, No. 4, 2017, pp. 1074–1081. doi:10.2514/1.G001739.
- [21] Schuet, S., Lombaerts, T., Kaneshige, J., Shish, K., and Stepanyan, V., "Stall recovery guidance using fast model predictive control," *AIAA Guidance, Navigation, and Control Conference, 2017*, 2017. doi:10.2514/6.2017-1513.

- [22] Crespo, L., Kenny, S., Cox, D., and Murri, D., “Analysis of control strategies for aircraft flight upset recovery,” *AIAA Guidance, Navigation, and Control Conference 2012*, 2012. doi:10.2514/6.2012-5026.
- [23] Doman, D., and Oppenheimer, M., “Improving Control Allocation Accuracy for Nonlinear Aircraft Dynamics,” *AIAA Guidance, Navigation, and Control Conference and Exhibit*, 2002. doi:10.2514/6.2002-4667.
- [24] Oppenheimer, M., and Doman, D., “Methods for compensating for control allocator and actuator interactions,” *Journal of Guidance, Control, and Dynamics*, Vol. 27, No. 5, 2004, pp. 922–927. doi:10.2514/1.7004.
- [25] Carbaugh, D., Rockliff, L., and Vandal, B., *Airplane Upset Recovery Training Aid Revision 2*, ICAO, 2008.
- [26] ICAO, *Doc 9803 AN/761 "Line Operations Safety Audit (LOSA)"*, 1st ed., 2002.
- [27] ICAO, *Doc 10011 AN/506 "Manual on Aeroplane Upset Prevention and Recovery Training"*, 1st ed., 2014.
- [28] Stengel, R., and Nixon, W., “Stalling characteristics of a general aviation aircraft,” *Journal of Aircraft*, Vol. 19, No. 6, 1982, pp. 425–434. doi:10.2514/3.57412.
- [29] Brandon, J., “Dynamic Stall Effects And Applications To High Performance Aircraft,” *Special Course on Aircraft Dynamics at High Angles of Attack: Experiments and Modeling*, , No. AGARD Report No. 776, 1995, pp. 2–1 – 2–15.
- [30] US Air Force, U., *Manual on Aeroplane Upset Prevention and Recovery Training*, MIL-S-83691A, 1972.
- [31] Kwatny, H., and Kim, H., “Variable structure regulation of partially linearizable dynamics,” *Systems and Control Letters*, Vol. 15, No. 1, 1990, pp. 67 – 80. doi:10.1016/0167-6911(90)90046-W.
- [32] Heller, M., David, R., and Holmberg, J., “Falling leaf motion suppression in the F/A-18 hornet with revised flight control software,” *AIAA Paper*, 2004, pp. 5281–5291. doi:10.2514/6.2004-542.
- [33] Eagles, R., *Guidance Material and Best Practices for the Implementation of Upset Prevention and Recovery Training*, Safety and Flight Operations, International Air Transport Association, 2015.
- [34] Engelbrecht, J., Pauck, S., and Peddle, I., “A Multi-mode upset recovery flight control system for large transport aircraft,” *AIAA Guidance, Navigation, and Control (GNC) Conference*, 2013. doi:10.2514/6.2013-5172.
- [35] Sieberling, S., Chu, Q., and Mulder, J., “Robust flight control using incremental nonlinear dynamic inversion and angular acceleration prediction,” *Journal of Guidance, Control, and Dynamics*, Vol. 33, No. 6, 2010, pp. 1732–1742. doi:10.2514/1.49978.
- [36] Smeur, E., Chu, Q., and de Croon, G., “Adaptive Incremental Nonlinear Dynamic Inversion for Attitude Control of Micro Air Vehicles,” *Journal of Guidance, Control, and Dynamics*, Vol. 39, No. 3, 2015, pp. 450–461. doi:10.2514/1.G001490.
- [37] Simplicio, P., Pavel, M., van Kampen, E., and Chu, Q., “An acceleration measurements-based approach for helicopter nonlinear flight control using Incremental Nonlinear Dynamic Inversion,” *Control Engineering Practice*, Vol. 21, No. 8, 2013, pp. 1065 – 1077. doi:{10.1016/j.conengprac.2013.03.009}.

- [38] Oppenheimer, M., Doman, D., and Bolender, M., *The Control Handbook, Second Edition: Control System Applications* (chap. 8), Electrical Engineering Handbook, CRC Press, 2010.
- [39] Lombaerts, T., Looye, G., Chu, Q., and Mulder, J., “Pseudo control hedging and its application for safe flight envelope protection,” *AIAA Guidance, Navigation, and Control Conference*, 2010. doi:10.2514/6.2010-8280.
- [40] Reiner, J., Balas, G., and Garrard, W., “Flight control design using robust dynamic inversion and time-scale separation,” *Automatica*, Vol. 32, No. 11, 1996, pp. 1493–1504. doi:10.1016/S0005-1098(96)00101-X.
- [41] Dorsett, K., and Mehl, D., *Innovative Control Effectors (ICE)*, Lockheed Martin Tactical Aircraft Systems, 1996.
- [42] Niestroy, M., Dorsett, K., and Markstein, K., “A tailless fighter aircraft model for control-related research and development,” *AIAA Modeling and Simulation Technologies Conference, 2017*, 2017. doi:10.2514/6.2017-1757.
- [43] van der Peijl, I., de Visser, C., and Niestroy, M. A., “Physical Splines for Aerodynamic Modelling of Innovative Control Effectors,” 2017. Unpublished thesis.
- [44] Matamoros, I., and de Visser, C., “Incremental nonlinear control allocation for a tailless aircraft with innovative control effectors,” *AIAA Guidance, Navigation, and Control Conference, 2018*, 2018. doi:10.2514/6.2018-1116.

B

Additional Results

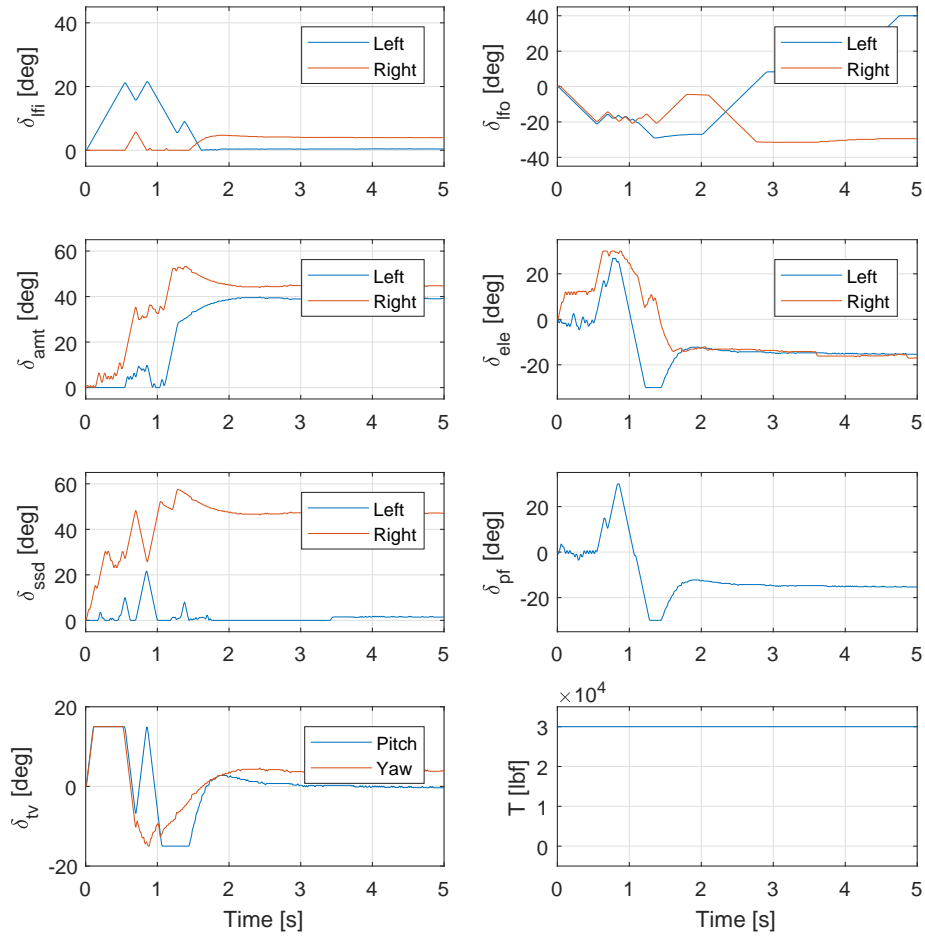


Figure B.1: Control effector inputs during low speed deep stall recovery

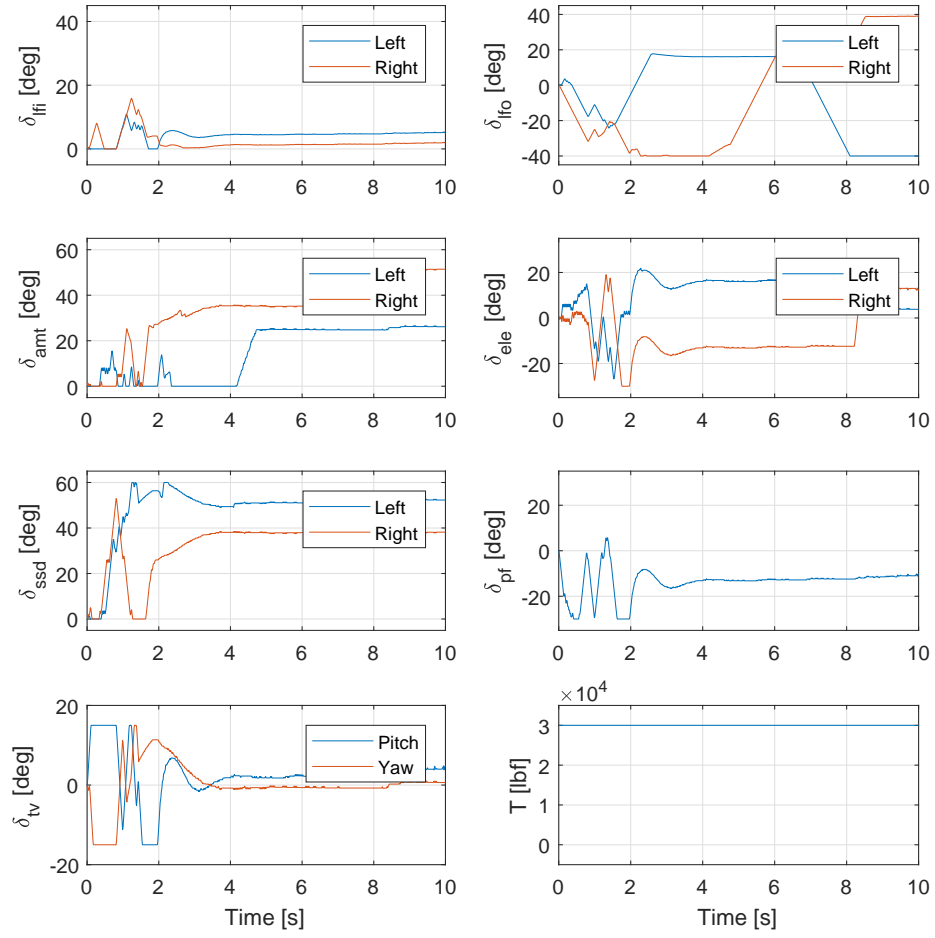


Figure B.2: Control effector inputs during zero speed deep stall recovery

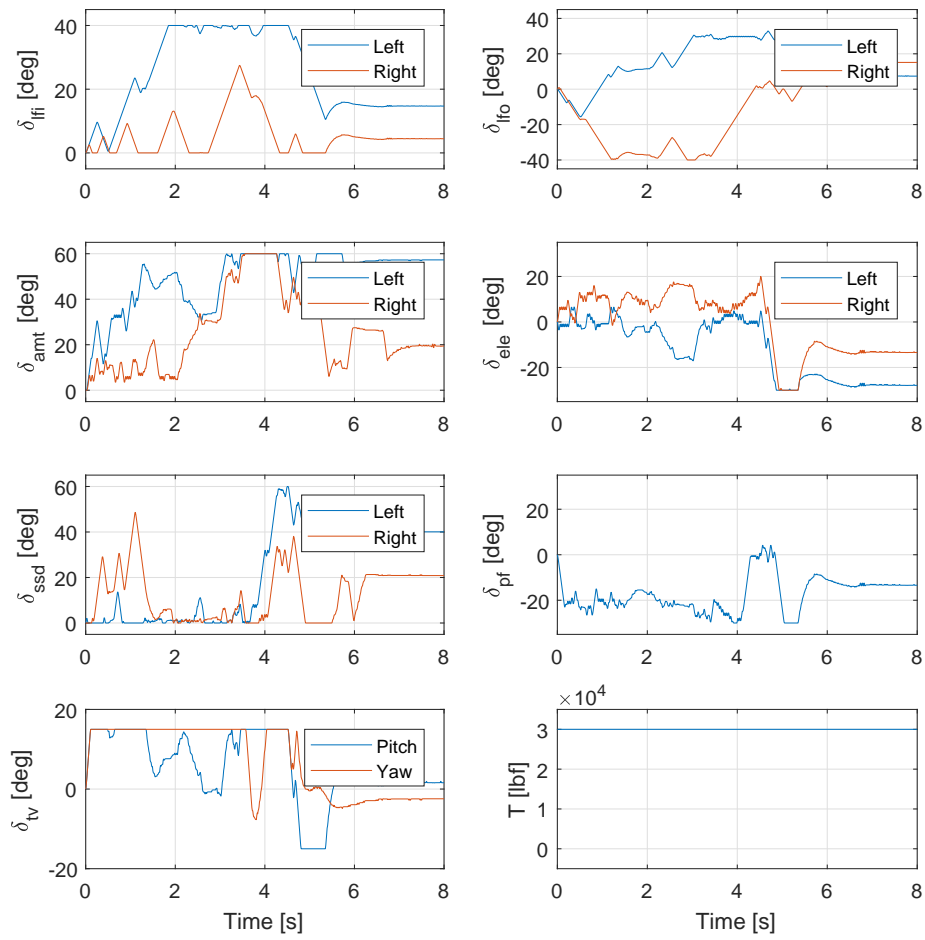


Figure B.3: Control effector inputs during yaw spin recovery

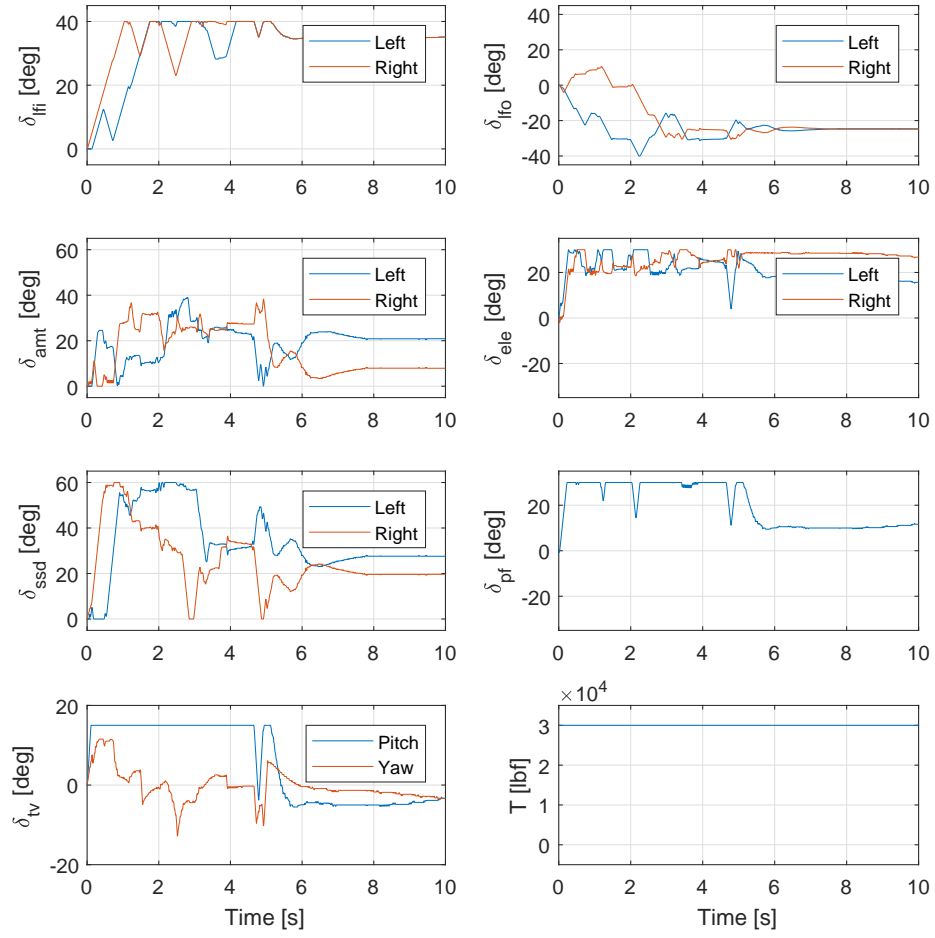


Figure B.4: Control effector inputs during pitch spin recovery

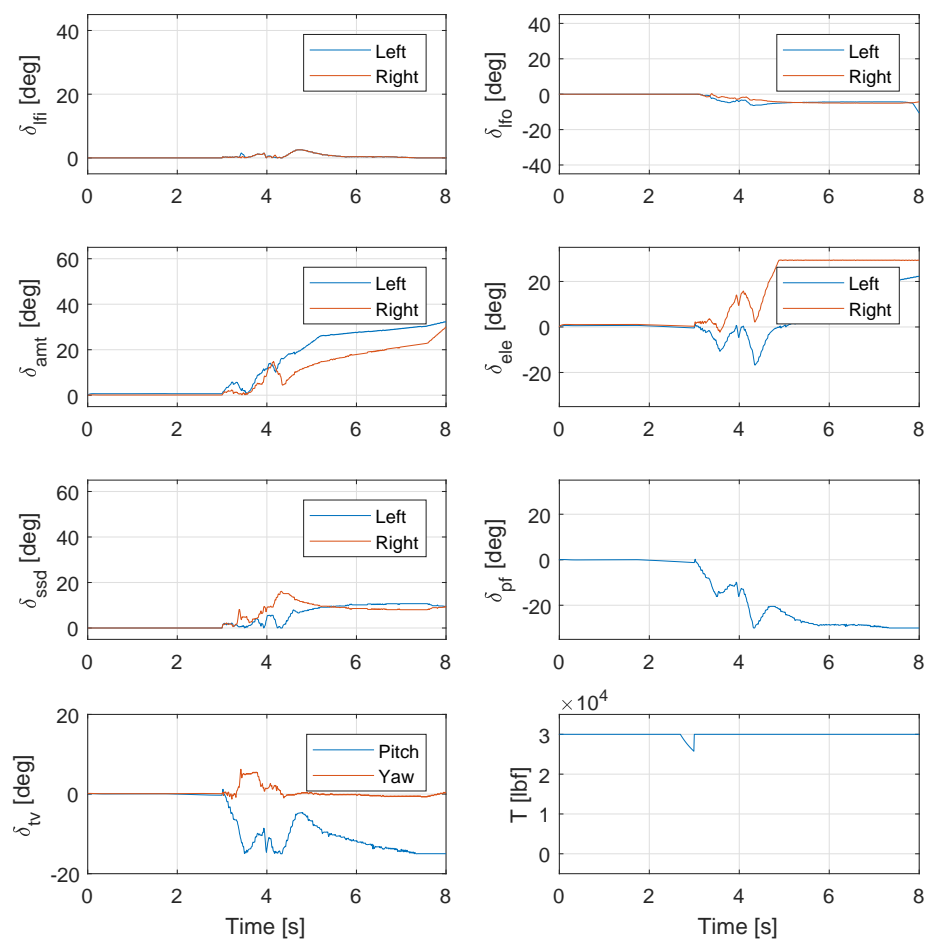


Figure B.5: Control effector inputs while encountering a 1,000 ft/s wind gust

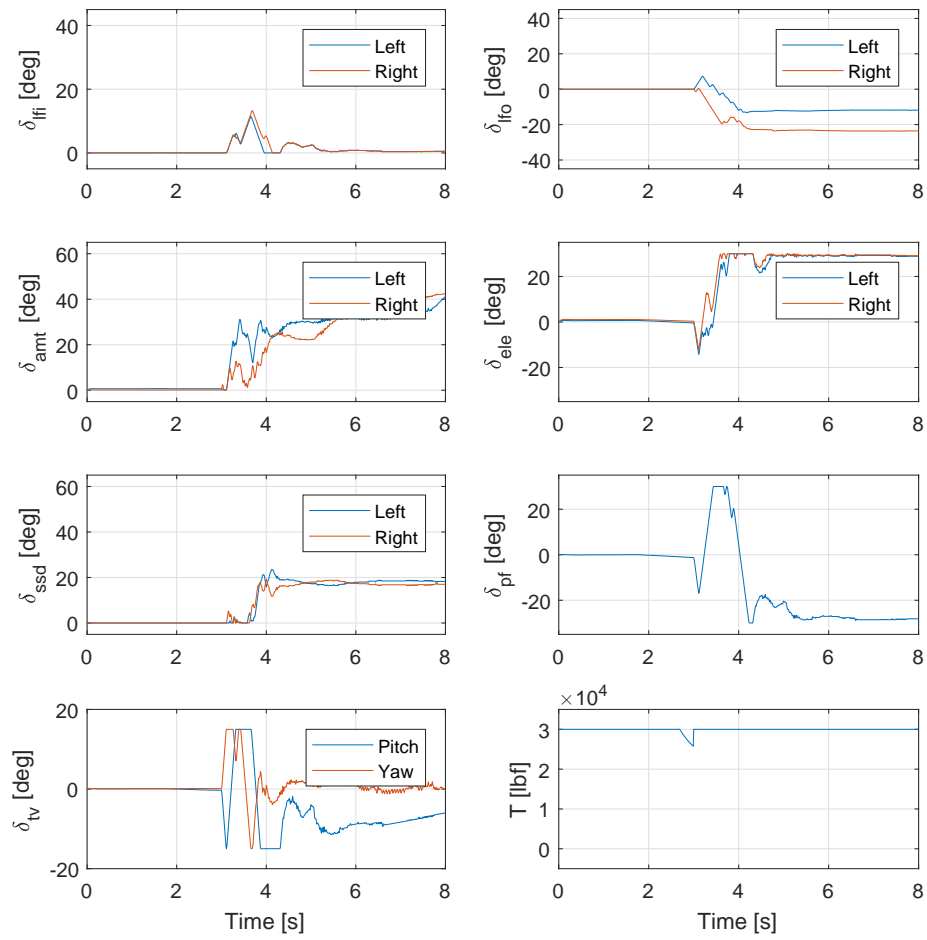


Figure B.6: Control effector inputs while being hit by missile

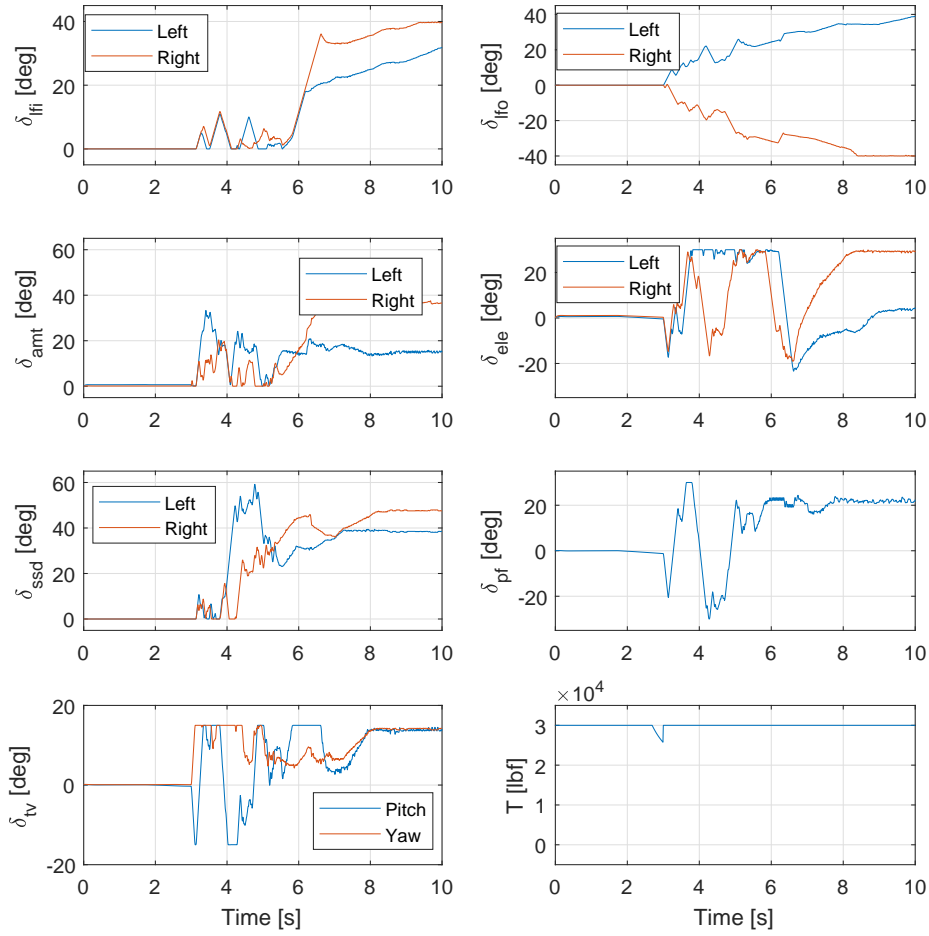


Figure B.7: Control effector inputs while being hit by missile, no failure in left wing control effectors

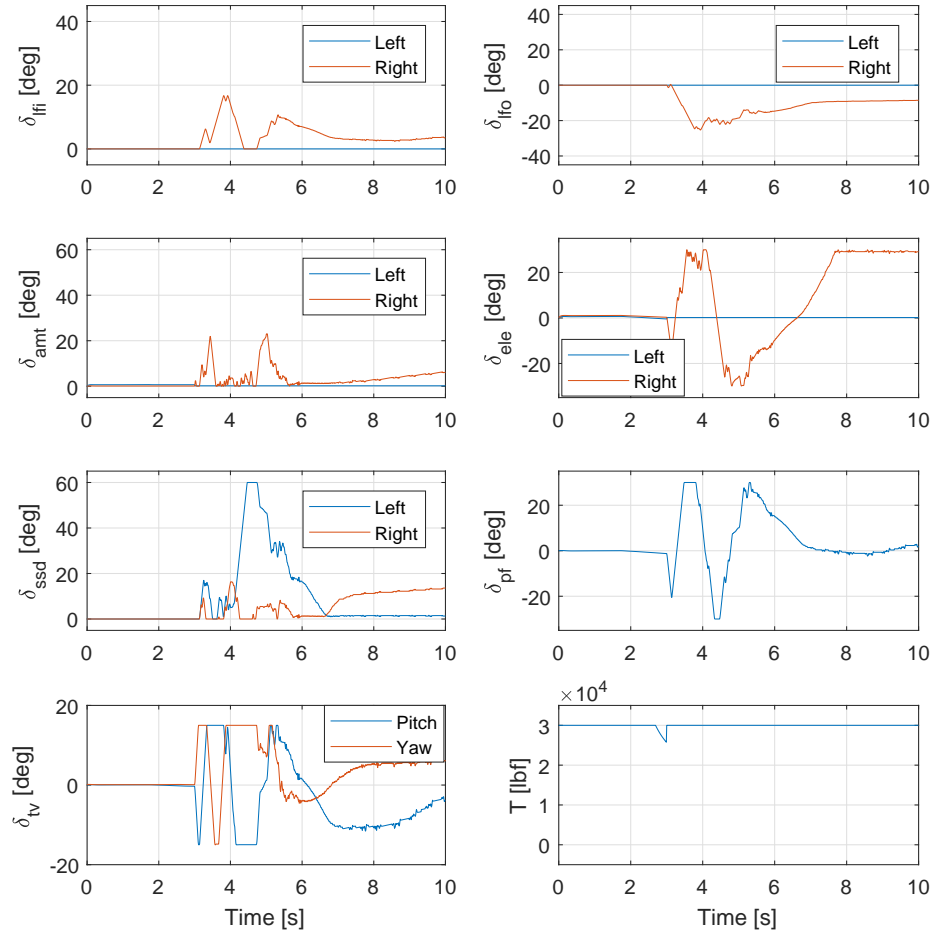


Figure B.8: Control effector inputs while being hit by missile, failure in left wing control effectors

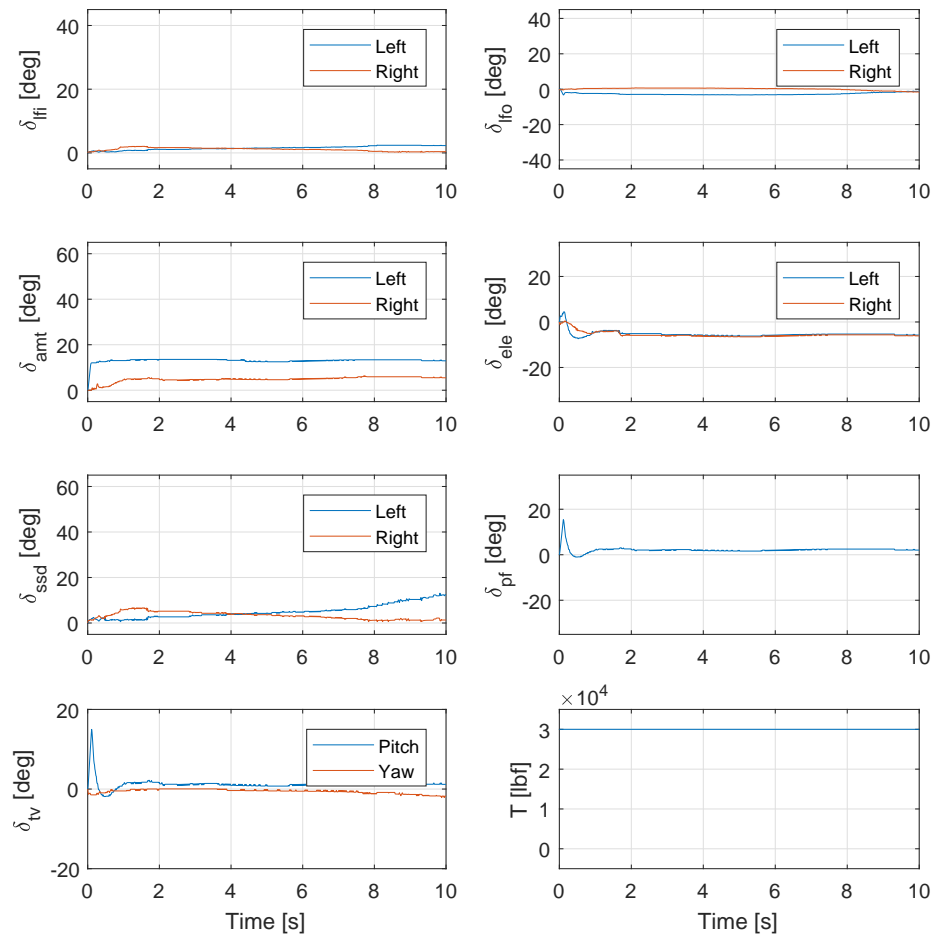


Figure B.9: Control effector inputs with low altitude control system during low altitude stall